The Relation between Clouds and Surface Water on Exoplanets

Master's Thesis

G.F. Mettepenningen

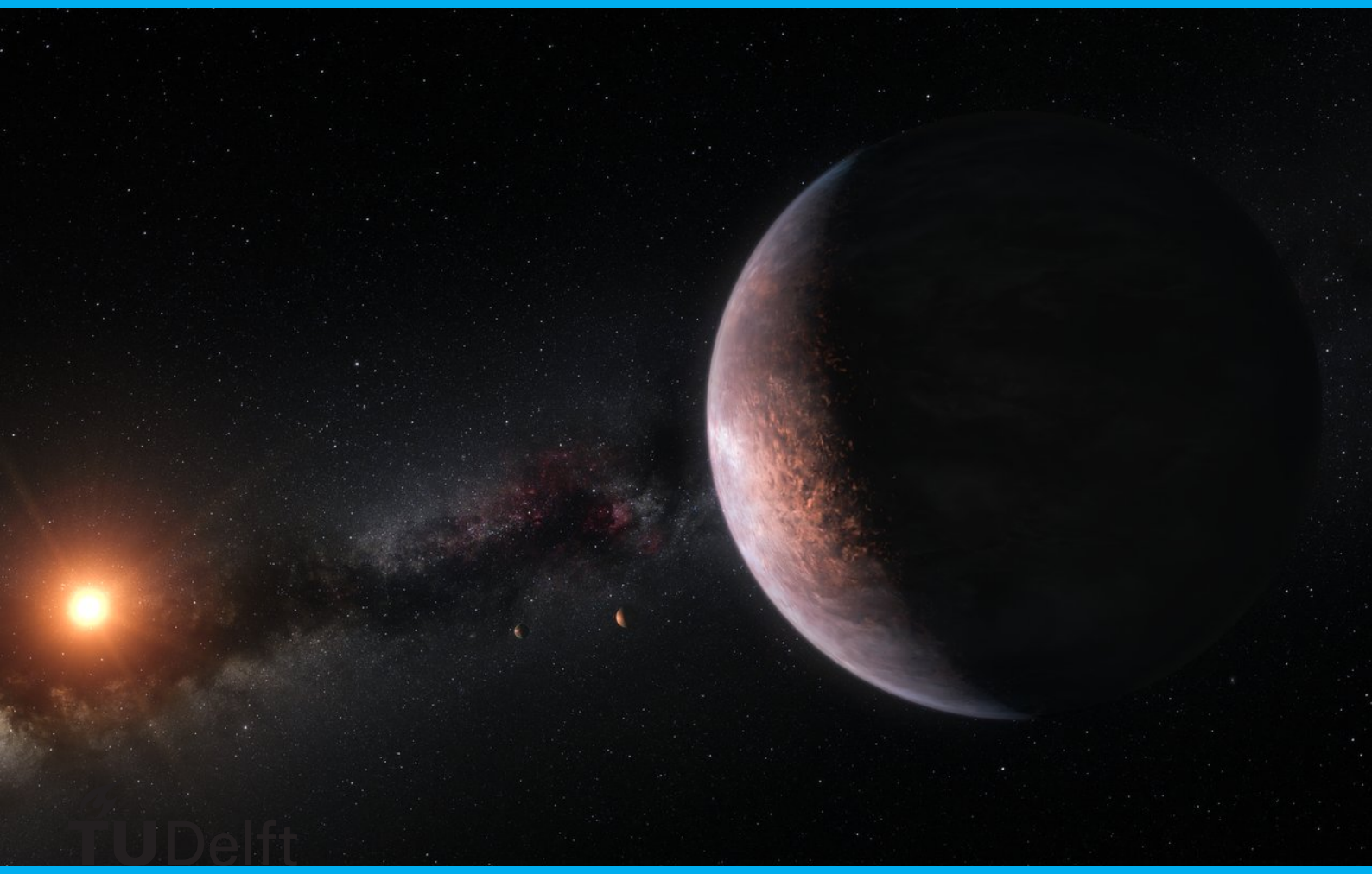

The Relation between Clouds and Surface Water on Exoplanets

Master's Thesis

by

G.F. Mettepenningen

to obtain the degree of Master of Science
at the Delft University of Technology.

Student number:	4682343	
Project duration:	December, 2021 – August, 2022	
Thesis committee:	Dr. D. Stam	TU Delft, supervisor
	Dr. E. Schrama	TU Delft, chair
	Dr. A. Menicucci	TU Delft, committee member
	V. Trees	TU Delft, committee member

An electronic version of this thesis is available at http://repository.tudelft.nl/.
The cover image is an artist's impression of the TRAPPIST-1 exoplanetary system, taken from ESO (https://www.eso.org/public/images/eso1805a/).

TU Delft

Preface

The five years I've spent in Delft were a rollercoaster on discovering what topics in aerospace engineering I find the most interesting, figuring out what I wanted to do in my studies and my career, and mostly finding myself. I'm very happy to end those five years with a great thesis project, where I could really give form to the project myself. It would not have been possible without my supervisor Daphne Stam, who gave me the guidance, responsibility and freedom to make this thesis to what it is now. Thank you for always having advice and ideas on how to continue, for giving feedback that I can benefit from in many future projects, and mostly for keeping the communication and cooperation low-threshold, easy and fun. I would also like to thank Victor Trees, for being critical and open, and calculating signals for me, nothing was ever too much to ask for you. Another thank you to Susan Branchett, Frank Selten and Fred Kucharski for helping me understand SPEEDY. Lastly I want to thank my family and friends to let me annoy you with unwanted information and for helping me where possible. I'm proud of the work I performed and what the thesis has become, and I hope you learn something about exoplanetary climates while reading it!

G.F. Mettepenningen
Delft, August 2022

List of Figures

List of Tables

Contents

Abstract

To answer the question of habitability of other planets, it is crucial to find liquid water. As a planet's surface might be difficult to characterise through observations, the observation of cloud composition and coverage could possibly reveal the presence of large bodies of surface water. Climate code SPEEDY is used to investigate relations between cloud patterns on rocky exoplanets with oceans for various planet parameters, such as obliquity and incident stellar flux, and the observable signals of such exoplanets are computed. SPEEDY is an open-source Fortran code that has been developed for climate computations of the Earth. It is very fast compared to traditional climate codes, because it is based on parametrisations of physical processes. SPEEDY was chosen for the modelling of rocky exoplanets, because of its speed, since our aim is to run simulations for various planet parameters, and its flexibility, since it allows the adaptation of planet properties such as the presence and distribution of continents. A disadvantage of SPEEDY is that the implemented parametrisations are valid for the Earth and might have a limited validity outside the typical Earth-values. Therefore the exoplanet models properties are kept close to those of the Earth itself. Four exoplanet models are used: an ocean planet, a planet with one large dry continent, a planet with one large vegetated continent, and the latter planet with polar ice caps added. Two types of oceans are used: one with a constant temperature and the other with a temperature gradient. Multiple parameters are varied to study their influence on the cloud coverage pattern: rotational period, obliquity, orbital eccentricity, surface pressure, relative humidity, and incident stellar flux. The planet's rotational period is found to have the most obvious influence on the cloud pattern: with increasing rotational speed, bands of clouds form, parallel to the equator, with the number of bands increasing with the rotational speed. The total flux and polarisation of starlight that is reflected by the planets with cloud bands as functions of the wavelength and the planetary phase angle are computed. For smaller rotational periods, the total reflected flux of the planet increases, but the degree of polarisation depends on the visibility of the glint, which in itself depends highly on the cloud pattern. Also the influence of the integration time of the observations on the reflected light signals is studied, and in conclusion the signal depends on how the cloud patterns are averaged over time. Our main recommendation for further research is to broaden the applicability of SPEEDY for exoplanet research by first gaining more insight into the parametrisations and then by adapting them where necessary to allow wider parameter settings.

1 Introduction

The search for life outside of our solar system has been fascinating mankind for many centuries. Over the last decades, more and more planets have been discovered in our galaxy. Now the question is if any of these planets could sustain habitable conditions. One of the essential ingredients for the existence of life is liquid water. The quest thus rose to find water on exoplanets. Although puddles in the soil or subsurface water would suffice, we started looking mostly at oceans, as they have large masses of water and are easier to detect. However, a problem was encountered: clouds blocked the signal of a possible surface ocean (Komacek et al., 2020). This thesis comprises the research that will try to overcome this problem, by finding a relation between observable clouds and underlying oceans. On top of this, the project goes a step further: the signals which the simulated cloudy and watery planets would emit, are calculated, to see what would need to be observed.

1.1. Context of the topic

Current technologies cannot detect many planetary features, such as clouds and oceans, yet. Therefore almost all research on exoplanet characterisation is based on models only. On the other hand, a lot of effort is invested in the future detection of features with telescopes, and it is expected that future technology will be able to characterise the planets in more detail, and also detect clouds (Luger et al., 2019).
Based on this, our research perspective is twofold: We try to characterise the climate of exoplanets with models, primarily because we want to know what our neighbours in the galaxy look like, and secondarily in the context of the quest to find habitable planets. This thesis can be seen purely in this context. Furthermore, there is hope to detect clouds in the near-future. Based on the relation this thesis tries to find, the cloud pattern for a planet with an ocean on its surface could be calculated. It can then be determined what signal to find with the future technology, to track down a planet with liquid water. This is denoted as the second step in this research, after finding the required relation. This second step would be a wonderful addition, but our research can already fulfil its objectives, and be of great value with the first step. Therefore the focus will lie therein.

The relation seeked should be at large scale, global, and can thus remain rather simplistic. It should be noted that looking for liquid water on the surface, only oceans are looked for. Other forms of water can also be present on a planet, such as in the atmosphere or in soil on the surface, where it can form puddles, but this defines an entirely different planet (Herbort et al., 2020, Kiang et al., 2021). The scope of this thesis only incorporates oceans, which exist of pure water. No more detailed description of the soil or ocean composition is needed at this stage of the research.
On Earth, there is a clear water cycle, based on evaporation of oceans and condensation of clouds. This cycle is formed by Earth's atmospheric composition, and planetary parameters such as surface pressure. Earth's climate is characterised by its seasons, which depend on its rotational period. It is expected that there could also be a relation between clouds and oceans on exoplanets, and the parameters that could determine this relation are modelled to find out. Eventually, when a relation between clouds and oceans is found, it suffices to detect clouds to be able to quantify the oceans.

It is believed that clouds are easier to be detected and observed than oceans, because of certain observation properties such as the rainbow.
This modelling will be done by an existing climate model, namely SPEEDY (Kucharski et al., n.d.). SPEEDY is a complete 3D model, developed based on Earth's climate. It is originally built at ICTP, but further developed at TU Delft and only recently in use at our faculty. The TU Delft's recent version ExoSPEEDY is flexible and can therefore be adapted to exoplanets as well. Because of its simplicity, its parametrisation is expected to be able to be projected onto other planets, although with limitations. It should be noted that for simplicity throughout the entire document the name SPEEDY is used (instead of both SPEEDY and ExoSPEEDY) to denote the climate model.

1.2. Research questions of the thesis

This section consists of two main parts: the research questions and the research objectives. These research objectives and questions are derived from the gap present in current scientific research, for which the context and relevance are described above.

1.2.1. Research Objective

The main research objective of this thesis can be stated as:

> "To find if a relation between clouds in the atmosphere and (liquid) water on the surface of exoplanets exists, and if so to define this relation, by the climate model SPEEDY".

To identify this relation, our research thus also needs to find out whether there even is a relation.
This goal will be reached through subgoals, listed chronologically as 'milestones' in the thesis. First, to determine the parameters and parameter ranges that will be varied in the experiment. The relevant parameters and their ranges are to be found in literature, and the ranges can be adjusted if deemed necessary during the process of running the model. The exoplanets to be looked at should be similar to Earth, but some variety should be introduced. This means that the values of the parameters will be varied, but will in any case lie close to the values of Earth.
Then, another objective is to implement and run the experiment with these parameters with the climate model SPEEDY, to generate the data. This looks straightforward, but generating useful data is essential for our research.
Finally, the last objective is to process and interpret the data to find and identify a relation (or not).

1.2.2. Research Questions

Some questions are formulated to aid the research into fulfilling its objective. The main focus of the thesis is on the question:

> "What is the relation between clouds and surface water on exoplanets?"

As this question is very broad, it is broken down into some sub-questions, listed below.

- How can climate model SPEEDY be used to find the relation between clouds and surface water on exoplanets?
- Which parameters have an influence on planetary atmospheres, and could thus have an influence on the relation between clouds and surface water on exoplanets?
- How should these parameters be implemented and varied in climate model SPEEDY and how large is their influence on the relation?
- What are the specific conditions of the planetary atmosphere and surface under which such a relation can be observed?

Finally, the second part of the thesis should answer the question: How can this relation be observed with a telescope? This is basically calculating the signal of the planet with a specific cloud pattern, such as the spectrum at different phase angles and phase curves at different wavelengths. It is seen as a bonus if this could be done, but it is not part of the main objective. The main objective can already be reached by answering the question(s) stated above.

1.3. State-of-the-art in exoplanet observations

Although at this day, many exoplanets are discovered, hardly anything is known about them. Over the past few years, a lot of effort has been invested to change this. Research topics shifted from detecting to characterising exoplanets, and this research area will continue to grow.
Exoplanet features are very difficult to detect, but many different scenarios can be modelled theoretically. The models vary greatly in complexity and detail, each revealing different properties of various planets.

1.3.1. It all starts with Earth

The research in the field of the climate of exoplanets is often tailored towards the search for liquid water, in light of the question of habitability. As a basis, the only inhabited planet we know is used, namely Earth. The climate model used for this research is initially based on Earth's climate, and further on projected onto exoplanets. Earth is known in detail and can be studied thoroughly, unlike other planets. The same physical and chemical laws that are discovered on Earth can be extrapolated to exoplanets (Guzewich et al., 2019).
Also direct detection methods start with Earth. "How would Earth look like if it were an exoplanet?" The signals Earth sends out are reconstructed (Gu et al., 2021, Cowan et al., 2009, Robinson et al., 2011). If such a signal can be found, it is possible that a planet with similar features as Earth is identified. This planet could exhibit a complex cycle of clouds in its atmosphere, and oceans of liquid water on its surface.

1.3.2. Commonly studied exoplanetary targets

Evidently, planets that are relatively easy to observe are favoured, such as closeby systems or planets with a high contrast. Focus often lies on M-dwarfs, as these stars have a low mass, low luminosity and are long-lived. This makes the contrast in both size and brightness of the exoplanet larger, and the habitable zone closer to the star. The advantage of this is that planets in that zone have a higher probability of transiting. It should be noted however that planets close to the star are often tidally locked, meaning that their rotational period equals their orbital period. Because a fixed side of the planet faces the star and the other side does not, this likely strongly influences their climate. Furthermore, M-dwarfs are simply by far the most common stars in our galaxy, as can be seen in Figure 1.1. (de Vera and Seckbach, 2021)
Examples of such nearby M-star systems with planets in the habitable zone are TRAPPIST-1 (Gillon et al., 2017) and Proxima Centauri (A. D. D. Genio, Way, et al., 2019). Because they might contain liquid water, their possible climates are studied in more detail.

Another target that is of interest for research on habitable exoplanets is Venus, because in its early history it could have had water oceans and a habitable surface temperature. In the beginning of our planetary system, Earth and Venus were very similar for a long period of time, but they evolved into a different fate (D. Genio et al., 2020). If Venus had a prograde orbit and a rotation period which is faster than it is today (although slower than Earth), it could have sustained a moderate temperature and liquid water for a significant period of time (Way et al., 2016).

1.3.3. Direct detection methods

The most informative method to detect certain features on exoplanets is direct detection, observing the signals directly originating from the planet. With current technology, not much is yet possible, because of resolution issues in spectral, spatial and temporal range. As technology is developing rapidly, this might change in the near future.
By far the mostly used method to detect and characterise exoplanets is the transit-method. Combined with spectroscopy, this method can characterise the upper layers of the atmosphere. A drawback is that the starlight cannot pass through an atmosphere with clouds. The clouds can cause the planet's radius to appear larger, or it can cause irregular variations in transit measurements. They can also lower the amplitude of spectral features (Komacek et al., 2020). However, if clouds would be detected by another method, transits can be used to determine their composition from gases in the atmosphere. Phase curves describe the apparent albedo or the reflected starlight of a planet at different angles as

[1] Image from https://www.nasa.gov/sites/default/files/thumbnails/image/stsci-h-p2006a-f.jpg, consulted on 13/06/2021

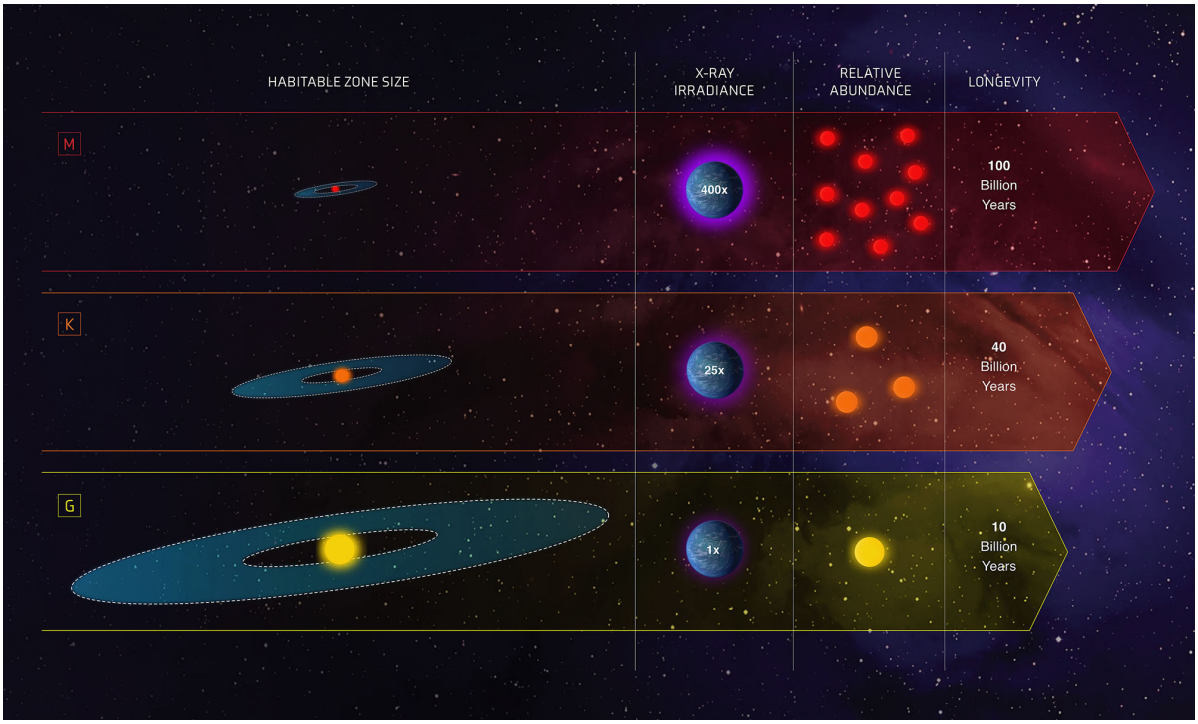

Figure 1.1: The habitable zone around different star types, accompanied by some features of the star type. The Sun is a G-star type, a M-star type is a common target for exoplanet detection.[1]

compared to the observer. In particular, oceans can show clear reflection patterns, called the glint effect. This proves to be an effective method to detect surface water. Nevertheless, again clouds can interfere or block this effect (Zugger et al., 2011). However, being based on stellar reflection, phase curves can also describe cloud patterns, as clouds are good reflectors (Grenfell et al., 2012).
Another feature of the signal emitted by exoplanets is polarisation. A light wave can travel through space in a certain direction or under a certain angle with respect to the reference plane, which is characterised by its polarisation[2]. From the type and degree of polarisation, it can be derived where and what clouds are present in the atmosphere (Klindzic et al., 2021). It is a novel development that will finetune its methods in the near future, and is expected to be used more and more later on.

1.3.4. Atmosphere of exoplanets

The range of conditions for liquid water to be sustained on the surface of exoplanets appears to be quite broad! Surface temperature and pressure play an important role in this. Generally, the water amount increases for an increasing surface temperature (Wunderlich et al., 2020). Also a relatively high minimum surface pressure should be maintained (Wordsworth and Pierrehumbert, 2013). The main reason why water could perhaps not be sustained on a planet is the runaway greenhouse effect. Under certain conditions, water can escape from the atmosphere, and planets can lose water amounts up to worth to Earth's oceans (Ishiwatari et al., 2019). This effect can be detected by certain compositions of the atmosphere, for example the ratio between hydrogen and deuterium could be an indicator. Another aspect to liquid water are the surface-atmosphere interactions. The presence of an ocean obviously has an influence on the climate, but not only because of its water cycle. It interacts with certain gases in the atmosphere, an ocean is for example a CO sink. This property could be used to identify an ocean, through the non-detection of CO (Wunderlich et al., 2020).
In Figure 1.2 possible atmospheric compositions for varying planet mass and equilibrium temperature can be seen. Planet mass is often a constraint, while equilibrium temperature is determined by the star and the atmosphere itself. The temperature of a planet can be derived from its absorption or emission spectrum. Atmospheric composition has a direct influence on oceans and clouds, as enough water

[2] An interested reader is directed to https://www.eso.org/public/announcements/ann13069/ for more information on polarisation and its connection to exoplanets

needs to be present in the atmosphere to create a sustainable water cycle. It also has large indirect influences: it influences the surface pressure and temperature, which influences both liquid water and clouds.

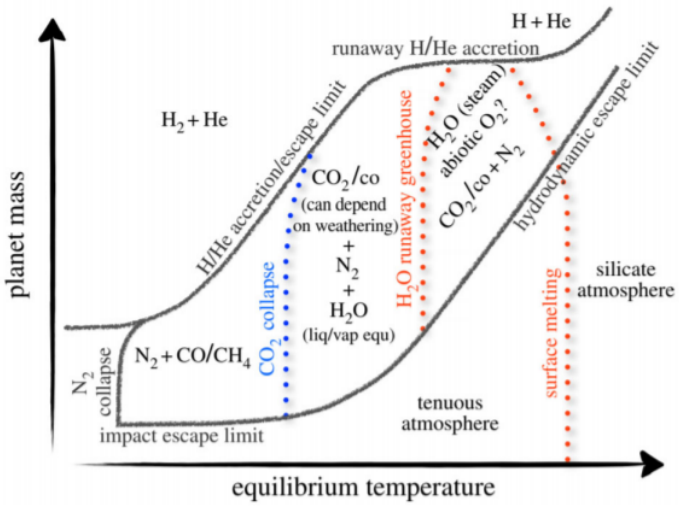

Figure 1.2: Possible atmospheres for given planet mass and equilibrium temperature (Grenfell et al., 2020). The limits for maintaining an atmosphere on the planet are also shown.

Tidal lock can induce large temperature difference over a planet. The planet can go as extreme as being an eyeball planet, with its surface covered entirely by ice except for the substellar point, which has an open ocean (Checlair et al., 2017). Generally, the planet has an extensive cloud cover on the dayside, while keeping a more clear nightside. Nevertheless, cloud feedback and heat transfer can moderate the climate, enlarging the ocean. Besides tidal lock, rotation period plays a role in planetary climates. In general, a faster rotating planet has a different cloud cover than a slower rotating one. This could be harmful for the cloud feedback.
At higher insolation, more clouds are present, but for a higher rotation period, the cloud coverage would diminish. A fast rotating, hot planet diverges from the classical Earthly water cycle. This planet would have a very humid atmosphere with thick steamy clouds, but very little surface water (Way et al., 2018, Jansen et al., 2019, A. D. D. Genio, M. J. Way, et al., 2019, Loftus and Wordsworth, 2021).

1.3.5. Cloud formation

In general, in literature it is commonly assumed that the greater the fraction of a planet's surface covered by water, the more clouds there are. More surface water consequences in a more humid atmosphere, and hence more clouds. On Earth, the principle of cloud feedback effects even each other out, but on other planets this will probably not be the case, as the clouds' properties differ, such as their altitude in the atmosphere (Yang et al., 2013, A. D. D. Genio, Way, et al., 2019).
The chemical processes that hide behind cloud formation, cloud feedback, and water vapour in the atmosphere are well-known. Clouds form at condensation nuclei and grow onto these particles. Surface pressure and temperature play an important role in this process, together with the composition of the atmosphere (Woitke et al., 2021).
Figure 1.3 is the cloud formation process. The essential ingredients are an excess of (water) vapour and so-called Cloud Condensation Nuclei (CNN's), tiny particles, for example dust, on which the water vapour can condensate to form a small cloud particle. An important factor for this condensation is temperature, therefore this type of clouds is called cooling clouds. Also direct chemical processes can fulfil this purpose. This type of clouds is evidently called chemical clouds. Now that small particles are formed, they grow into large clouds through collision. Wind can either add small particles, often dust, to the cloud or blow them away. Finally large particles fall from the clouds, or as we know it: rain. During this sedimentation, the water becomes liquid. This rain ends up in water bodies, such as rivers and oceans. To be able to close the cycle and form clouds again, the water needs to evaporate.

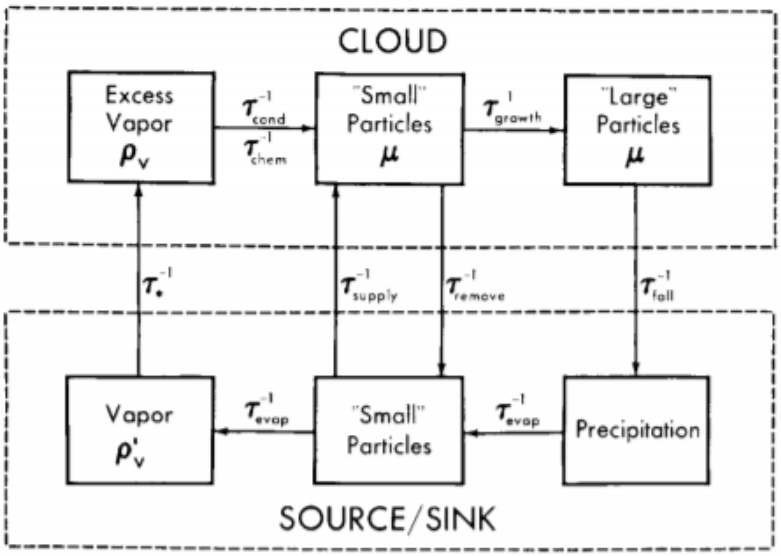

FIG. 1. Block diagram of a simple conceptual model of an aerosol or cloud. Symbols are defined in the text.

Figure 1.3: The cloud formation process as described by Rossow, 1978 (symbols are explained there). The various states of gases and particles are represented in the blocks, while the arrows show transition or transportation processes.

For the presence of (excess) water vapour, surface temperature and pressure play an important role. Both need to be high enough to be able to form water vapour. The threshold for nucleation or condensation is often generalised into a critical vapour density in the atmosphere.
It is assumed that the temperature of the particles is similar to that of the atmosphere. If this would not be the case, other microphysical processes might dominate. For example in ice clouds, the particle growth depends on the crystal structure. Other aspects that affect the growth rate are the size of the particles itself, the sticking efficiency of the particles, and impurities the particles might have. Also, it is assumed that the wind is turbulent, and as a consequence similar over the entire atmosphere.

1.4. State-the-art in climate models: introduction to climate code SPEEDY

As many other studies, this thesis will be based on a climate model. The model selected is SPEEDY (version 41, Kucharski et al., n.d.), in which TU Delft has a large contribution. The model is fast, and incorporates all features needed for this research, while still being simple. This section lays out the general mechanisms of GCM's and available codes. After, the next chapter is entirely dedicated to SPEEDY. There its specific parameters and variables are discussed in detail.

1.4.1. Global Climate Models (GCM's)

Already 40 years ago, scientists started building models to simulate the climates of other planets (Rossow, 1983). Up to date, models are the main source of research in the field, as exoplanets are simply really difficult to detect. Most models are based on Earth's chemistry and physics and extrapolated towards exoplanets. The most basic climate models are limited to 1D (Petralia et al., 2020), but currently many 3D models are available. The abbreviation GCM stands for either Global Climate Model or General Circulation Model, used interchangeably. The term does not have a clear definition, all different 3D climate models currently available fall under it. This means that the list of models can have a variety in things taken into account or not.
In a model, often a trade-off needs to be made between complexity and computational speed. This highly depends on the purpose of the model. Some models take into account the surface wind, waves

in the ocean, the local composition of the soil, etc. Others do not even bother about the rotation of the planet. In this research, SPEEDY makes up a good balance: only global characteristics are seeked, so it may be not detailed, allowing for a very fast model, which is handy for many runs with many parameter sets.
As an example, clouds are a generic part of the climate for us, but cloud formation is often not included in the models. Cloud formation is very complex, and first separate cloud formation models on a microphysical basis needed to be set up in order to be able to incorporate them in other models (Zsom et al., 2012, Ohno and Okuzumi, 2017). Still, because of its uncertainties, clouds remain a big factor in causing differences between models.
The way clouds are processed in SPEEDY, does not take all microphysical mechanisms into account. It simply assumes that a certain amount of water vapour and condensation nuclei cause a certain amount of clouds to appear.

The thesis will remain restricted to planets similar to Earth. This means a combination of oceans and land on the planet's surface, a similar composition of the atmosphere, and similar planetary and stellar features, such as rotation, surface pressure, eccentricity, incoming flux, etc.

At this day, Ocean Heat Transfer (OHT) is a highly discussed topic (Way et al., 2018). OHT is the lateral transport of heat through an ocean, which makes the ocean dynamic. Its importance is already proven, but despite that it is often not taken into account in models, for computational purposes (Yang et al., 2019). Generally, OHT evens out the surface temperature and climate of a planet. The climate sensitivity lowers, so the climate itself is more sturdy. The water freezes more slowly, so the ocean ice fraction is also lower. OHT even has an influence on clouds, mostly the low level clouds, as they are closest to the surface and ocean. This also means that the greenhouse radiative cloud feedback will be smaller (Way et al., 2018).
In the version used, SPEEDY does not use OHT, for simplicity and computational speed. As mostly experimental runs are intercompared, the physical effect of OHT will not influence the conclusions drawn in this thesis. More on SPEEDY's ocean model and other properties can be found in Chapter 2.

1.5. Overview of the report

As explained, the aim of the thesis is twofold: The main objective is to find a relation between clouds and surface water on exoplanets. To achieve this aim, first exoplanets are incorporated in the used climate model SPEEDY. Chapter 2 gives an overview of the working of this model. The process of building exoplanets is described in Chapter 3. Secondly, parameter variations are performed to give form to the seeked relation. These are discussed in Chapter 4. From these parameter variations, a specific case is selected to be studied in further detail. This deeper analysis can be found in Chapter 5.
The secondary objective of the project is to calculate the signals of the simulated planets. These signals are shown and intercompared in Chapter 6. Finally, conclusions of the thesis can be found in Chapter 7, and further recommendations in Chapter 8. As some code is developed and the models are adapted, verification and validation needed to be done, which is reported in Appendix A. Appendix B contains a list of experiments run in SPEEDY.

2

Climate model SPEEDY

The basis of this thesis project is climate model SPEEDY. SPEEDY will provide the tools to simulate the atmosphere and its clouds for a given exoplanet. As introduced in Chapter 1, SPEEDY was originally built to be applied to Earth. A large part of this thesis project comprised to extend its features to be able to use the model for different Earth-like exoplanets. As the model is flexible, it should be possible and relatively easy to adapt it to work with other planets.
A planet implemented in SPEEDY is defined in two ways: parameters that can be varied by the user, such as mass, radius, rotation, insolation and so forth, and the definition of the planet in the source code, such as the orography or Sea Surface Temperature (SST). This thesis goes further than simply varying parameters through the user interface, by also adapting features in the source code.

This chapter gives an overview of the workings of SPEEDY, together with its features and limitations relevant to the project. For any further features not covered here, the reader is directed to SPEEDY's documentation (Kucharski et al., n.d.).

2.1. Model description

SPEEDY is based on a dynamical core with as model variables vorticity, divergence, temperature, surface pressure and specific humidity. Its documentation can be found on http://users.ictp.it/~kucharsk/speedy_description/km_ver41_appendixA.pdf, the main aspects are summarised here. Its architecture and working sequence can be seen in Figure 2.1. The advantages of this model are that it is fast and flexible. On the other hand, these features bring along that the model is limited in complexity. On top of that, the model is very recent, which makes sure it uses most up-to-date technology, but it has not fully proven its purpose of being applied to exoplanets yet. Hence, we do not know to what extend the parametrisation based on Earth will work or will not work on exoplanets. This aspect is to be clarified in this thesis through simply using the model and discovering its limits.
The inputs that can be changed are the planetary, time-stepping, dynamics and physics parameters. Also the land and sea/ice model can be adapted. The physical parameters consist of convection, condensation on a large scale, short-wave and long-wave radiation. Clouds are determined from relative humidity, and they decrease the long-wave transmissivity. Surface fluxes of momentum and energy between land and sea are also part of the physical parameters. Finally, vertical diffusion is taken into account, which consists of the redistribution of dry energy and moisture within the lower layers, the diffusion of water vapour in the troposphere and the diffusion of dry energy if the lapse-rate is larger than the dry adiabatic limit. For the mathematical formulation of these physical parameters, the reader is directed to the documentation. The model is constrained by boundary conditions, amongst others the topographic height, land and sea mass, surface temperature, deep soil temperature, sea-ice fraction, soil moisture, snow depth, bare-surface albedo, and the land covered by vegetation. These boundary conditions should be specified on a monthly or annual basis.

The model is written in Fortran, in which also the output analysis will happen. The code calculates

its results on a latitude-longitude grid, reduced to $48x96$ points. An experiment in SPEEDY for 3 years takes about 20 minutes cpu-time. The mathematics behind the model will not be modified for this research. The results roll out in GRADS files, which can easily be used in the GRADS processing package of Fortran to process the data. More on this and details on SPEEDY in context of the thesis project can be found in Section 2.2.

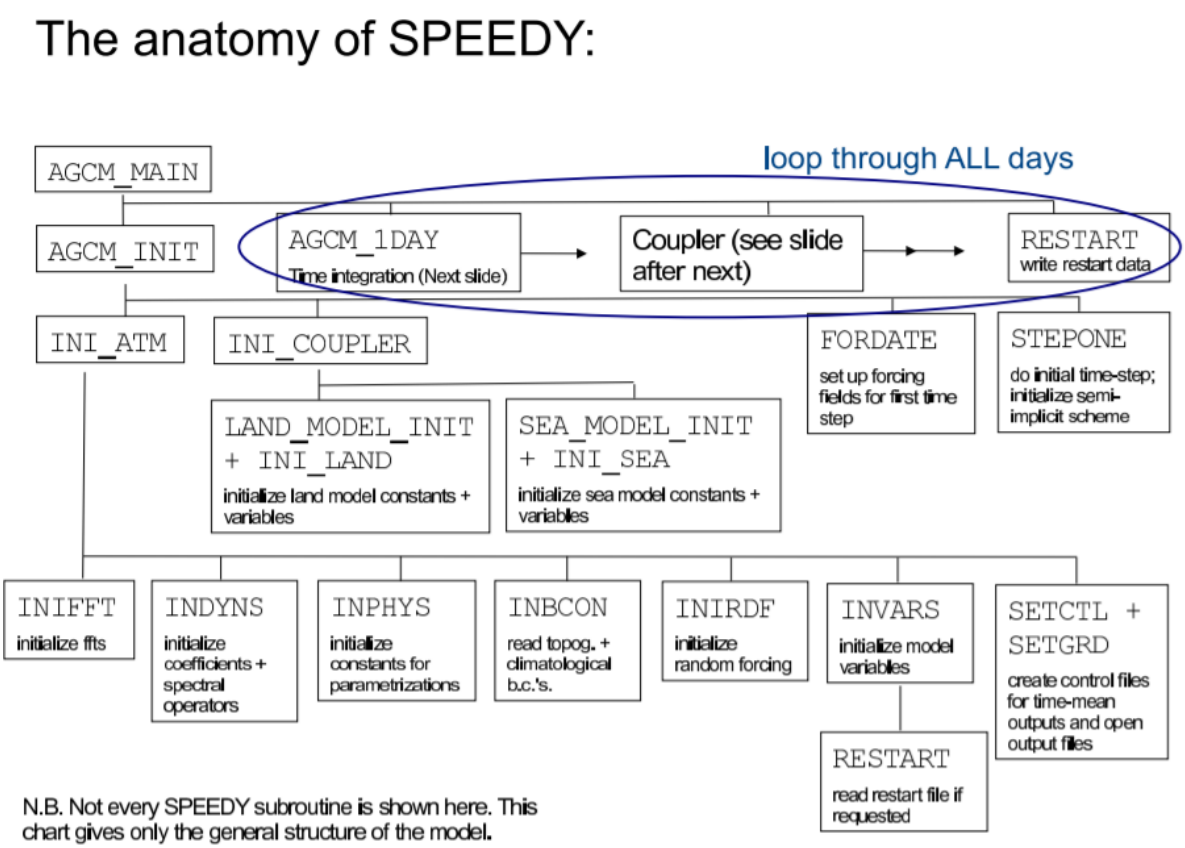

Figure 2.1: The anatomy of the SPEEDY model, version 41 as built by Kucharski et al., n.d. The blocks represent source code blocks, explaining their function under the name of the designated subroutine.

2.2. Features & Limitations

A benefit of SPEEDY is that it is a rather simple model, but this also causes some limitations to take into account. This section lists some of the model's features which greatly influence the results and conclusions. Their implications and assumptions are elaborated upon.

Many contributors & Different definitions of parameters

SPEEDY is the result of many building blocks, which are the work of various contributors. The code was unified and centralised by Susan Branchett (TU Delft), making sure it is overviewable and user friendly. Nevertheless, this can only be done to a certain extent, and as a result there are still some irregularities. Some parameters are defined differently in different subroutines. For example, one year consists of 365 days for the simulation time of the model, but for radiation purposes a year of 360 days is used. This has as a consequence that subroutines do not always cooperate smoothly when adapting the model.

The slab ocean model

The implemented ocean model is a mixed-layer slab ocean. This means that there is no lateral heat transfer. Also, automatic freezing of the ocean is not taken into account. This means, that even when the ocean becomes for example -30 degrees, it will still have its liquid properties, such as the same

process of evaporation. However, known from personal communication, SPEEDY developers are incorporating this freezing/melting feature into the next version of SPEEDY.
Furthermore, the vertical heat transfer is split up into the slab on the surface of the ocean, and deep ocean heat transfer. The deep ocean heat transfer is simply parameterised into one deep ocean heat flux. The depth of the slab is determined by the following formula (Kucharski et al., n.d.):

$$d_o = d_{omax} - (d_{omax} - d_{omin}) \cos^3 lat \tag{2.1}$$

Which ranges between d_{omax} 60m at the poles and d_{omin} 40m at the equator. This depth becomes important when the ocean and atmosphere are coupled, because of the ocean heat transfer described in Chapter 1, which is not applicable to this thesis, but SPEEDY has the option to incorporate it.
The standard ocean model is always based on prescribed Sea Surface Temperature (SST). If no coupling is enabled, the SST remains constant throughout the experiment. If coupling is enabled, the ocean is forced by the atmosphere, so the SST can vary over time. If more coupling is desired, an external ocean model can be loaded into SPEEDY.

Parametrisation based on data input
To guarantee simplicity, some parameters are not modelled in SPEEDY, but read in from data bases. An example of this is the SST. In the unadapted version of SPEEDY, this is taken from a database for the full duration of the experiment, which usually begins at 1st of January, 1979. If the experiment runs for three years, the SST will simply remain the one from the database, regardless the evolution of other parameters.
When the database for SST at a certain point does not match the land-sea mask, the missing datapoint is set by a predetermined value. In case of the SST it is the freezing temperature of pure water 273.15K, irrespective of the coordinates of the datapoint. All read in databases are checked for faulty points and complemented before use in the model.
As the databases are only available for Earth, this feature of SPEEDY cannot be extrapolated onto exoplanets. It should therefore be adapted, as will be described in Section 3.1.

Cloud formation
Aforementioned, it was described that SPEEDY's cloud formation is based on many assumptions, to keep the model fast and simple. For every grid point, the cloud cover is the sum of two terms:

1. A weight factor (given as input) multiplied by the squareroot of precipitation rate. The precipitation rate comprises both convective precipitation and large-scale precipitation.

2. The square of the maximum relative humidity in the troposphere. This term is only taken into account if the relative humidity is higher than the threshold. If the relative humidity is lower than the threshold, no clouds from this term are assumed.

Stellar flux absorption
The stellar flux is split into wavelength bands, to designate the according amount of flux to an according absorption band. These bands are based on the absorption from gases in the atmosphere and defined as follows. On one hand there is the shortwave radiation, which comprises the visible (including UV, for ozone absorption) and near-infrared. On the other hand, there is the longwave radiation, which comprises four wavelength bands, between 5 and 15μm: the 8.5-11μm band, the CO_2 absorption band around 15μm, the weak water vapour absorption, and the strong water vapour absorption (Kucharski et al., n.d.).

Decoupling of parameters
To keep the model simple, many parameters are merely seen as input data and are not mathematically computed, hence they are decoupled from one another. For example, the stellar flux does not depend on variations in the orbit of the planet, nor on its planetary rotation or its obliquity. Flux at different locations is simply derived from the stellar constant and absorption through the atmosphere and set per location on the planet.

GRADS output files & Processing software
SPEEDY produces various output files, an overview of the different file types:

- GRADS files, consisting of control and grid files. Grid files are binary files which simply contain the data, while control files contain all the information on how to read the data in the grid files. In a control file, a.o. the grid on which the data is produced and the parameters that were calculated are specified. These two types of data files should be processed together.
- The raw data is saved in textfiles. These are matrices with numbers, without documentation of what is what, such as is the case in the GRADS files. The benefit of this is that these textfiles are more accessible and easier to work with than those GRADS files.
- A file containing the run status of the experiment.

GRADS files (the combination of control and grid files) can easily be processed by the GRADS module in Fortran. This module can plot the parameters on the specified grid and times, plus a (limited) number of built-in functions, such as minimum, maximum, magnitude of vectors or average. It is a rather basic processing module, but very easy in use.
To process data in Python, the needed parameters are distilled from the raw data in the textfiles. For the purpose of this thesis project mostly time-mean output fields (monthly and daily) were used, but also (co)variance and diabatic heating fields output are available.

2.3. Stability of the model's parametrisation

At the start of this project, the applicability of SPEEDY to other planets than Earth was unknown. The closer the planetary properties are to Earth, the more accurate and representative the extrapolation of the model will be. Checks are built into SPEEDY to guarantee the possibility of the situation really existing. For example if the temperature gets below 180K, the simulation stops. However, the simulated data from before this moment is still available. This can be used to study the physical processes as desired, or to see what went wrong right before the experiment blew up. The implications of these instability issues in the context of this research and their effects on the results are discussed in Section 4.1.
The parametrisation of SPEEDY can thus not be applied to a wide exoplanet range. It is left as a recommendation to expand the scope of the model.

3

Building exoplanet models

Now the workings of SPEEDY are known in a bit more detail, the use and application can start. Figure 3.1 shows all parameters which are relevant to the project, in terms of model parametrisation, study cases to be defined and parameter variations done on these cases.
First, SPEEDY needs to be adapted to be able to be applied to exoplanets. The way this is done, can be found in Section 3.1. As the infinitive amount of possible exoplanets cannot all be studied, some study cases are defined, which are described in Section 3.2.

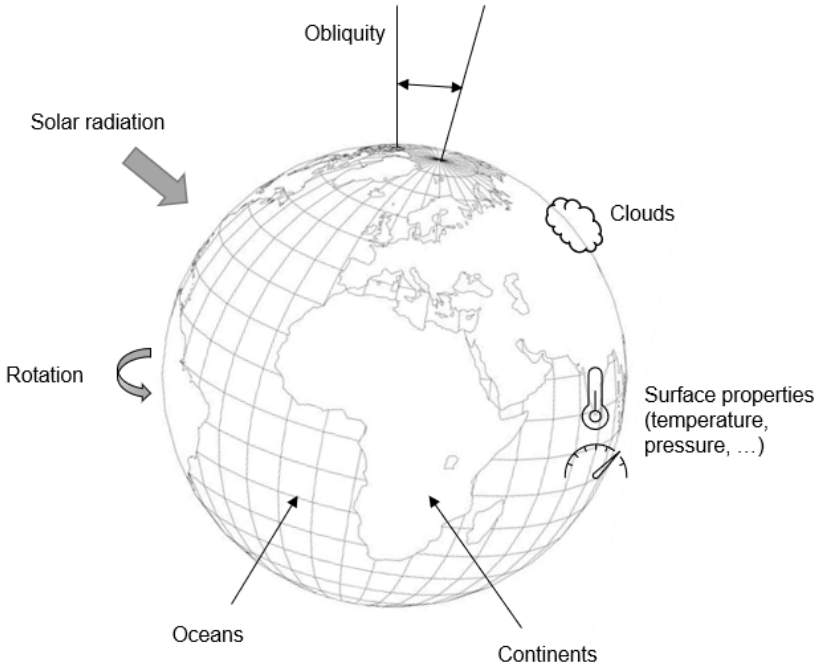

Figure 3.1: Visualisation on our known planet Earth of the parameters that play a role in the parametrisation of SPEEDY, the defined cases and parameter variations of this thesis.

3.1. Methodology

This section explains how the surface of the planet is adjusted in SPEEDY. The adjustments are done in the source code for each planetary surface separately, having the disadvantage that a new version of the source code needed to be developed for every individual case.

First, the oceans, continents, sea ice and orography of Earth are taken out. These are mainly databases that are loaded in and are now disabled. Then, the land and oceans applicable to a certain case are implemented. The source code is adapted to be able to set the values of these parameters by hand. The orography is kept zero for all cases.
To keep the exoplanets straightforward and guarantee simplicity, the cases described in this thesis all have uniform properties. That is, the ocean or land on the surface is horizontally homogeneous, in terms of temperature and albedo. For example, oceans have a temperature of 0^oC, no height variations, and an albedo of 0.07, based on oceans on Earth. The specifications of all cases are described in the next section.
Furthermore, the subroutines to correct datafiles and smoothen planetary properties (as described in Paragraph 2.2) are disabled, so are the anomalies in all fields.

Figure 3.2 shows the methodology and build-up of cases schematically. It lists the parameters that are reset at the start of the simulation and the features that are added for each case. The explanation of these features (and why case 4 comes before case 3) is elaborated upon in the next section.

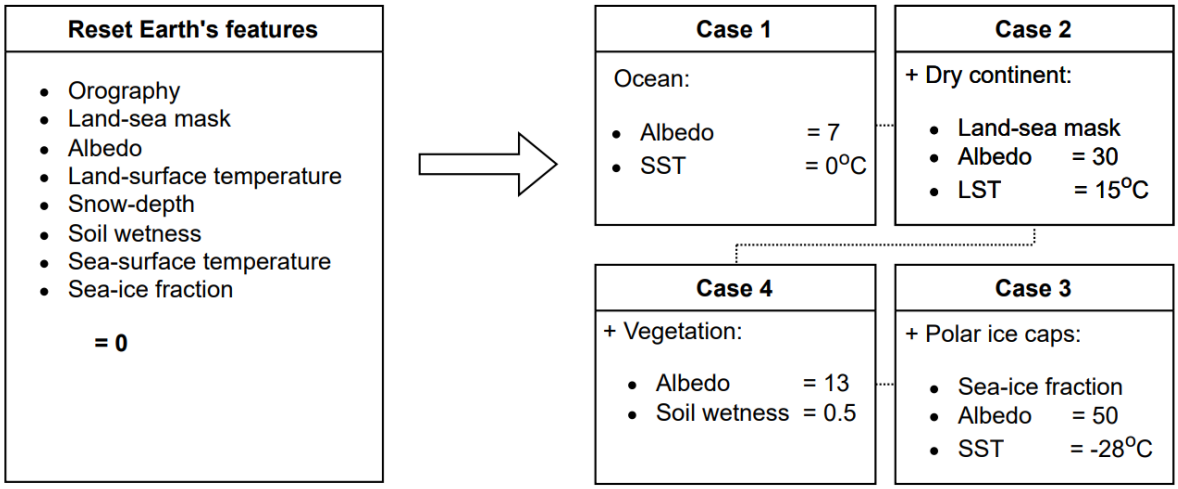

Figure 3.2: Methodology of case implementation. On the left side the properties which were loaded from Earth's databases are shown, which are reset to 0 for implementing exoplanets. These properties are overwritten for each case, by the values shown on the right side. The ocean defined in case 1 is kept for all other cases, with additional properties shown in the boxes. Each consecutive case adds features.
Note: case 4 comes before case 3, as it was defined afterwards as an intermediate case.

3.2. Cases

The cases to be studied are introduced in Section 3.1. This section lists the properties of each case, as well as describing the motivation behind the selection of the case.

Case 1: Ocean planet
In this case, the planet's surface is fully covered with oceans, a so-called water planet. There are multiple options for diffusion in the ocean of the planet. For Earth, simply the sea surface temperatures over the years are loaded as data in SPEEDY. For exoplanets this is of course not possible, so the temperature has to be determined manually.
First, a constant temperature of 0 degrees (freezing temperature of clear water) was selected. Unfortunately, these planets often yield instable atmopheres, but nevertheless some interesting results and insights are presented in Chapter 4. The effects observed on these planets are often similar as the effects with another type of ocean, described below.
Secondly, a linear gradient in sea surface temperature was introduced. The temperature icreases from -28^oC on the poles, to 27^oC on the equator. This yields a stable situation, for which the results are also discussed in Chapter 4. With these options for the SST, there are two case 1 planets defined, both in a separate experiment. This is the same for all cases, thus four cases yield eight different planets.

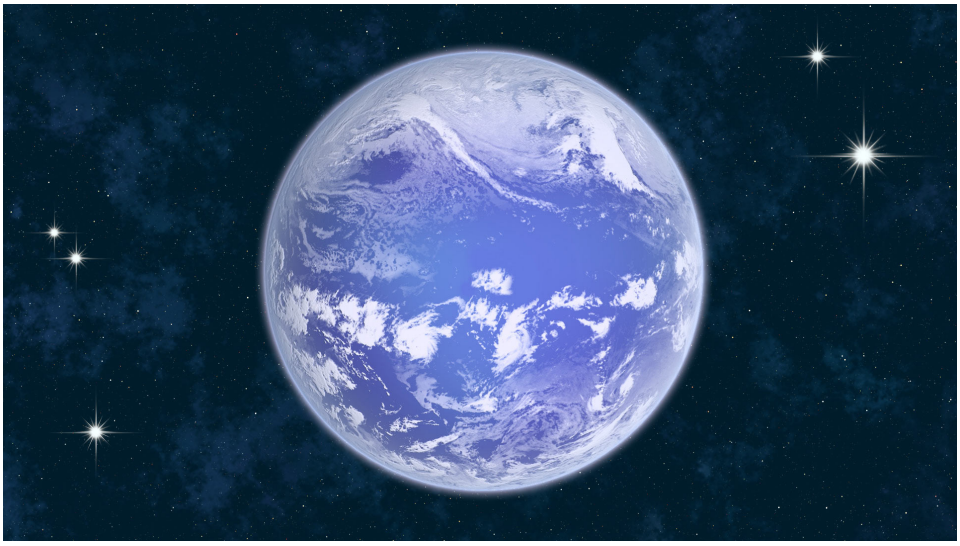

Figure 3.3: Self-made impression of a water planet.[1]

Case 2: Desert continent

In case 2, a continent is introduced. It is a round continent in the middle of the map. In SPEEDY, longitude-latitude grid of the planet is reduced to a grid of $96x48$ pixels, as described in Section 2.1. The radius R of the round continent is 20 pixels, with an origin in pixel (48,24), lying on the equator. Land is thus present in pixel (i,j) if it adheres to the following equation:

$$R^2 \leq (i-48)^2 + (j-24)^2 \tag{3.1}$$

As the map is a distorted representation of a globe, on a real planet this continent would actually be oval. All land used in the described cases has a temperature of 15^oC, so does this continent. It is completely dry and has an albedo of 30, based on the Sahara desert (assuming a similar colour of sand would be present on the exoplanet). The rest of the planet is still covered by an ocean, with the same properties as in case 1, including both ocean types, defining two different planets belonging to the same case.

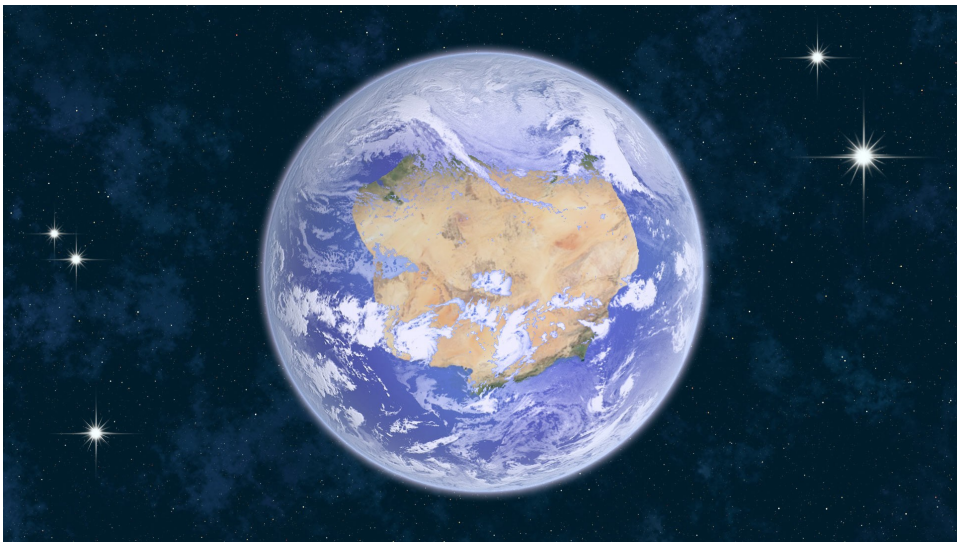

Figure 3.4: Self-made impression of a planet covered by oceans with a large dry oval continent in the middle, resembling a desert. The picture does not have smooth coasts, to represent a real planet. The model case is thus a simplification, justified by the global characterisation of our research.

[1]Based on http://cdn.sci-news.com/images/enlarge5/image_6365e-Water-World-Exoplanet.jpg, consulted on 31/03/2021

Case 3: Vegetated continent + polar ice
In case 3, the same continent as case 2 is present, but now completely covered with vegetation. As a result, the soil wetness is 50%. The albedo drops to 13, based on the Amazone rainforest.
Case 3 also has the addition of a band of ice at both poles. The band is 5 pixels wide and spreads over all longitudes, thus yielding a northern band of pixels (i,1 to 5) and a southern band of (i,43 to 48). This ice has a temperature of $-28^{o}C$ and an albedo of 50, based on the North pole in winter. An important note, on Earth, the North and South pole are completely different. The North pole consists of sea ice, while the South pole is land with snow on top. Here, the same configuration as the North pole is used for both polar ice caps.
Case 3 is a representation of a ”simplified Earth”, because it contains certain important features that define our habitable home planet.

Figure 3.5: Self-made impression of a planet covered by oceans with a large vegitated or wet oval continent in the middle, resembling a rainforest, and ice caps on the poles. Again, the picture does not have smooth coasts, to represent a real planet. Also the ice caps are not circular around the poles in the figure, but have an irregular, more natural shape.

Case 4: Vegetated continent
Case 4 also has the vegetated continent described in case 3, but no polar ice caps. This case was created as an intermediate between case 2 and 3, because two additions were done going from case 2 to 3 and an observed effect can as such not be attributed to either one addition. To keep the numbering of experiments consistent, this case is denoted as case 4 and not switched with case 3.

Control case: Earth
For validation purposes, all parameter variations described later on are also performed on Earth. Are the observed effects still present for a known case? With varied parameters, the planets created are not technically Earth anymore, but the trends can be traced back more easily than for unknown exoplanets. For example, we know what happens on Earth when it gets warmer, is that also represented in the results? Are the effects the same as for exoplanets? This case is not described in the results, but is used for tracking correctness of the simulations. A note beforehand: Earth is a far more complicated planet than the cases described above. As a consequence, it will be more difficult to extract the same effects from its results.

[2]https://climate.nasa.gov/news/2206/earth-from-space-15-amazing-things-in-15-years/, consulted on 31/03/2021

Figure 3.6: Self-made impression of a planet covered by oceans with a large vegitated or wet oval continent in the middle, resembling a rainforest. Similar to Figure 3.4, the picture does not have smooth coasts, to represent a real planet.

Figure 3.7: Our own planet Earth as seen from space.[2]

4

Parameter variations

Some planetary and stellar parameters influence the cloud pattern on the planet significantly, and some do not. To see what the influence of certain parameters is, some parameter variations are done. The same parameters are varied for all model cases described in Chapter 3. The parameters are varied between 50% and 150% of Earth's value. The parameters that are varied are the following:

- Rotation, including tidal lock as a special case
- Obliquity, including zero obliquity as a special case
- Orbital eccentricity
- Atmospheric surface pressure
- Incoming stellar flux
- Relative humidity thresholds

This list is selected from literature. Mainly their influence on deep clouds is studied. The way stratospheric clouds are implemented in SPEEDY imposes a minimum cloud cover above land. This easily leads to the false conclusion that if no stratospheric clouds are present, no land is present. To avoid this, stratospheric clouds are usually not taken into account in the analysis, only if their analysis has a clear added value. Other parameters such as temperature, wind and pressure vertical velocity (the vertical movement of air in the atmosphere) are studied to aid in drawing conclusions on the cloud pattern.

Some parameter-variations were combined, but the effects do not seem to add up as expected. As SPEEDY is a rather simplified model, not all parameters are as tied to each other as they really are on Earth. For example, planetary rotation and stellar flux are connected through night and day, but this diurnal variation is not incorporated in SPEEDY. The results discussed below are thus solely the consequence of the single parameter variation, and are not entangled with other parameters.
It should be noted that all figures are titled with an experiment number. For every run in SPEEDY, an experiment number needs to be specified, which is linked to input parameters. In Appendix B a list can be found, explaining the parameter settings of each experiment (or experiment series). Lastly, a map of Earth is printed on every figure. The displayed continents are not part of the experiment and are not used in any way to generate the results shown on the plot. They are simply left for easy visualisation and orientation on the planet.

4.1. A note on stability and the limits of the implemented parametrisations and approximations

Based on the way SPEEDY is built up, for certain parameter combinations it can get unstable. For example, the gradients in the output parameters get nearly infinitive, causing the Eddy kinetic energy

to raise incredible high values. This effect is demonstrated in Figure 4.1, which shows the deep cloud cover for an ocean planet without temperature gradient, at half insolation (in this experiment the stellar flux is set to 50% of the solar flux on Earth, based on parameter variations explained hereafter). The results of unstable experiments are not taken into account for drawing conclusions, but they can be relevant in understanding how everything works.

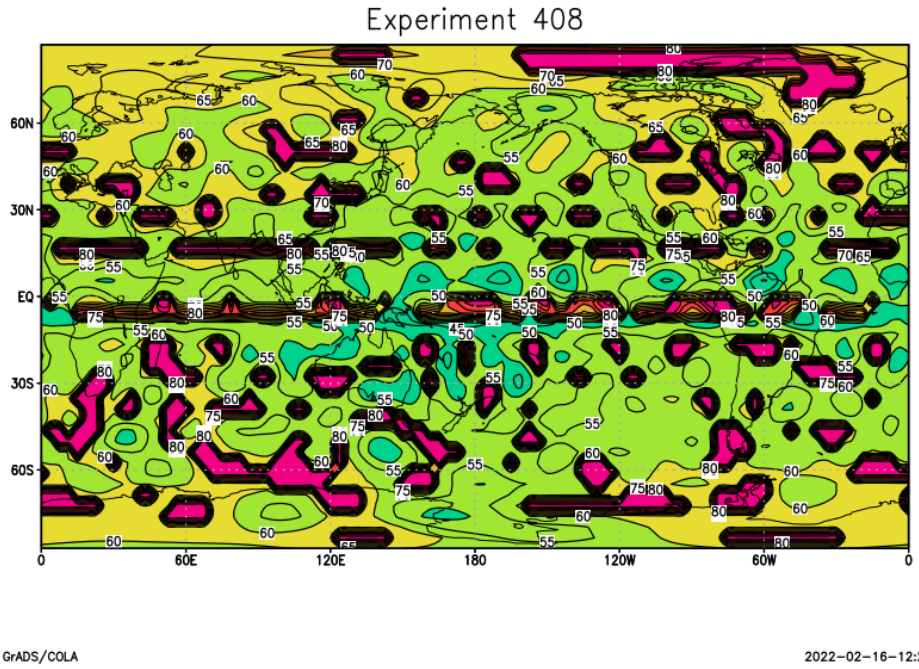

Figure 4.1: Deep cloud cover over an ocean planet for 50% insolation. This experiment only runs for one month propagation time. The red/pink colour shows high values, close to 100% cloud cover, while blue colours show low values, close to 0% cloud cover. In between, green and yellow show intermediate values, around 50%. This is a monthly average, hence no cloud cover or 100% cloud cover nearly never occurs.

As described in Section 3.2, for each case two types of oceans are investigated: one with constant temperature and one with a SST gradient. To define the propagation length of the experiments, an optimum needs to be found between convergence or stability of the results, and computational time. The optima are defined by trial and error. For the constant-temperature ocean, the propagation time is set to 3 months, when a (temporarily) stable situation is reached, but before divergence of the atmospheric energy. For the gradient-temperature ocean, the propagation time is set to 3 years, well after convergence to a stable situation was reached. An experiment in SPEEDY for 3 years takes about 20 minutes cpu-time.

4.2. Results

This section presents the results of the parameter variations on the cases described in Section 3.2. For every parameter variation, maps can be made from various output parameters. The map used the most in this thesis for comparison of the described cases and parameter variations is the deep cloud cover, as it represents the cloud pattern on which the effects are studied. These maps all have the same generalised colour scale. Often the temperature is looked at as well, to aid in explaining the effects seen in cloud cover. Here the colour scale is not generalised and colours can vary per temperature range. Lastly, maps comprising a wind vector as arrow in every pixel and a colour scale representing the pressure vertical velocity are made, to study convection.
Furthermore, the more complexity is introduced in the surface of the planet, such as a continent or polar ice, the less flexible the SPEEDY run becomes, e.g. the less parameter-combinations are stable. On top of that, for a complex planetary surface, the clouds seem to be more chaotic, which makes it

hard to identify relations. Therefore the results mostly focus on case 1, the water planet.
A general remark, which can be seen on all simulated planets as well as on Earth: The clouds can appear in different patterns, but areas of more and less cloud cover generally alternate. This is the natural local convection effect of high-pressure and low-pressure areas. This also translates in other parameters, such as the wind vector and temperature. The wind blows from a high-pressure area towards a low-pressure area, taking the clouds along. As such, a high-pressure area has a clear sky, why a low-pressure area is covered by clouds. This effect is shown in Figure 4.2. This results from a high-pressure area having a low temperature and a low-pressure area having a high temperature. From the pressure vertical velocity, it can be seen that in low-pressure areas, the air descends (green/blue colour), while in high-pressure areas, the air rises (orange/red colour). This can have many explanations as not all processes are studied: temperature variations over altitude, precipitation releases energy in the air, cloud feedback can be active, etc. Lastly, the precipitation follows nicely the cloud patterns.

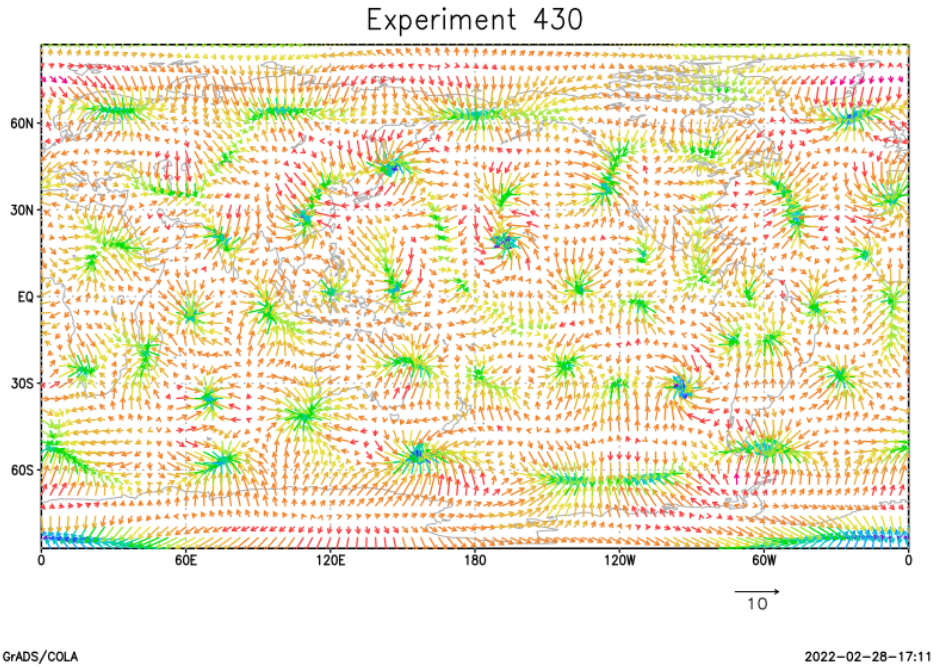

Figure 4.2: Wind vectors coloured by pressure vertical velocity, on an ocean planet without gradient. The vectors are scaled with a unit vector stated below the figure, the colours range from a downward vertical velocity in the blue to an upward vertical velocity in the red. Planetary rotation is zero, but stellar flux is equal to Earth's. This figure illustrates the high-pressure and low-pressure areas pattern.

The results shown in this section are based on monthly averages, to limit short-term variations and clearly see long-term effects. A day defined in a SPEEDY experiment equals an Earthly day of 24 hours. As we do not know the rotational period of an exoplanet a priori, this 'day' is kept as time span and used consistently throughout the experiments and intercomparisons.

4.2.1. Default ocean planet

The default ocean planet (default meaning Earth's value for all parameters) is given as a basis to compare the results from the parameter variations to. Case 1, the water planet without continents, is selected, because it provides the most clear cloud patterns. The studied output is the cloud cover, temperature and wind. The resulting maps for the default planet are shown in Figures 4.3-4.5 and 4.6-4.8, for the planet with and without temperature gradient in the ocean respectively.

In these figures, the influence of the sea surface temperature gradient from a low temperature on the poles to a high temperature on the equator, together with some general effects can be seen. Ob-

viously, temperature on the gradient-planet shows more variations than on the constant-planet. The gradient-planet has an average temperature of 274.0K, while the constant-planet has an average temperature of 265.9K. From these numbers it can be derived that for a constant SST, the temperature is lower than the pre-set value, which means the planet naturally tends to cool down to a lower equilibrium temperature. This observation confirms that a planet with gradient is more (initially) stable, than without gradient. The equator receives more incoming flux than the poles, thus an ocean which has the same temperature everywhere is illogical, explaining this stability difference.
The cloud cover follows the pattern of temperature: there are more variations on a planet with gradient. The average cloud cover percentage of both planets remains similar: 64.9% for a planet without gradient and 60.8% for a planet with gradient. This small difference can be due to seasonal variations or other temporary effects.
Visible in both instances, although more extensively in the gradient-one, is the convection in Hadley cells. Around the equator, there is a more active zone, and the clouds form longitudinal bands. This effect for both planets is studied in more detail in Chapter 5, as an effect of rotation.
As the gradient-planet has a more dynamic atmosphere as explained before, the wind and vertical velocities will also be higher. This effect can be seen in the figures: the reference vector in Figure 4.5 has a value of 6m/s, while in Figure 4.8, it is 10m/s. Usually, the value is assumed to lie around 7m/s, which is close.

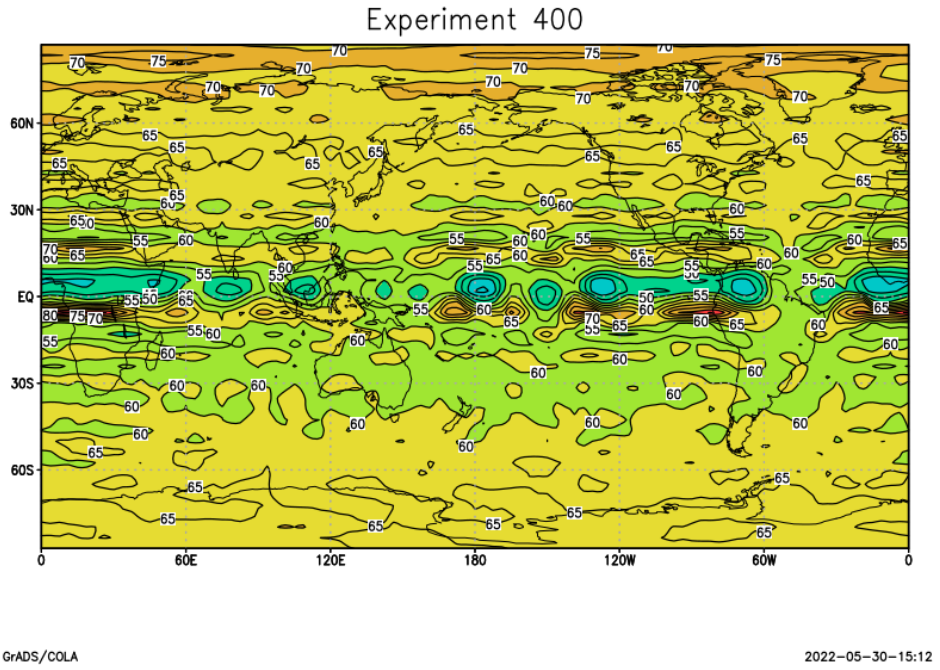

Figure 4.3: Deep cloud cover over an ocean planet with constant SST, case 1, with parameter settings at 100%, equal to Earth. This a monthly average after 3 years of simulation. The colour scale used is the same in all cloud cover maps and ranges from blue/purple at 0% cloud cover to red/pink at 100%.

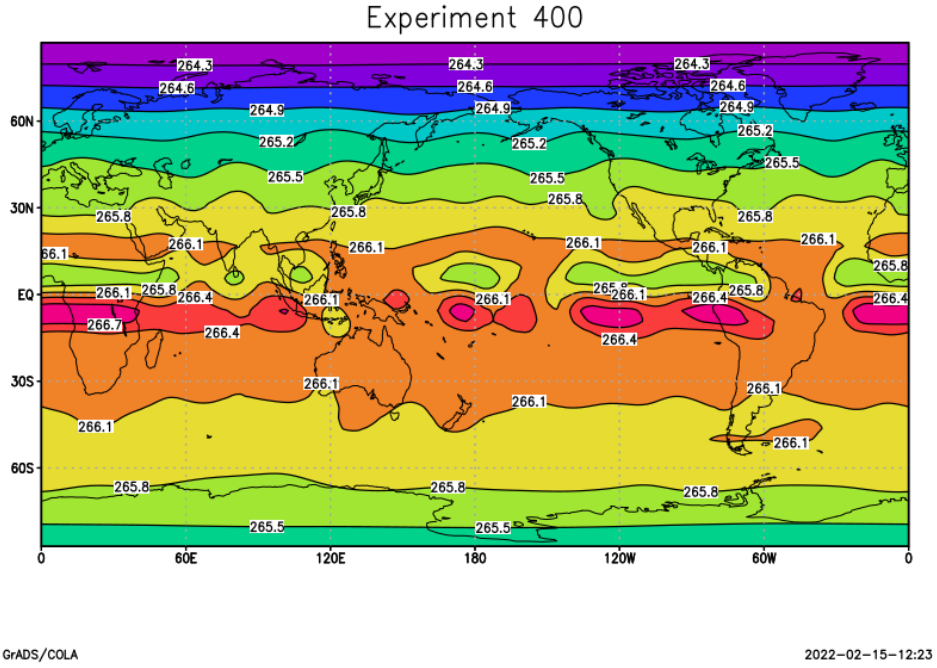

Figure 4.4: Temperature on an ocean planet with constant SST, case 1, with parameter settings at 100%, equal to Earth. This is the same experiment as Figure 4.3. The colour scale in temperature plots can vary, as the values can also vary significantly over experiments. Nevertheless, blue/purple denotes a low temperature and red/pink denotes a high temperature.

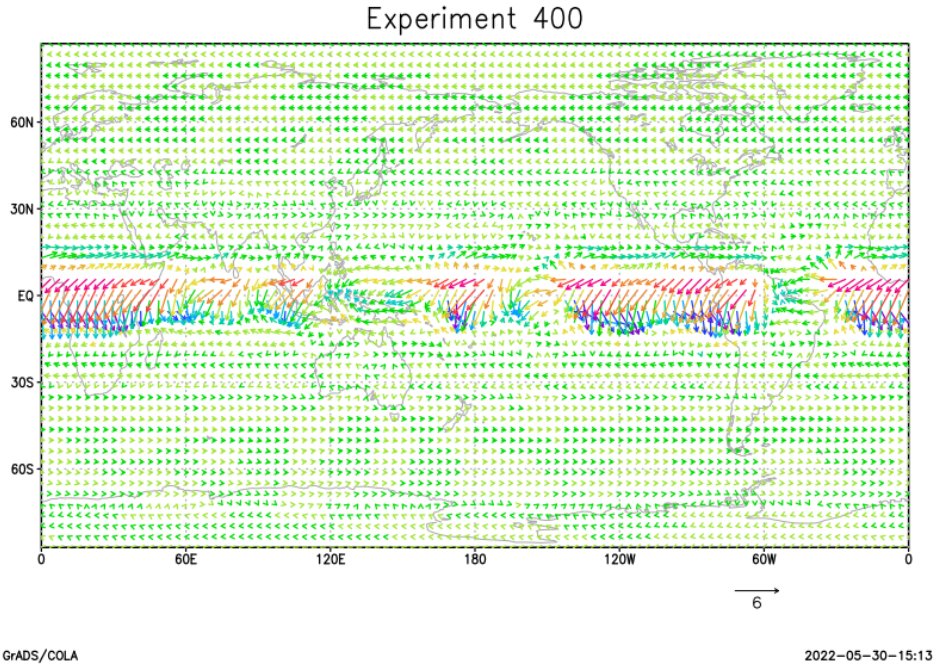

Figure 4.5: Wind vectors and pressure vertical velocity (colour scale) over an ocean planet with constant SST, case 1, with parameter settings at 100%, equal to Earth. The wind vectors are referenced by a unit vector in the right corner below, which denotes the scale of the vectors in m/s. The colours of the arrows are defined by the pressure vertical velocity at that location, again ranging from low values in the blue/purple and high values in the red/pink.

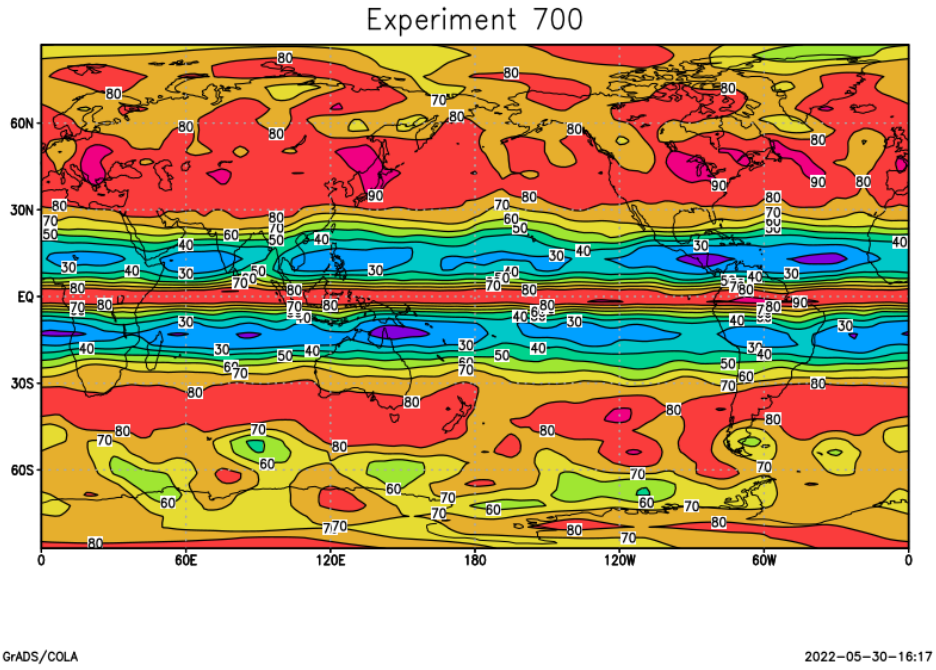

Figure 4.6: Deep cloud cover over an ocean planet with gradient in SST. The figure has the same properties as Figure 4.3, with the introduction of a SST gradient.

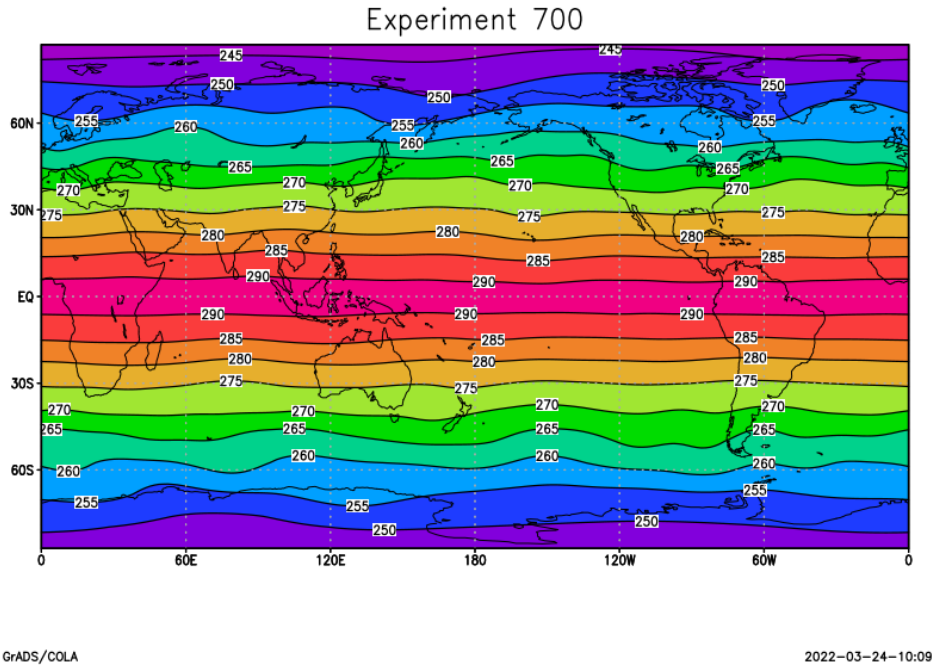

Figure 4.7: Temperature on an ocean planet with gradient in SST. The figure has the same properties as Figure 4.4, with the introduction of a SST gradient.

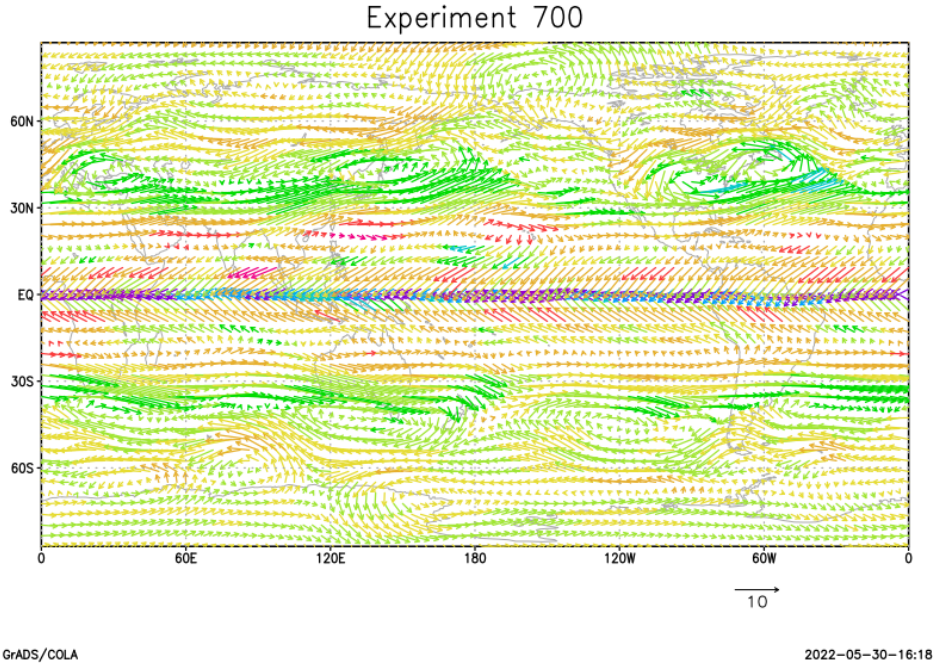

Figure 4.8: Wind vectors and pressure vertical velocity (colour scale) over an ocean planet with gradient in SST. The figure has the same properties as Figure 4.5, with the introduction of a SST gradient.

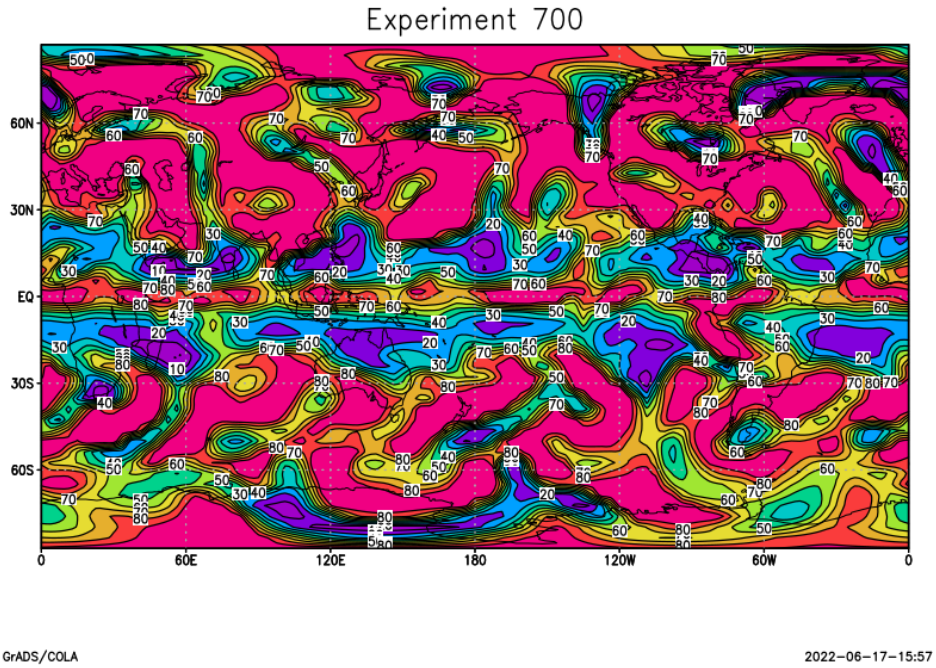

Figure 4.9: Deep cloud cover over an ocean planet with gradient in SST (case 1, parameter settings 100%), on a daily basis. The day shown is the last day of three years simulation, and hence the last day of the month on which the monthly output is based.

4.2.2. Daily output

As mentioned, the presented results are based on monthly output from SPEEDY simulations. Nevertheless, SPEEDY is also able to provide daily output. This output is relevant to study short-term effects and to see how the dynamics of the clouds behave. These results will also be used for the signal calculations. In this chapter, the daily output is not analysed further, but it is worthwhile showing. An example of a daily cloud pattern can hence be found in Figure 4.9, for the default water planet with gradient after three years of simulation. As can be seen, the atmosphere forms patchy clouds, resembling Earth's cloud cover.

4.2.3. Parameter variations

Per parameter that is varied, the resulting cloud maps and possibly other output is shown and discussed. The effects of the parameter values on the planets climate are addressed and explained.

Rotation

For a rotating planet, the cloud pattern forms bands, as can be derived from Figure 4.10. These bands get more narrow when the planet rotates faster. This can also be seen on an ocean planet with gradient, in Figure 4.11. As this effect is mostly present above an ocean surface, the bands in the cloud pattern could be an indicator for surface water. Therefore, this effect is studied in more detail in Chapter 5.
Pressure vertical velocity is a measure for the vertical movement of the air in the atmosphere. Smaller bands pair with a larger pressure vertical velocity, as equal air masses are moved in smaller convection cells. The wind velocity remains generally unchanged over rotational speed. Also the temperature remains unaffected.

The local wind vector is a good indicator of the dynamics of the atmosphere. In Figure 4.12, this wind vector is shown for both 50% and 150% rotational speed. The magnitude of the wind remains unaffected by rotational speed, as it is unit 10 here, as it was for 100% rotational speed in Figure 4.8. Next the mutual differences on a large scale are touched upon. From the figures, it can be seen that at a smaller rotational speed, the movement of the air is fairly consistent over the planet, the atmosphere seems to make one big movement. At a higher rotational speed, the convection is larger: the vertical velocity is higher and the horizontal atmospheric movements are on a much smaller scale. The 100% rotational speed case lies nicely inbetween. Lastly, it should be noted that for all instances, the equator is the most dynamic zone, which follows from Hadley cell convection. From these observations, it can be concluded that the higher the rotational speed, the more dynamic the atmosphere becomes. At high rotation, the conditions of a location on the planet vary quickly all the time.

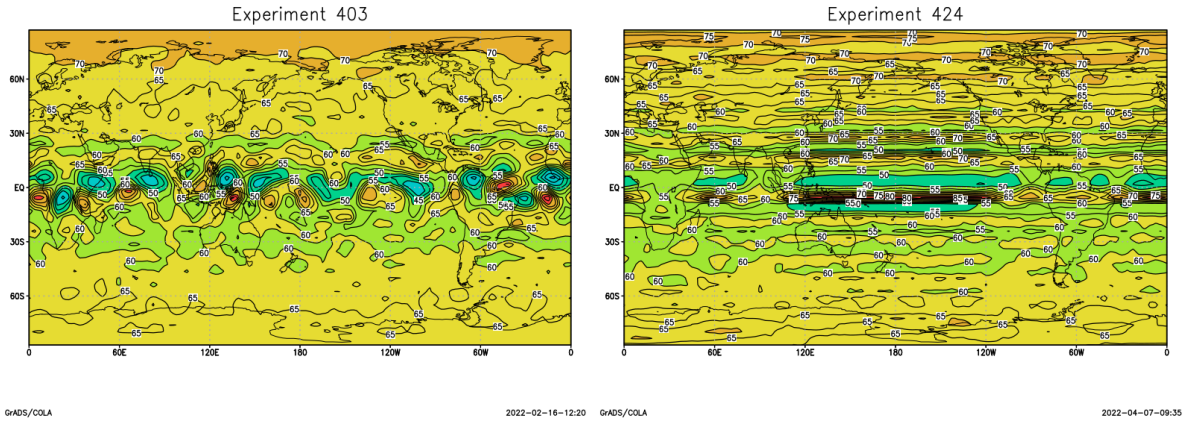

Figure 4.10: Deep cloud cover on ocean planet without gradient, case 1, at 50% rotational speed on the left and 150% rotational speed on the right. The same colour scale as in Figure 4.3 has been used.

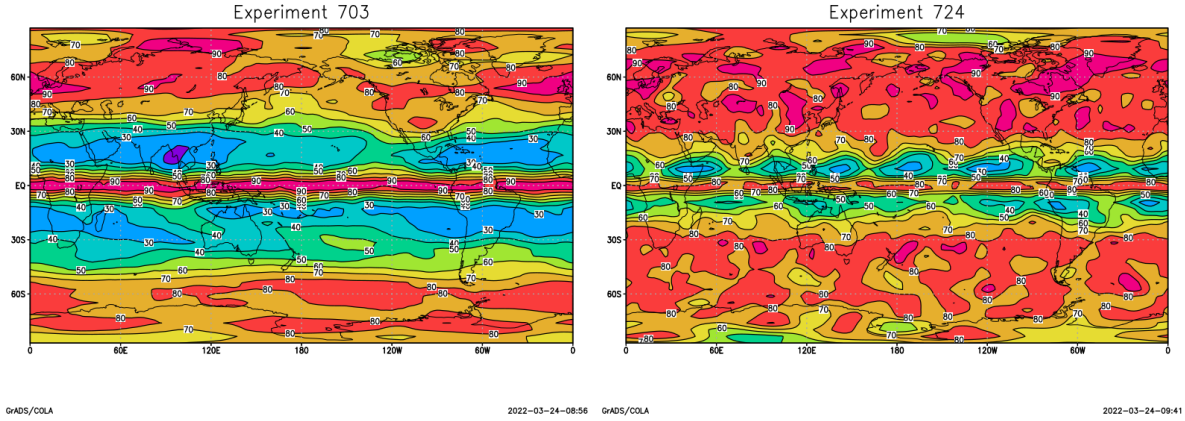

Figure 4.11: Deep cloud cover on ocean planet with gradient, case 1, at 50% rotational speed on the left and 150% rotational speed on the right. The same colour scale as in Figure 4.3 has been used. This figure can be compared to Figure 4.10, as the introduction of a SST gradient is the only difference.

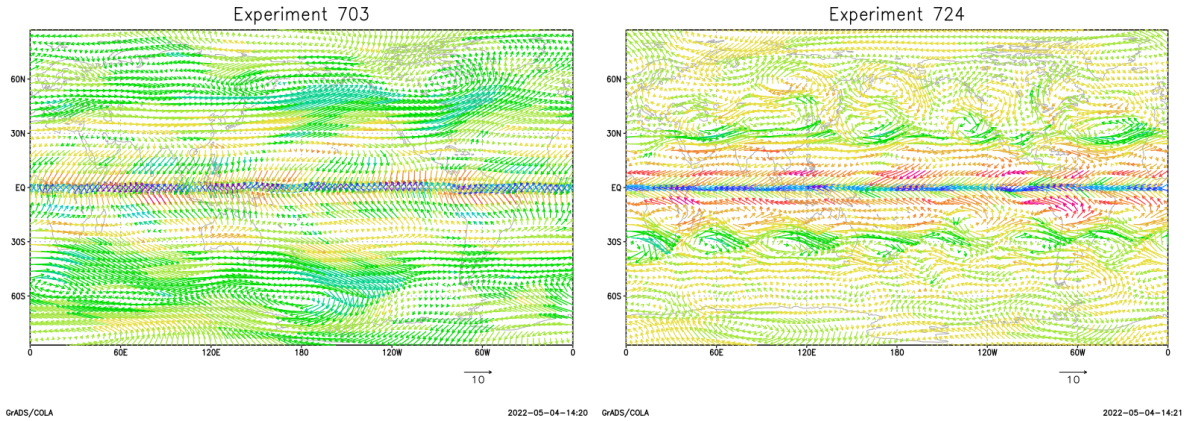

Figure 4.12: Horizontal wind vector (arrows, with scale defined in the lower right corner) and pressure vertical velocity (colour scale) on ocean planet with gradient at 50% rotational speed on the left, and 150% rotational speed on the right.

Obliquity

Also the obliquity is varied from 50% to 150% compared to Earth's obliquity. At first sight, obliquity does not seem to have a large influence on the cloud pattern. From literature (Colose et al., 2019), it was concluded that highly oblique planets tend to have higher average temperatures. This phenomenon is confirmed in the parameter variation in Figure 4.14: it can be observed that the temperature on the equator remains almost the same, but this warmth is spread out more over the summer-hemisphere when obliquity increases. As the difference in temperature over the studied obliquity range is small (it is between 0 and 10 degrees) the influence on the cloud pattern will remain limited. At an oblique planet, seasons can be observed. Generally, in winter there are more clouds than in summer. As a larger obliquity is induced, the seasons become stronger, as can be observed in Figure 4.13. This effect diminishes when a gradient is introduced in the sea surface temperature, because the effect of the stellar radiation is decreased.

As a special case, zero obliquity is studied as well, shown in Figure 4.15. The clouds on the planet are nicely symmetrical, which is a confirmation that everything works as it should.

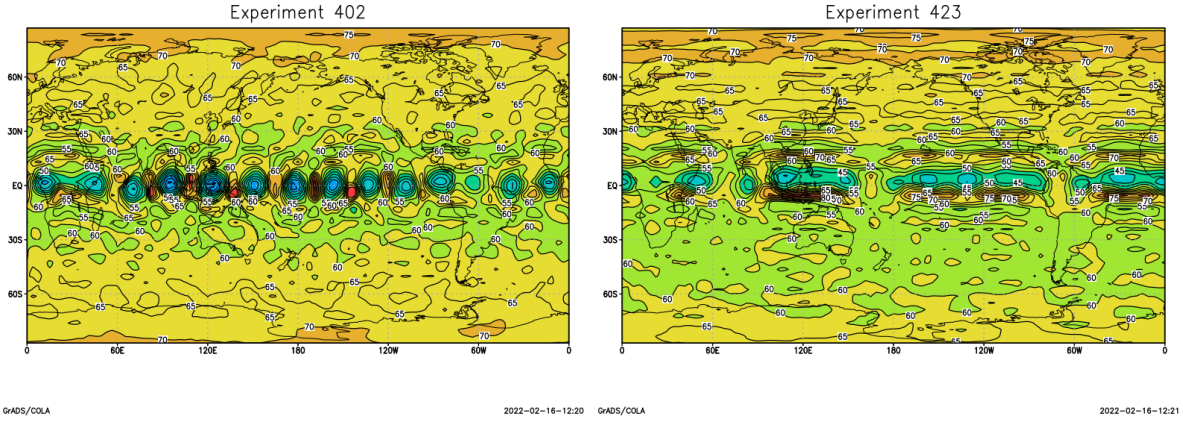

Figure 4.13: Deep cloud cover on ocean planet without gradient, case 1, at 50% obliquity on the left and 150% obliquity on the right.

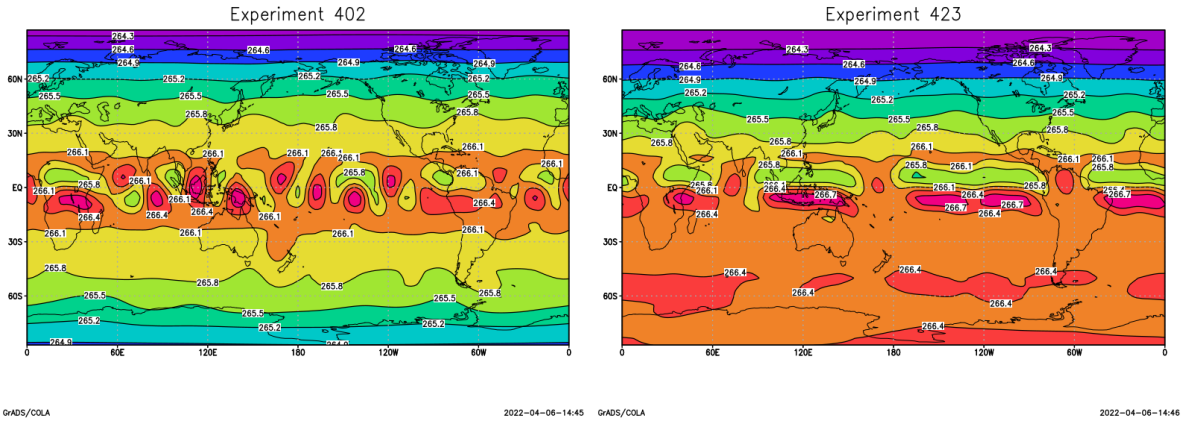

Figure 4.14: Temperature on ocean planet without gradient, case 1, at 50% obliquity on the left and 150% obliquity on the right.

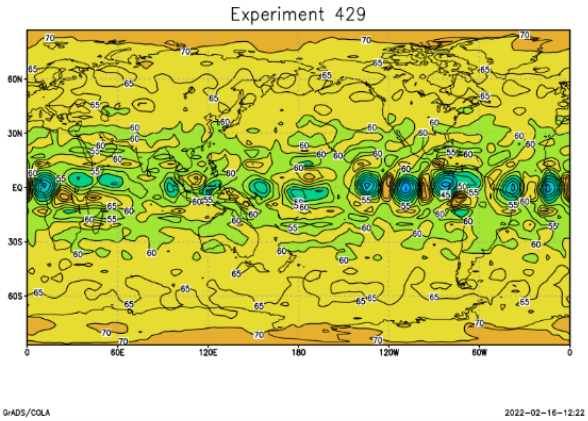

Figure 4.15: Deep cloud cover on ocean planet without gradient, case 1, at zero obliquity. This figure can be compared to Figure 4.13, which compares obliquity settings.

Orbital eccentricity

Regarding variation of eccentricity, no influence on the cloud pattern is identified. Because of the

decoupling of parameters described in Section 2.2, the stellar flux is not adapted according to the eccentricity. This parameter will therefore not be discussed further.

Atmospheric surface pressure

Changing the surface pressure has a direct influence on cloud formation in the atmosphere. For both a higher and lower pressure than on Earth, more clouds can be observed, as shown in Figure 4.16. Cloud formation, dynamics and cover go together with convection processes, which are described further on. The cloud cover lies above 80%, for a planet with constant SST and 150% surface pressure. For a constant-SST planet with 50% surface pressure, the average even rises above 90%. On a planet with gradient in SST, the same increase in cloud cover for a lower pressure can be seen, although at a slightly lower average percentage. A higher surface pressure, this planet becomes unstable, so no conclusions can be drawn based on these results.

It should be noted that the clouds for a lower pressure are higher in the atmosphere, and clouds for a higher pressure are as low in the atmosphere as at normal pressure (here it should be taken into account that SPEEDY does not have the exact altitude of the clouds as output, but only a cloud cover in a certain range of altitude). In a thicker atmosphere, for a higher pressure the critical vapour density is more easily reached. Regarding a thinner atmosphere, the explanation is bit more complicated. There is equally as much evaporation from the ocean surface (or even more as the pressure is lower), as the parameters are uncoupled and hence other properties are not influenced. However, the mixing ratio of water vapour as compared to other gases in the atmosphere is higher, to make sure the pressure is lower. As a consequence, there is a relatively larger amount of water vapour present in the atmosphere, which allows for forming more (water) clouds. This effect should be studied with another climate model to be sure it is not simply a consequence of SPEEDY's parametrisation.

It should be noted that the increase in cloud cover is more present above an ocean than above land, which makes it easier to identify oceans. It is desirable that these effects are not present above land, otherwise one could conclude false-positively that if more clouds are present, an ocean is observed. Nevertheless, for a large increase/decrease in pressure, the effect captures land as well, not entirely excluding the risk. In addition, a lower pressure counteracts the band-formation effect from rotation, which makes it harder to detect oceans again.

For a difference in surface pressure, a change in convection can be seen. This is shown in Figure 4.17, comparing 50% and 150% surface pressure. As can be seen from the scale of the arrows, the wind velocity in a thin atmosphere can be about 17 times higher than in an Earth-atmosphere and even 33 times higher than in a thick atmosphere. The explanation is rather simple: A thinner atmosphere requires less energy to be moved than a thicker one, hence allowing for more dynamic convection. One might attribute this very high wind velocity to the instability of the atmosphere, but even in cases that have been stable for a long time with a thin atmosphere these high velocities can be observed.

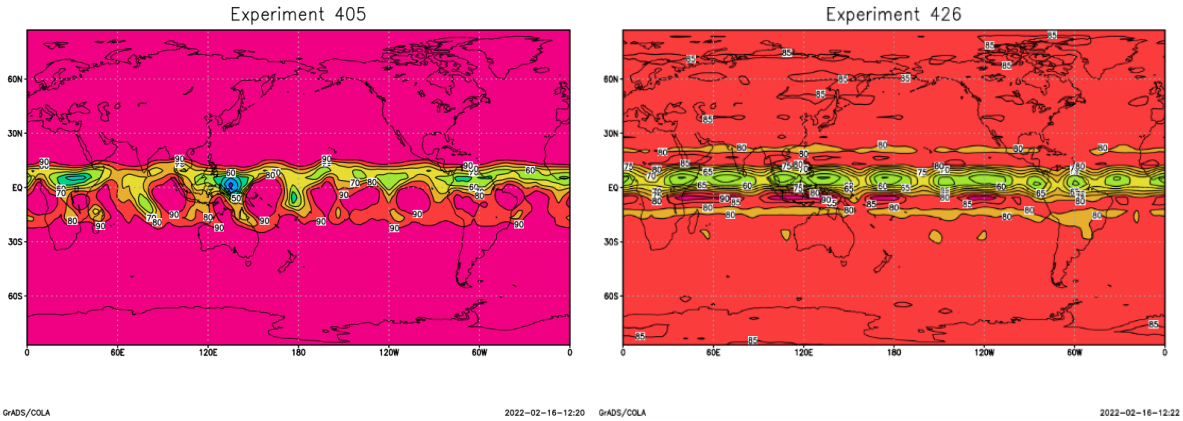

Figure 4.16: Deep cloud cover on ocean planet without gradient, case 1, at 50% atmospheric surface pressure on the left and 150% atmospheric surface pressure on the right.

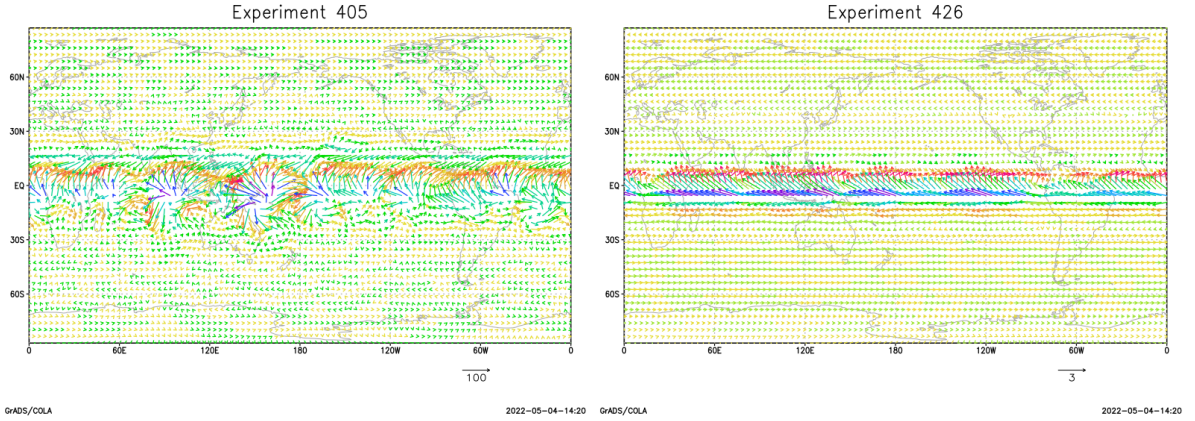

Figure 4.17: Horizontal wind vector (arrows, with scale defined in the lower right corner) and pressure vertical velocity (colour scale) on ocean planet with gradient at 50% atmospheric surface pressure on the left, and 150% atmospheric surface pressure on the right.

Surface pressure also has a large influence on temperature. A planet (both with and without SST gradient) with a lower surface pressure, can have temperatures easily above 300K. This could be the result of the atmosphere being heated up more by stellar radiation as it is thinner. In experiment 426 (higher surface pressure, no gradient in SST), the temperature drops to only 240K. This could be due to the extensive cloud cover, which causes a cool-down effect through feedback via reflection. It could also be due to an unstable environment, because also the planet with SST gradient becomes unstable at higher surface pressure.
Lastly, it should be noted that the described effects are often counter-intuitive, or data lacks to be able to draw conclusions. Therefore the influence of surface pressure on planetary atmospheres should be studied more deeply, perhaps with another more detailed climate model than SPEEDY.

Incoming stellar flux
The stellar flux is a rather complicated parameter in the simulations. A lower flux than on Earth causes the temperature in the SPEEDY simulation to get in a downward spiral and makes sure the planet gets too cold to sustain a gaseous atmosphere. This instability is represented in cloud cover in Figure 4.18 on the left. A higher stellar flux unchains some feedback reactions. The star heats the surface, causing more water to evaporate from the ocean's surface, making sure the atmosphere gets humid. The hot air rises faster to colder regions, where it condensates into more clouds. This effect is shown in Figure 4.18 on the right and mostly present in the hemisphere where it is summer. Because of the increase in temperature, the air also rises more persistently, causing the clouds to form at higher altitudes. This effect is most existent around the equator. This follows from the Hadley cell convection, where air around the equator rises. On top of that, the stellar flux increase mostly effects the equatorial region. Warm air can hold more water gas, causing the relative humidity to decrease and less clouds to form. Netto, this effect is not present in the results, but it should not be forgotten.
As a consequence, for a higher stellar flux, the seasons become more extreme. This effect is shown in temperature in figure 4.19. A clear dichotomy between the northern and southern hemisphere in summer and winter can be seen.

Relative humidity thresholds
Setting the relative humidity thresholds, as how they are defined in SPEEDY, causes the following effects: if the threshold is set lower, less clouds are formed, if the threshold is set higher, more clouds are present.

The performed parameter analysis brought a lot of clarity on answering the research questions. The conclusions regarding the relation between cloud patterns and surface water, drawn from the variations, can be found in Chapter 7.

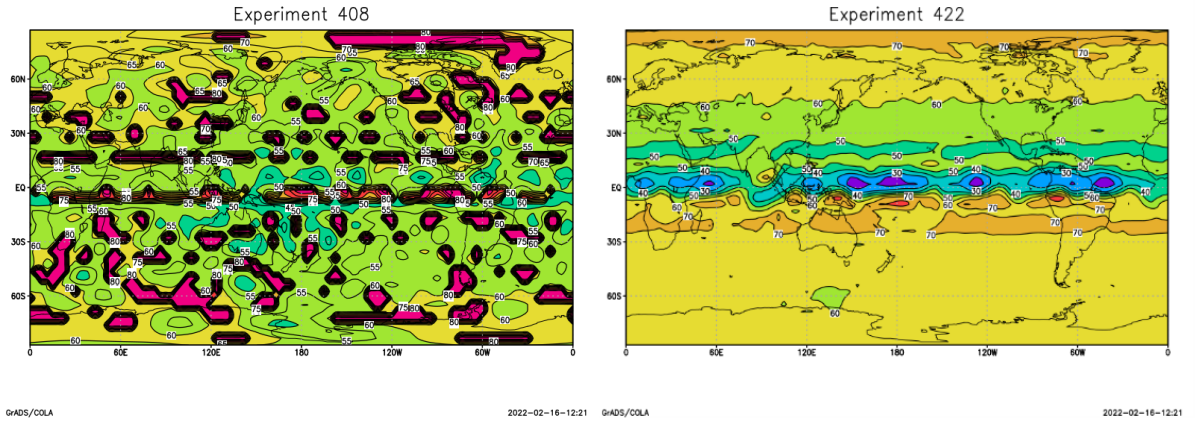

Figure 4.18: Deep cloud cover on ocean planet without gradient, case 1, at 75% incoming stellar flux on the left and 150% incoming stellar flux on the right. The experiment at 50% stellar flux could not be used here as it was unstable.

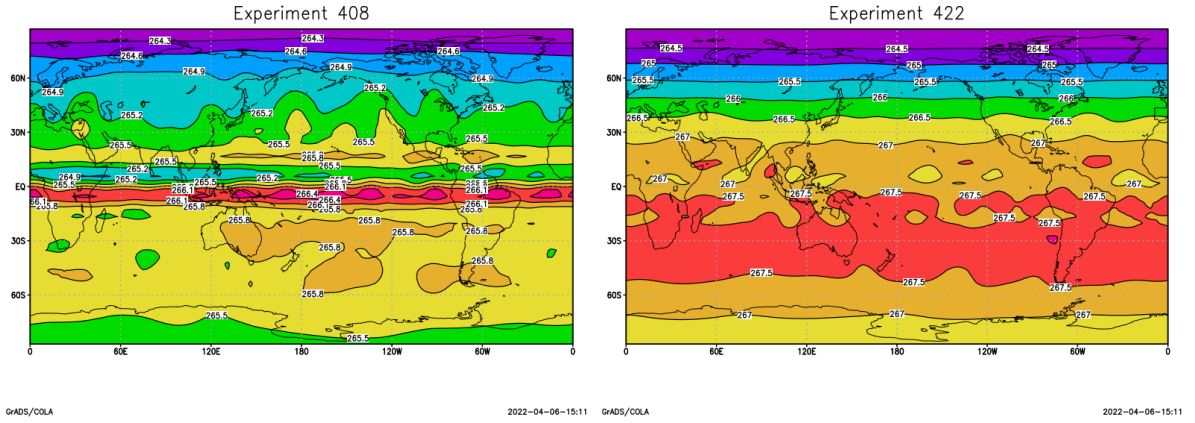

Figure 4.19: Temperature on ocean planet without gradient, case 1, at 75% incoming stellar flux on the left and 150% incoming stellar flux on the right. The experiment at 50% stellar flux could not be used here as it was unstable.
Note: The colours in the plots do not correspond to each other, the same colour does not necessarily represent the same value in both plots. The plots use a different colour scale because the variations in the left plot are smaller than in the right plot (the seasons become more extreme, as explained in the text). This is only the case in this figure on temperature, not Figure 4.18 on cloud cover.

4.2.4. Other cases: the influence of land

The previous section focused on case 1, the ocean planet, but case 2, 3 and 4 which include continents, cannot be left unanalysed. As mentioned before, a continent introduces complexity in the model, which makes it harder to recognise the effects from the parameter variations. Therefore this section will focus on describing the general differences in cloud cover, temperature and convection for the cases, rather than focusing on the parameter variations of these cases itself. As the cases become more complex, more and more experiments become unstable and thus unusable, which made this focus shift a logical step. Because of this instability issue, only planets with a temperature gradient are discussed here.

A generally accepted concept in literature is the more water, the more clouds. There are more clouds above an ocean than above a continent, even when it is vegetated and wet. The default experiment's cloud cover for every case is shown in Figures 4.20, 4.21 and 4.22.

Case 2

Case 2 comprises a desert continent of 15 degrees and an albedo of 0.3, in both the gradient and gradient-less SST ocean. The cloud cover over a desert continent is very limited. The cloud pattern

over the ocean is clearly disrupted by the land. The temperature, as shown in Figure 4.20 on the top right, is more extreme on land than over the ocean, which is similar to Earth. Because of the clear sky, the land can become warmer and because of the warmth, the land stays clear. From the temperature over land, it can be clearly seen that these results are taken at a time where the northern hemisphere is in winter and the southern hemisphere is in summer, which in this case is December. The boundaries between land and ocean can be derived from the convection map in Figure 4.20 on the bottom as well. When air bumps against a coastline, it will turn around. This dynamic enhances convection, making the wind blow harder.
In general, the dichotomy between land and ocean results in clear variations in atmospheric parameters. Regarding the cloud pattern (Figure 4.20 on the top left), these differences make it easier to distinct oceans from land.

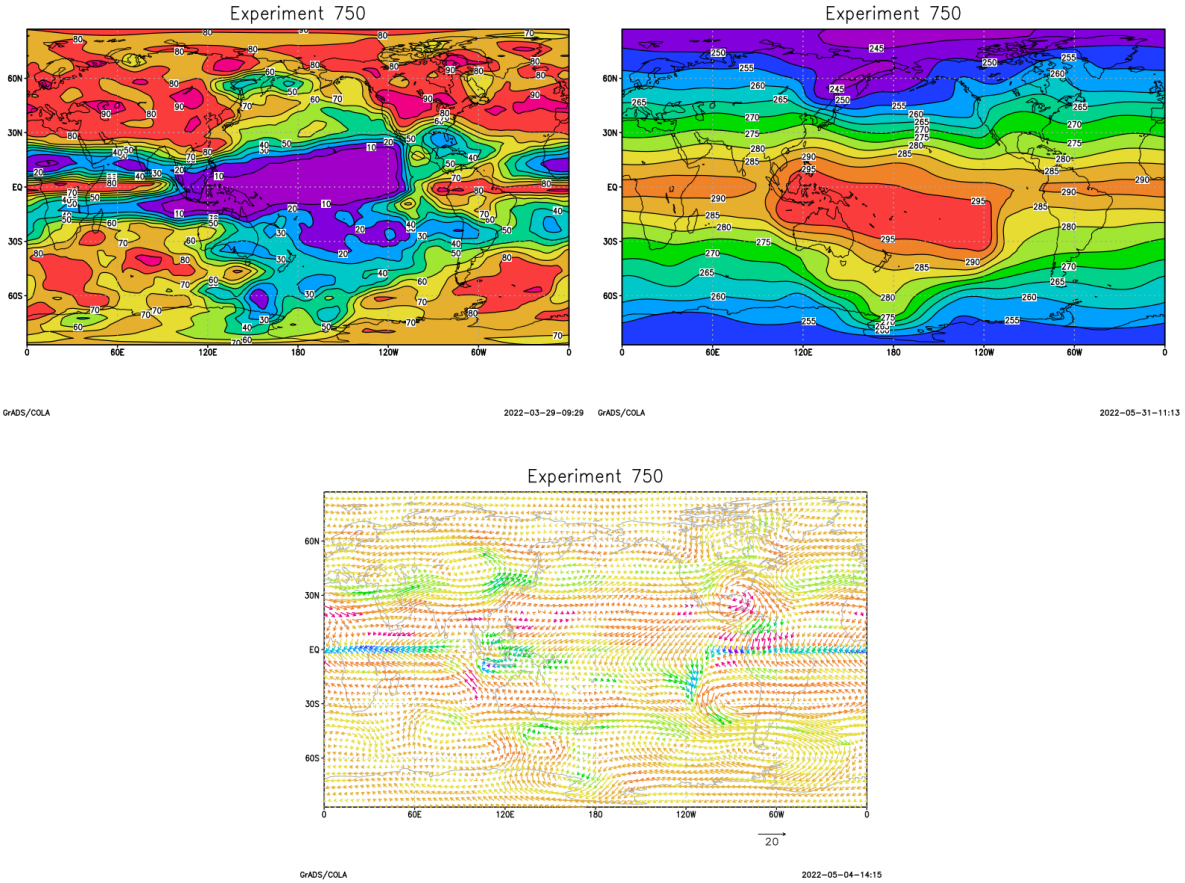

Figure 4.20: Case 2, a planet with desert continent, at 100% parameter settings. The figure on the top left shows deep cloud cover, the figure on the top right shows temperature and the figure on the bottom shows wind vectors coloured by pressure vertical velocity, to characterise convection.

Case 4

Case 4 comprises a continent of the same size and temperature and in the same oceans as case 2, but it is completely covered by vegetation with a soil wetness of 50% and an albedo of 0.13. Generally, vegetation on the continent does not have a large effect on the studied output parameters in Figure 4.21. This suggests that the effects described for case 2 are due to the presence of land, rather than the land being dry. The same observations thus hold, although to a less extent. The slightly less pronounced dichotomy mediates the effects a bit. The temperature is for example slightly higher at the North pole and slightly lower in the tropics. Also the convection is slightly less, although the atmosphere is still dynamic and the turnaround effect at the coastlines is clearly present.
Because of this mediation, the band-like cloud pattern from above oceans can break through and can be seen above land as well. On the one hand it is nice to see the cloud pattern get a little more structured,

but on the other hand makes this it harder to characterise the planet's surface from clouds. When a large continental structure is present such as on this model planet, the convection could possibly aid in finding it. Nevertheless when the land fractures are smaller, the convection pattern can be ascribed to high- and low-pressure areas, remaining unnoticed.

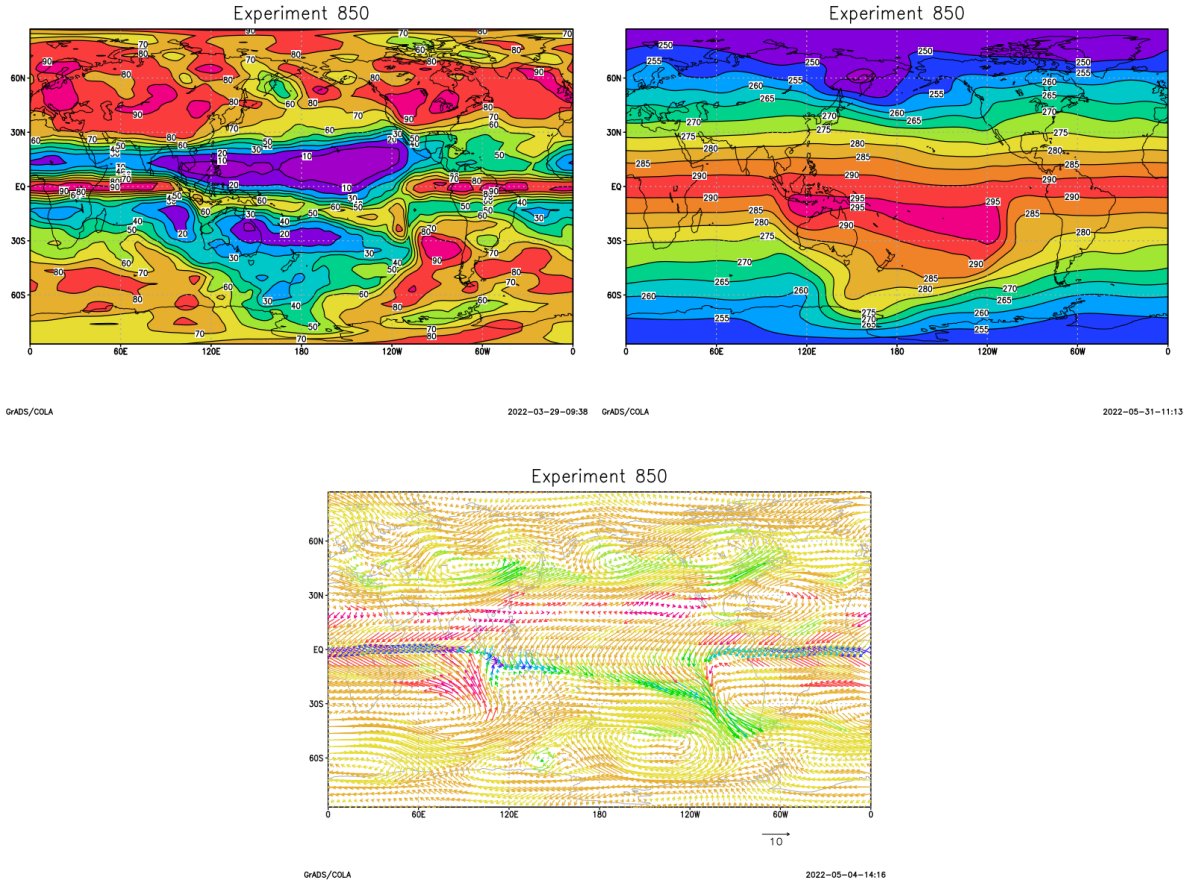

Figure 4.21: Case 4, a planet with vegetated continent, at 100% parameter settings. The figure on the top left shows deep cloud cover, the figure on the top right shows temperature and the figure on the bottom shows wind vectors coloured by pressure vertical velocity, to characterise convection.

Case 3

Case 3 is the same as case 4, with the addition of polar ice caps. In Section 2.2 was explained that in SPEEDY the ocean does not freeze nor melt automatically from temperature differences. This means that the fraction of sea ice defined at the start of the simulation remains to have its properties until the end, and so does the ocean. The way sea ice is implemented in SPEEDY, it does not affect many parameters a priori. For example, the difference in evaporation of ice and water is small, and within sea ice there still seems to be heat transfer. The depth of sea ice is undefined in SPEEDY's source code, so that might play a role in this. Other parameters, such as temperature and albedo, which are set by hand, are very different for ice and water. The results the model provides, shown in Figure 4.22, are very different from case 4, which is remarkable, taking into account the small contribution from ice to the model dynamics in SPEEDY. It could be attributed to the large difference in albedo, but in case 2 we did not see such a large difference coming from albedo alone. As after three years of simulation, the model is still stable, this cannot be a numerical effect and it should have a physical explanation.
There are a lot more clouds, but the band pattern remains visible around the equator. The temperature effects described in the other cases are still present, but in general the planet is a lot warmer, up to 25 degrees in both polar and equatorial regions. This observation is contradictory to the presence of ice. The convection is extremely high, especially around the equator. The turnaround effect at the coastlines nevertheless remains present. What causes these results remains unexplained at the

moment and more research is needed in where the large difference between case 4 and case 3 comes from.

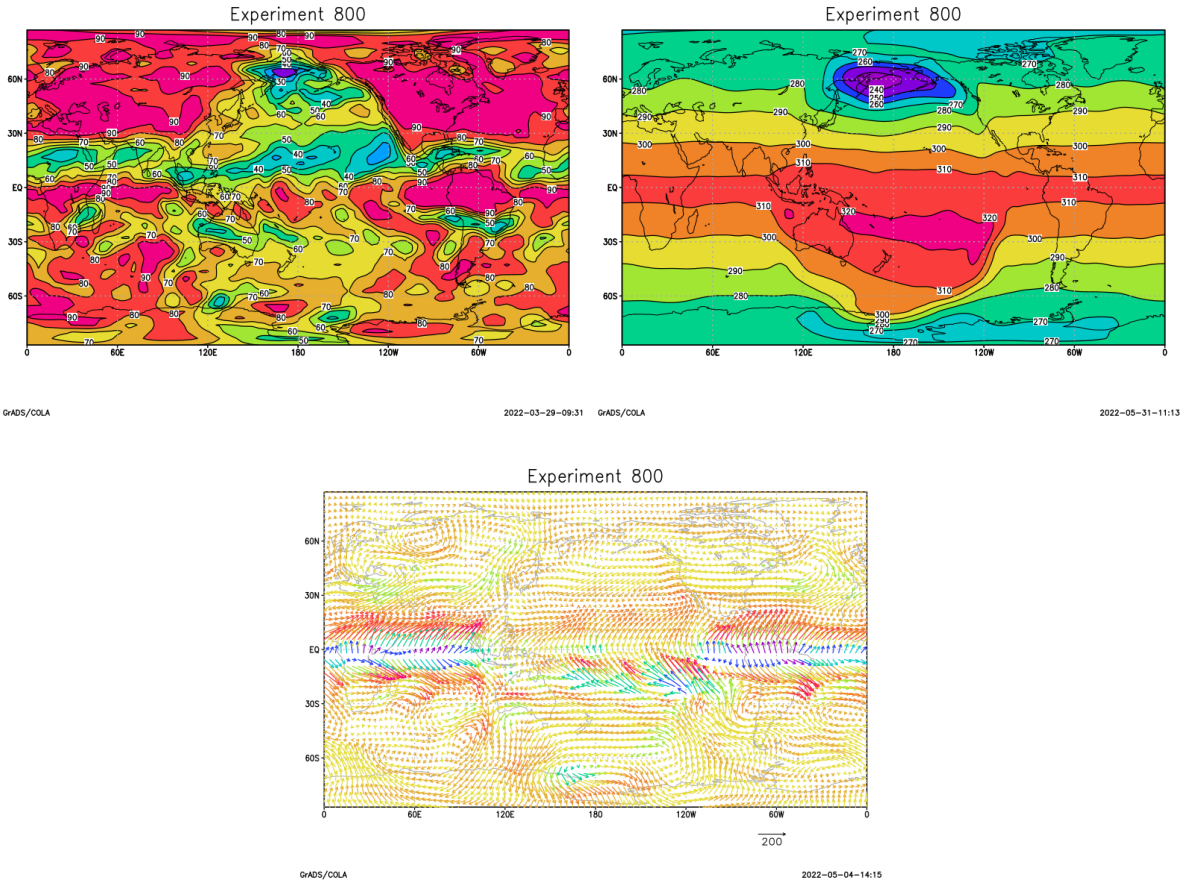

Figure 4.22: Case 3, a planet with vegetated continent and polar ice, at 100% parameter settings. The figure on the top left shows deep cloud cover, the figure on the top right shows temperature and the figure on the bottom shows wind vectors coloured by pressure vertical velocity, to characterise convection.

5

Rotation of a water planet

From the parameter variations in Chapter 4 it was seen that the variation in rotation on a water planet is particularly interesting, because it causes the clouds to form bands. Clear variations in cloud pattern could be seen, which could be attributed to a variation in rotational speed. As these effects are mostly visible on a water planet, this chapter zooms in on this case. It is believed that if this effect from rotational variation can be observed in signals, something convincing can be said about the presence of water on the planet.

This chapter goes deeper into two aspects of the rotation of a water planet. First, it tries to quantify the cloud pattern and its relations to rotation, to create a tool that can be used in further research. Secondly, a special case of rotation is studied more closely, namely tidal lock. To realise this, SPEEDY needs to be adapted, as in essence a new planet is created.

5.1. Longitude averages per latitude

The clear band pattern in fast-rotating planets was the inspiration to select the average of cloud cover per latitude as metric for further analysis. The relevance of using this metric is shown in Figure 5.1, which shows these averages for a water planet with gradient. Convection in the form of Hadley cells can clearly be seen: as the air rises or comes down, an alternating pattern between more and less clouds can be seen. As the planet rotates faster, this alternating pattern gets narrower, which corresponds to the expectation that more convection in smaller Hadley cells takes place.
Figure 5.1 shows this effect for a water planet, but also on planets with continents this effect can be seen, although to less extent, shown in Figure 5.2. Depending on the disturbance of the continent, e.g. how large it is, the amplitude of the band averages will get smaller. On land, the seasons also become more clear, there are more clouds in winter than in summer. Nevertheless the same pattern will be visible, as the clouds are averaged over longitude. In general, the band pattern really denotes plenty of water on a rotating planet, and the higher the amplitude the more water.

The effect of the rotation appears to be quantified by the width of the bands, which is as aforementioned the effect of Hadley cell convection. As the cloud cover drops in the tropics and rises again above the equator, the width is defined per tropic band, from peak to peak. Both bands should be similar and can be compared for validation. The results are shown in Table 5.1 below. The widening of the bands can clearly be seen. Over a range of 50% to 150% rotation, the bands widen about 79% (average of both sides). If it is assumed that this process is linear (it is not, as seen from the data, but later on will be described why such assumptions can be made), this means that when the rotational speed of the planet is doubled, the cloud bands will widen a factor 1.6, which is quite large on a global scale. This gives the good prospect that in planet signals that reach a telescope, differences for differently rotating planets will be observable.
As can be seen in Figure 5.1, only 48 latitudinal datapoints are available. This is very little to be able to draw significant conclusions on the width of the bands, as in Figure 5.1 it is sometimes unclear where the exact peak lies. On top of that, cloud cover is a complex parameter which holds many uncertain-

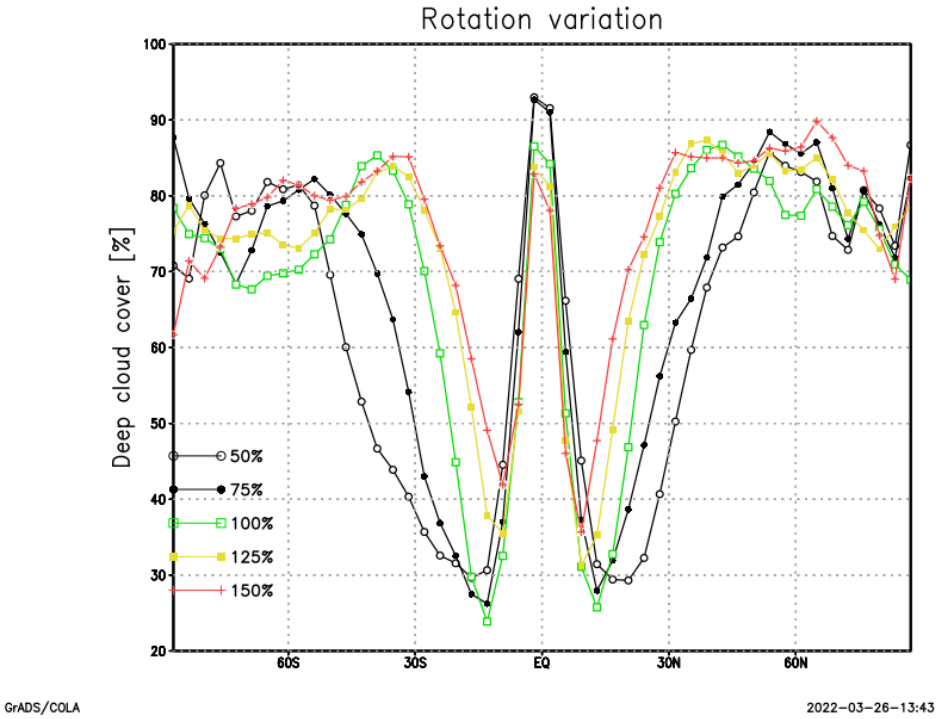

Figure 5.1: Average cloud cover per latitude for an ocean planet with gradient, case 1, for a variation in rotational speed. The percentages denote the parameter value compared to Earth's.

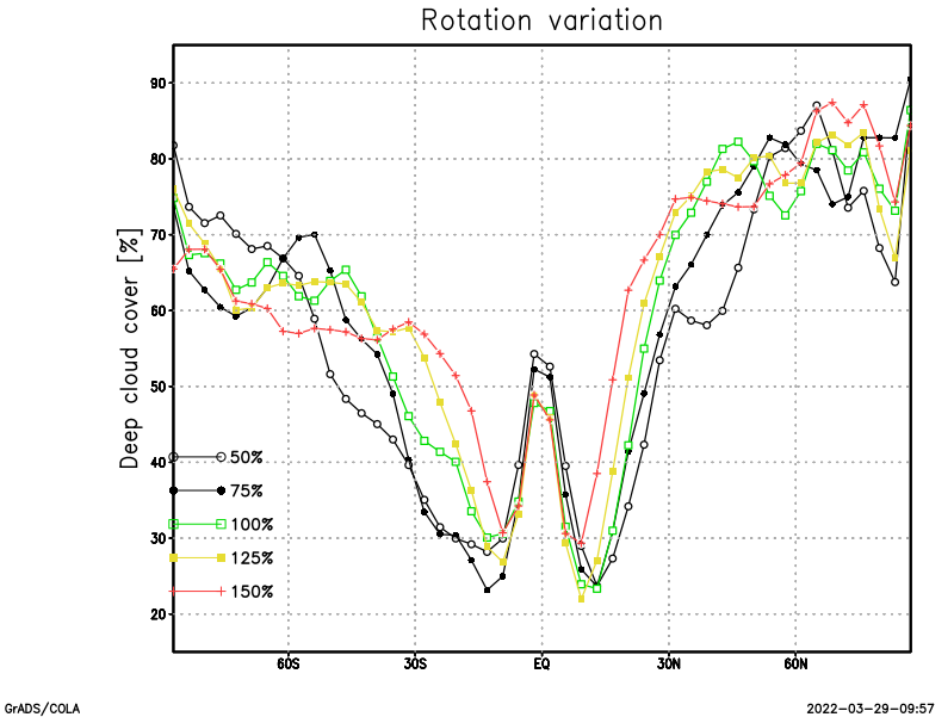

Figure 5.2: Average cloud cover per latitude for an ocean planet with desert continent with gradient, case 2, for a variation in rotational speed. The percentages denote the parameter value compared to Earth's. This figure can be compared to Figure 5.1, as now land is introduced.

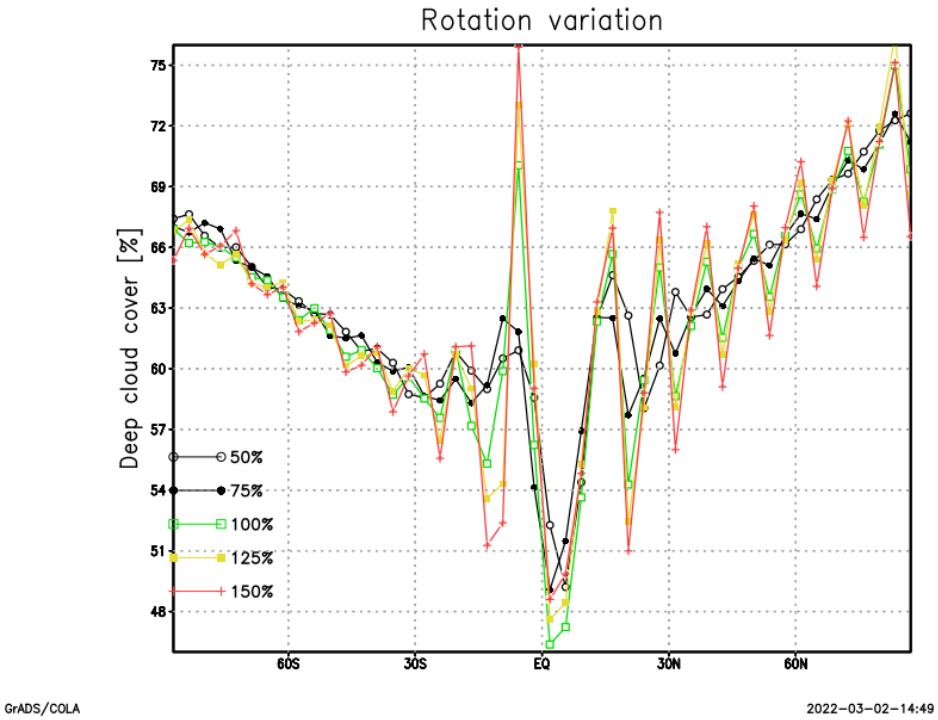

Figure 5.3: Average cloud cover per latitude for an ocean planet without gradient, case 1, for a variation in rotational speed. The percentages denote the parameter value compared to Earth's. This figure represents Figure 5.1, if no SST gradient would be present. The strong instabilities combined with the obliquity of the planet cause the climate not to be centred around the equator.

ties. This is partly counteracted by averaging over time and longitude, but it still plays a big role. One should keep this in mind when studying the data in Figure 5.1 and Table 5.1, and should not take these values as hard numbers. They should rather be seen as an indication of magnitude, and should also be treated like that. This is why the coarse assumption of linearity is a good approximation here.

Table 5.1: Width of cloud cover bands in degrees latitude. The band width is calculated peak to peak based on graph in Figure 5.1.

	Left band	*Right band*
50%	31	32
75%	35	39
100%	39	39
125%	54	54
150%	58	54

In Figure 5.3, the same result for a water planet without gradient is displayed. This figure shows that the faster the planet rotates, the stronger the difference between the cloud cover in the bands becomes, as can be seen in its amplitude. It should be noted that the latitude of the bands remains the same for each rotation variation, as the peaks lie at almost the exact same location.
This is completely the opposite of what is expected from convection in Hadley cells as described above. Generally, an atmosphere gets most of its heat from the ocean below, rather than from stellar radiation. As the ocean is forced to have a constant temperature, as no gradient is allowed, the atmosphere is pushed towards having a constant temperature as well. If this is the case, no convection is introduced. This is represented in Figure 4.5, showing the wind vectors of this situation. In general, there is very little wind, as no energy transfer is induced. However, as the influence of stellar radiation is not negligible, there will be energy transfer. Forcing the atmosphere to have a constant temperature through the ocean in the end causes an imbalance. This imbalance causes heavy local variations, which are the effects seen in the convection map and the peaks in Figure 5.3. As most stellar radiation is received at

the equator, the effect is mostly present in that region. When rotational speed is increased, it is even harder for the atmosphere to transfer the heat and mediate the imbalance, causing the cloud cover peaks to get higher. As explained before, eventually this imbalance causes the energy gradients to get very high and the simulation unstable.

5.2. Tidally locked water planet

A special case in the rotation of a planet is tidal lock, which means that the planet's rotation equals its orbital period, and thus the same side of the planet always faces the star. When real dynamics are used, the rotational speed can be set equal to the orbital period of the planet, and other parameters, such as stellar flux and temperature distribution, will adapt automatically. However, SPEEDY is based on parametrisations, so there is more to it to realise a tidally locked planetary model. Therefore this section will first explain the methodology of implementing tidal lock in SPEEDY, and then give an overview of the results.

5.2.1. Methodology

Tidal lock was imposed by setting the rotational period of the planet at one year as an input parameter. As explained in Section 2.2, many parameters in SPEEDY are decoupled. Therefore also the stellar flux and SST need to be adapted by hand. For every point on the surface of the planet, instead of varying over time due to rotation, the stellar flux was fixed at one timestep, to make sure it is always the same per location. The sea surface temperature gradient was adapted according to the incident stellar flux. The SST ranges from 27^oC at the substellar point to -28^oC at the anti-stellar side of the planet. These values are taken to be the same as the SST gradient of the ocean in the parameter variation cases, for easy comparison. Both the incoming flux and sea surface temperature then show a pattern as described in Figure 5.4, which shows the SST.

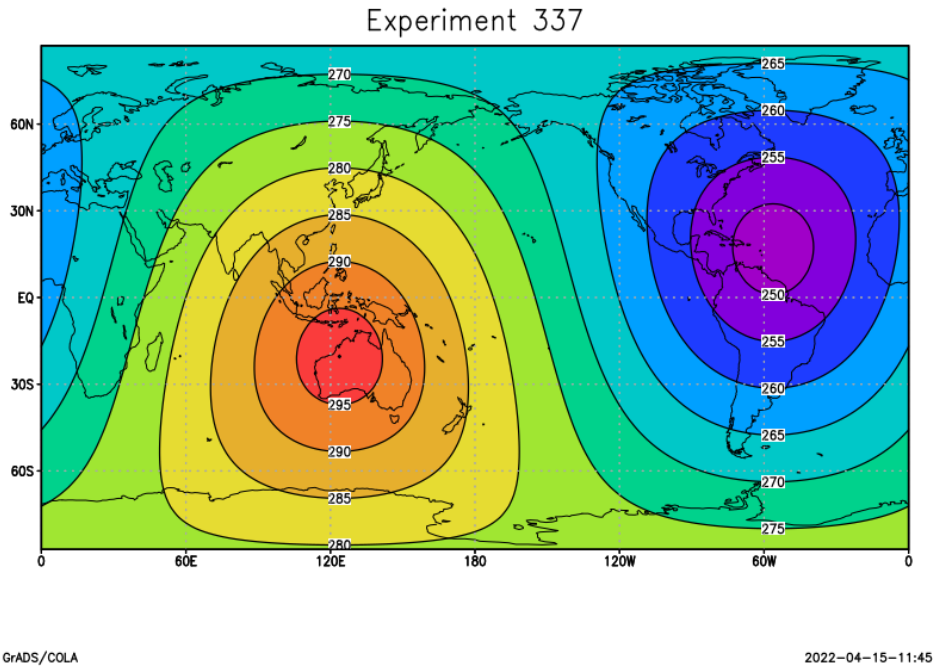

Figure 5.4: Sea surface temperature on a tidally locked water planet, showing a gradient from the substellar point to the back of the planet. Other parameter settings are kept equal to Earth.

5.2.2. Results

As the atmosphere is kept similar to Earth's, it appears to be too thin to provide enough energy transfer for this planet to be stable in tidal lock. However, certain cases and the influence of parameters on

this unstable situation can be discussed. What is remarkable, is that experiments which form more clouds are stable for a longer period of time, which shows that cloud feedback plays an important role in stability of the atmosphere.
From literature (Checlair et al., 2017, Yang et al., 2019), it was concluded that a tidally locked planet has extensive cloud cover on the dayside, while keeping a more clear nightside. This is confirmed by the experiments with SPEEDY, as it was the case for almost all experiments on the tidally locked planet. It seems like one massive cloud is formed over the substellar point, while no clouds can be found on the backside of the planet. The cloud pattern of the tidally locked water planet is displayed in Figure 5.5.
Complementary to the deep clouds, there are stratospheric clouds above the night side of the planet. These could be ice clouds, which are hard to quantify or observe in reflected starlight. Because this is an unknown and the cloud pattern does not change in other experiments, it is not taken into account in the process of drawing conclusions.

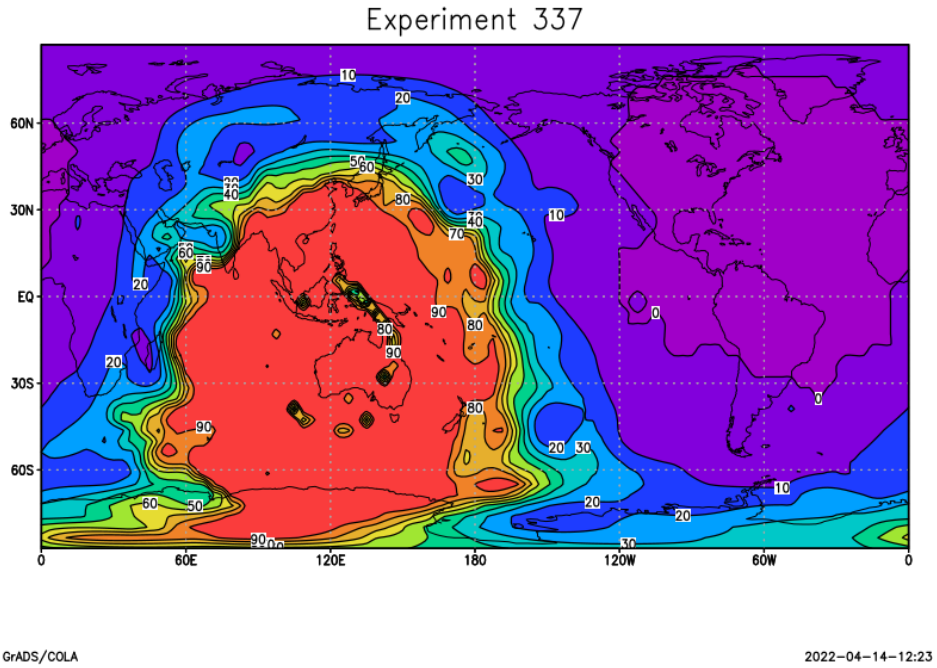

Figure 5.5: Deep cloud cover on a tidally locked water planet, with temperature gradient as shown in Figure 5.4. The colour scale used is the same as in other cloud cover maps (Figure 4.3). The substellar point exhibits many clouds, while the antistellar point exhibits no clouds.

Two approaches are taken for further analysis of the tidally locked planet. Firstly, some adaptations are made to try to get the planet more stable. The pressure is raised to create a thicker atmosphere, as it is believed that the atmosphere is too thin to be stable. Unfortunately, this creates even more instability, however now numerical rather than physical. To visualise the problem, the irregular behaviour of the cloud pattern is shown in Figure 5.6.

Another adaptation is the introduction of land, either dry or vegetated. Again, it exists of a round continent in the middle of the map. The substellar point then lies above the land, near the southwest coast. This point was chosen completely arbitrarily, to not be in the center of the land or ocean, nor on the equator or poles. The results for temperature and deep cloud cover are displayed in Figure 5.7. Regarding temperature, the land provides the effects expected from previous case studies (Section 4.2.4). The warming effect enlarges the area affected by the hot substellar point. Nevertheless the instabilities can be seen again, especially in Figure 5.7 on the bottom right. Regarding cloud cover, the land creates extreme gradients, which makes it uncertain to extract observations as numerical irregu-

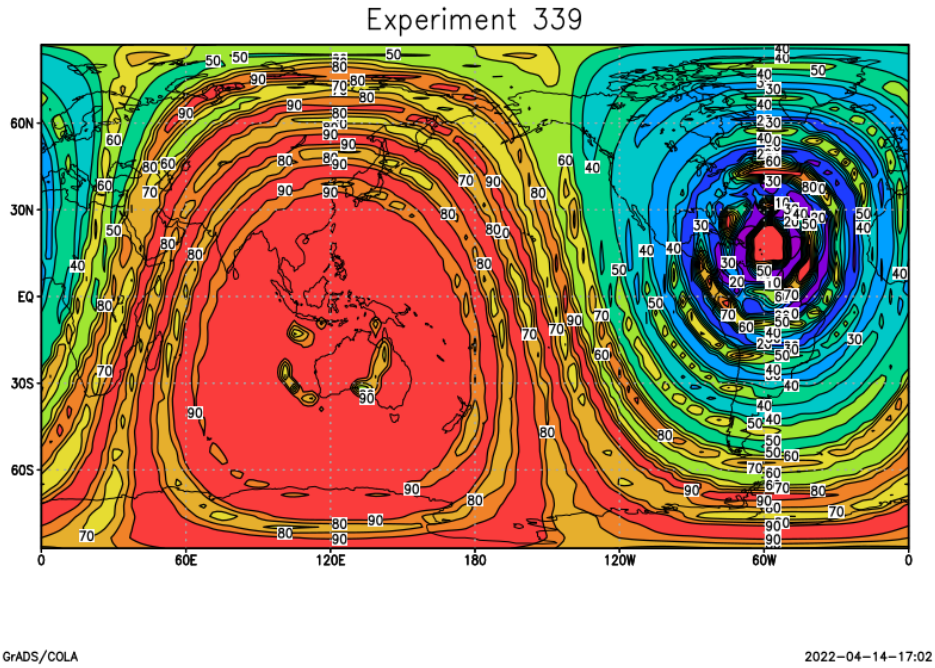

Figure 5.6: Deep cloud cover on a tidally locked water planet with the same properties as Figure 5.5, except with high surface pressure. The figure displays numerical instabilities.

larities are introduced.

The second approach is to pursuit the same parameter variations as on the cases in Chapter 4, except for rotation, because that is fixed, and eccentricity, as it did not have a significant influence before.
Many experiments are influenced by numerical problems: high cloud gradients, a completely different pattern for a small change in one parameter, an increase and then decrease in cloud cover for an increasing parameter, etc. For example, a 1% change in relative humidity induces a 30% change in cloud cover, while a 50% change in relative humidity induces the exact same 30% change in cloud cover.
After many experiments from which the results could find no explanation, it is concluded that forming a stable tidally locked planet in SPEEDY requires more invasive adaptations to the code than currently possible within the scope of the thesis. It is therefore added as a recommendation.

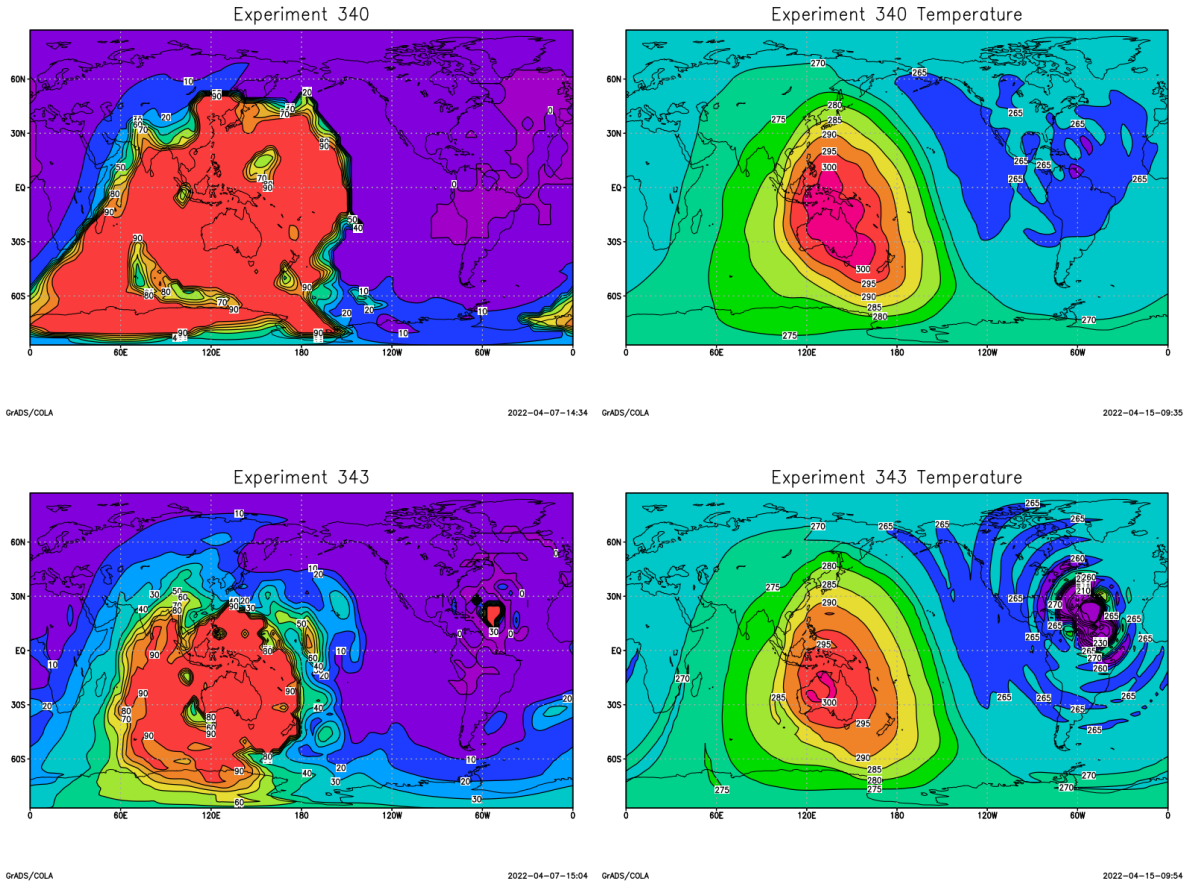

Figure 5.7: The effect of land on a tidally locked water planet, displaying both deep cloud cover on the left as temperature on the right. The top row shows a tidally locked water planet with a dry continent, while the bottom row shows a tidally locked water planet with a vegetated continent. Also here, numerical irregularities are present.

6

Reflected starlight signals

Determining a cloud pattern is one thing, observing it is a whole other challenge. After the cloud pattern is simulated, the signal that the planet reflects from its starlight can be determined. This is a novelty in the research field: calculating signals based on actual simulations. This signal is computed with DAP and PIXX, a code by Daphne Stam and Victor Trees (described in Trees and Stam, 2022, based on the software described in Rossi et al., 2018).

This code uses the files from DAP, a radiative transfer code that computes flux and polarisation of starlight that is reflected by a locally plane-parallel atmosphere and surface, for a range of incident light directions and a range of reflected light directions. This DAP code produces Fourier files that serve as input for PIXX.
PIXX computes for every pixel on the planet, the reflected flux and polarisation, using the Fourier file for the local atmosphere-surface conditions and the local illumination and viewing geometries. The latter geometries depend on the phase angle of the planet and the latitude-longitude of the pixel on the planet. These codes are both Fortran codes.

6.1. Methodology

PIXX takes as an input a map of the planet in question, with every longitude-latitude point assigned to a certain Fourier file, based on whether the pixel is covered by clouds or not. The cloud pattern put out by SPEEDY should thus be reduced to such a map. To this end, the daily output (as explained in Section 4.2.2) is used instead of the monthly output. It is deemed more representative of the real observation situation. Furthermore, only the water planet with gradient in SST was used to calculate signals. The scope of the calculations needed to be limited and from previous results this case was selected as most interesting. As SPEEDY's output is on a grid with less points than required for PIXX, the cloud cover was first interpolated. This was done linearly, with at the boundaries taking the closest lying value.
For an ocean planet, the maps are generated as follows: if the cloud cover in a point is larger than 50%, this point is assumed to be fully clouded, while if the cloud cover in a point is smaller than 50%, it is assumed to be cloud-free. For accurateness in the spectrum calculations, the calculations of the Fourier files are weighted with the cloud cover. For other visualisations, this was not done for simplicity.
To find out about the mathematics on how the signal is calculated, the reader is directed to Trees and Stam, 2022. As an output, PIXX standardly provides the total flux F, total degree of polarisation P, and values for the linearly polarised fluxes Q and U. The polarisation P is defined as follows:

$$P = \frac{\sqrt{Q^2 + U^2}}{F} \tag{6.1}$$

The reflected fluxes and polarisation are computed for every required phase angle. When U is much smaller than Q, an alternative definition for the polarisation can be used, namely:

$$P_s = -\frac{Q}{F} \tag{6.2}$$

When P_s is positive, the light is polarised perpendicular to the reference plane, if it is negative, parallel. The reference plane is defined as the plane through the planet, its star and the observer. (Trees and Stam, 2022)
Generally, these parameters are given for an unresolved disk (meaning the planet is seen as a single dot), to represent the low resolution of current observation techniques. Nevertheless, to study spatial variations on the planet or for visualisation purposes, the output can also be given for the resolved disk. Furthermore, the sub-observer point on the planet should be specified. To account for rotation of the planet, the signal is calculated for multiple sub-observer points.

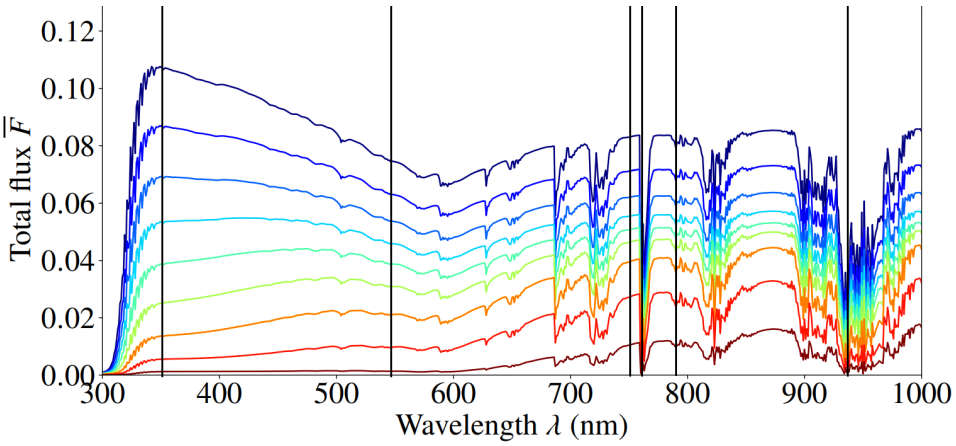

Figure 6.1: An example spectrum is shown to visualise the wavelengths selected for further analysis (350nm, 550nm, 750nm, 760nm, 790nm and 940nm) by black vertical lines.

The PIXX code can calculate the entire spectrum, but as this is computationally expensive, the instances for which this is done are limited, only for three different rotational speeds and three cases to study integration time, as are described in Section 6.2 and Section 6.3 respectively.
First, the general shape of the spectrum is elaborated upon briefly, following the example in Figure 6.1. The colours represent the phase angle at which the observation is done, ranging from 90 degrees in dark blue to 170 degrees in dark red, with steps of 10 degrees. The phase angle of an observation is the angle between the observer and the star, measured from the planet in orbit at the time of observation. This phase angle directly influences the visibility of the planet from Earth, and hence the intensity of the signal. Under 340nm, the light is absorbed by ozone. In the continuum after 340nm, the signal is governed by Rayleigh scattering of the gases, and the decrease in flux follows from that scattering. At higher wavelengths, absorption bands start to emerge. First, the large ozone dip between 340nm and 700nm can be observed, followed by a variation of shallow and deep bands relating to various gases. (Trees and Stam, 2022)
To get more specific information at more phase angles, the spectral range of the analysis is narrowed down. Based on the spectrum, wavelengths λ interesting for further study are selected. These are shown on a spectrum in Figure 6.1 and listed below.

- 350nm: a 'control' wavelength where there is no absorption, which represents the gases in the atmosphere, as at this wavelength the clouds are minimally represented in the results. The gases above the clouds in the atmosphere strongly scatter the light, and as such the fluxes are insensitive for the clouds.
- 550nm: to visualise the transition between where gases and where the surface and clouds of the planet govern the results.
- 750nm: right before the O_2A absorption band. This wavelength lies outside of any absorption band, displaying features of the surface of the planet in case there are no clouds.
- 760nm: inside the O_2A absorption band. Oxygen is present at every altitude of the atmosphere, below as well as above and also inside the clouds.

- 790nm: inside a shallow H_2O absorption band. Water is mostly present below the clouds, and its signal is thus blocked when clouds are present.
- 940nm: inside a deep H_2O absorption band. At this wavelength, the scattering by the gas in the atmosphere will be minimal, and mostly the clouds will be represented (and the surface if there are no clouds).

The binary cloud cover maps and signals can be visualised by the code as actual planets at various phase angles. Figure 6.2 is an example of such a visualisation based on a cloud map of the water planet of experiment 700 after three years of simulation at 0 degrees phase angle. The clouds are coloured white and the oceans blue.

Figure 6.2: Full-planet plot of a water planet at the last day of 3 years simulation (experiment 700), at a phase angle of 0 degrees. The figure is coloured in white for the clouds and blue for the oceans, based on a binary cloud cover map. This planet represents an integration time of one day at a rotational speed equal to Earth's.

Before going into the results, a disclaimer should be given. SPEEDY's output is determined on a latitude-longitude grid, a so-called geographical grid. When focusing on a part of the planet on this grid, one always sees the same location on the planet, evolving over time. On the other hand, when observing an exoplanet in the sky, one sees the planet at the same angle with respect to its star. This translates to for example seeing the part of the planet which is in morning, varying over planet's location. This is the so-called sub-observer grid.
To be fully correct, the cloud pattern from the geographic grid needs to be transformed onto the sub-observer grid. However, SPEEDY's calculations are designed to be performed on a geographical grid, and it is not known how reliable they would be on another grid. Therefore, it is decided to not transform the simulated cloud patterns and to simply calculate the signals on a geographical grid. To validate this approach, it is assumed that on a planet rotating at the same speed as Earth, the cloud cover during the day does not vary significantly, meaning it does not matter if the morning or evening side of the planet is looked at. Hence, the induced error will remain limited.

6.2. Rotation features

From the parameter variations in Chapter 4, it could be seen that the rotation of the planet influences the cloud pattern. This effect could especially be seen on a water planet. The question is whether this influence on the pattern is represented in observable signals. This section analyses this, based on the wavelengths previously chosen.

Already from a simple visualisation in Figure 6.3, some features can be seen, compared to the default case in Figure 6.2. For 50% rotation, the band pattern cannot yet be recognised, the cloud free areas are more located in zones. For 150% rotation, the bands get narrower, with more clouds covering the planet.

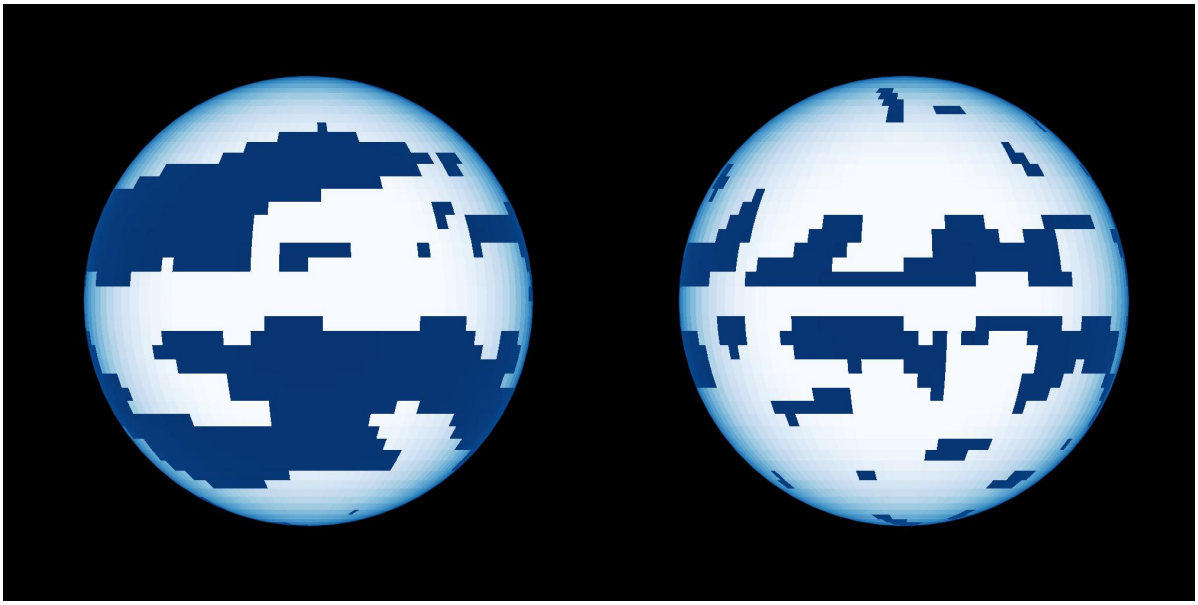

Figure 6.3: Full-planet plots of a water planet with 50% rotational speed on the left and 150% rotational speed on the right, both at 0 degrees phase angle. Blue denotes oceans and white denotes clouds. The figures represent a binary cloud cover map to compare different rotational speeds.

The cloud pattern can vary over the planet: the backside can have a different pattern than the frontside at the same point in time. To see whether the observations hold for the entire planet, the signal was calculated for every location around the planet and compared. The variation in signal over the planet turned out to be two orders of magnitude smaller than the variation of other parameters such as rotational speed, hence the observations are valid.

6.2.1. Spectra and phase curves

In Figure 6.4 the spectra for the different rotational speeds can be seen. At a first look, it can be seen that the flux in Figure 6.4 on the left rises when rotational period decreases, as an effect of increasing cloud cover. The curves of phase angles 120^o to 150^o lie close to each other, while for smaller and larger phase angles they are more stretched out. If a certain phase angle, often larger phase angles, does not follow that pattern, it is a sign of glint reflection from the oceanographic surface being present. The glint, when it is visible, increases the flux, as it is a reflection, which adds light. Also the depth of the absorption bands in both the F- as P-spectrum are affected by the glint.
This glint can more clearly be seen in the polarisation spectrum, as the lines of various phase angles cross, namely higher phase angles are more strongly polarised than lower phase angles. Furthermore, there are little dips in the spectrum within the absorption bands, which without glint would have been little peaks. These traces can be seen in the P-spectrum in Figure 6.4 on the right, and already here it should be noticed that they are not the same for all rotational speeds. The lower the wavelength, the smaller the glint contribution becomes, because the optical thickness of the atmosphere increases and less light reaches the surface. The described results are consistent with the observations denoted in Trees and Stam, 2022.
The glint is more visible when it is not covered by clouds, which depends on the simulated cloud pattern. As the differences between the signals of different rotational speeds are small and hard to see on the full spectrum, phase curves will be studied more deeply for the pre-selected wavelengths described in Section 6.1. These can be seen in Figures 6.5 and 6.6.

The phase curves where the clouds and surface are dominant (from 750nm onwards) generally

show a similar shape. This shape is determined by the shape and size of the cloud particles, which is constant for all signal calculations in this chapter. The lower wavelengths show a different pattern: 350nm is not much affected by the rotation, and 550nm shows a smooth transition over wavelengths. The reflected flux rises for increasing rotation, in agreement with the spectrum described above.
Some general spectral properties can be recognised in the phase curves. The wobble around a phase angle of 10 degrees, which can be seen in all fluxes, is the glory. Around 30°, the rainbow effect can be seen in both Q and P. This rainbow slightly shifts phase angle over wavelength. At 350nm, the effect of the surface and clouds is not yet visible, although a little hint towards the rainbow is already given. At higher phase angles, clouds are negatively polarised, which can be seen at 940nm where the effect of the gases is gone. At the other wavelengths, the positively polarised gas draws the curves up. Lastly, it is worth noticing that regarding polarisation, the curves all cross at the same phase angle. What the cause of this is, is yet unkown, but it has also been observed in other signal calculations (Trees and Stam, 2019).
The peaks in polarisation at higher phase angles are due to the glint. The significance of the glint peak depends on how visible the surface is at that particular wavelength, as is described above. It is remarkable that the highest glint can be seen at a rotation similar to Earth's. The glint is the strongest around the equator, and will thus be most visible in cloudfree pixels in that area. At a low rotational speed, the cloud pattern is more patchy than in bands, cloudy and cloud free zones spread around the planet. In addition, at a high rotational speed, the cloud cover in general is increased. Combining these effects, for in the in-between case of 100% rotational speed, the band pattern will have drawn the cloud free zones to group around the equator just enough, without increasing the cover too much, to observe the strongest glint signal.
At wavelengths lower than 750nm, the 50% case has the largest polarisation. At these wavelengths, the gas is still dominant, hence the instance with less clouds, namely 50% rotation, will increase in polarisation. Lastly, it should be noticed that at low phase angles, a large portion of the planet is in view, evening out local effects. As a consequence, the glint is less or even entirely not recognisable in the signals.
An interesting conclusion can be drawn from these observations. An increase in total flux can have many other reasons beside rotational speed. However, combining this with the described glint features, it might be an indication of a rotating water planet!

As will be described in Section 6.3, there can be a large variation in signal over days. For example the glint peak can become wider or higher. This raises the question whether the conclusions from the phase curves are reliable, or whether they could be simply temporal effects. In order to clear this issue, the phase curves were calculated for different days, at the described rotational speeds. As expected, the signals varies significantly over time, but the mutual differences between the rotational speeds remain the same. In conclusion, the statements made earlier in this section remain valid over simulation time.

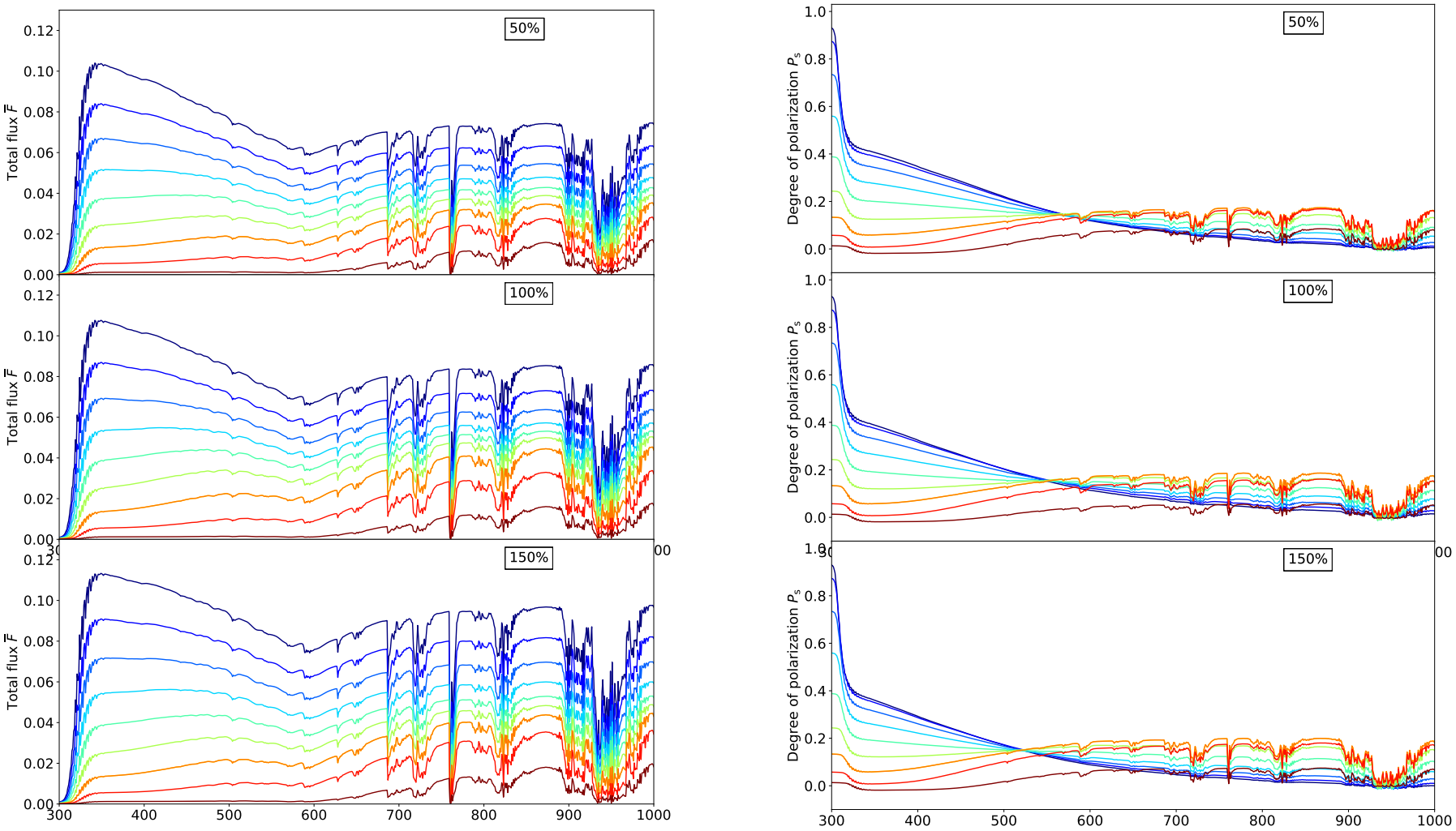

Figure 6.4: Spectra for various rotational speeds, for phase angles 90° (dark blue) to 170° (dark red) in steps of 10 degrees. The left figure shows the reflected flux F against wavelength, while the right figure shows the degree of linear polarisation P against wavelength. The rotational speed used is shown in the left upper corner: 50% of Earth's value on the top, 100% in the middle and 150% on the bottom.

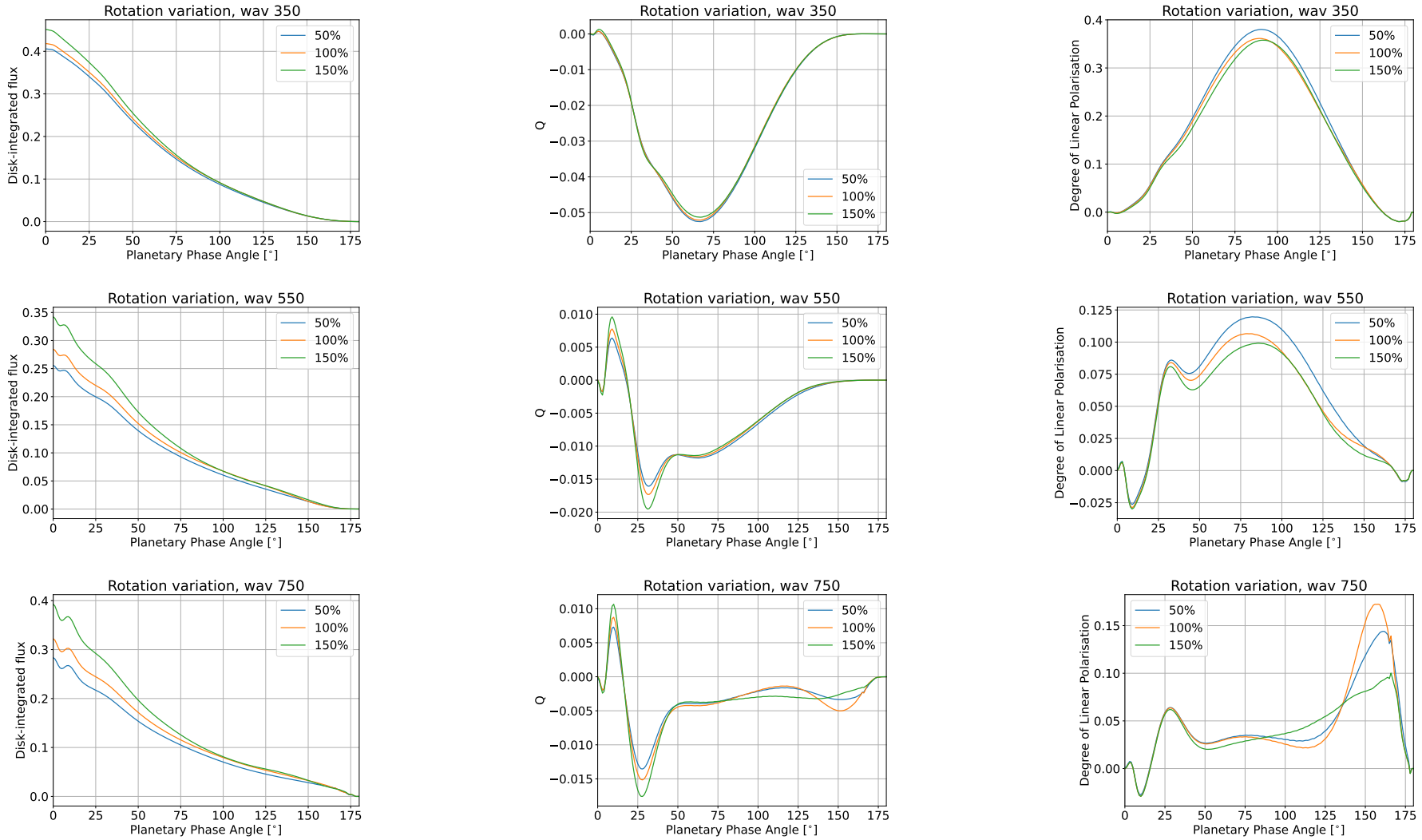

Figure 6.5: Phase curves for various rotational speeds, on wavelengths 350nm (top row), 550nm (middle row) and 750nm (bottom row). The properties shown are flux (left column), Q (middle column) and degree of linear polarisation (right column). The rotational speeds used in all phase curves are 50% (blue), 100% (orange) and 150% (green) of Earth's value.
Note: the little wobble around 165 degrees phase angle in Q and P originates from a little bug in the signal calculation code, but it does not affect the results or conclusions whatsoever.

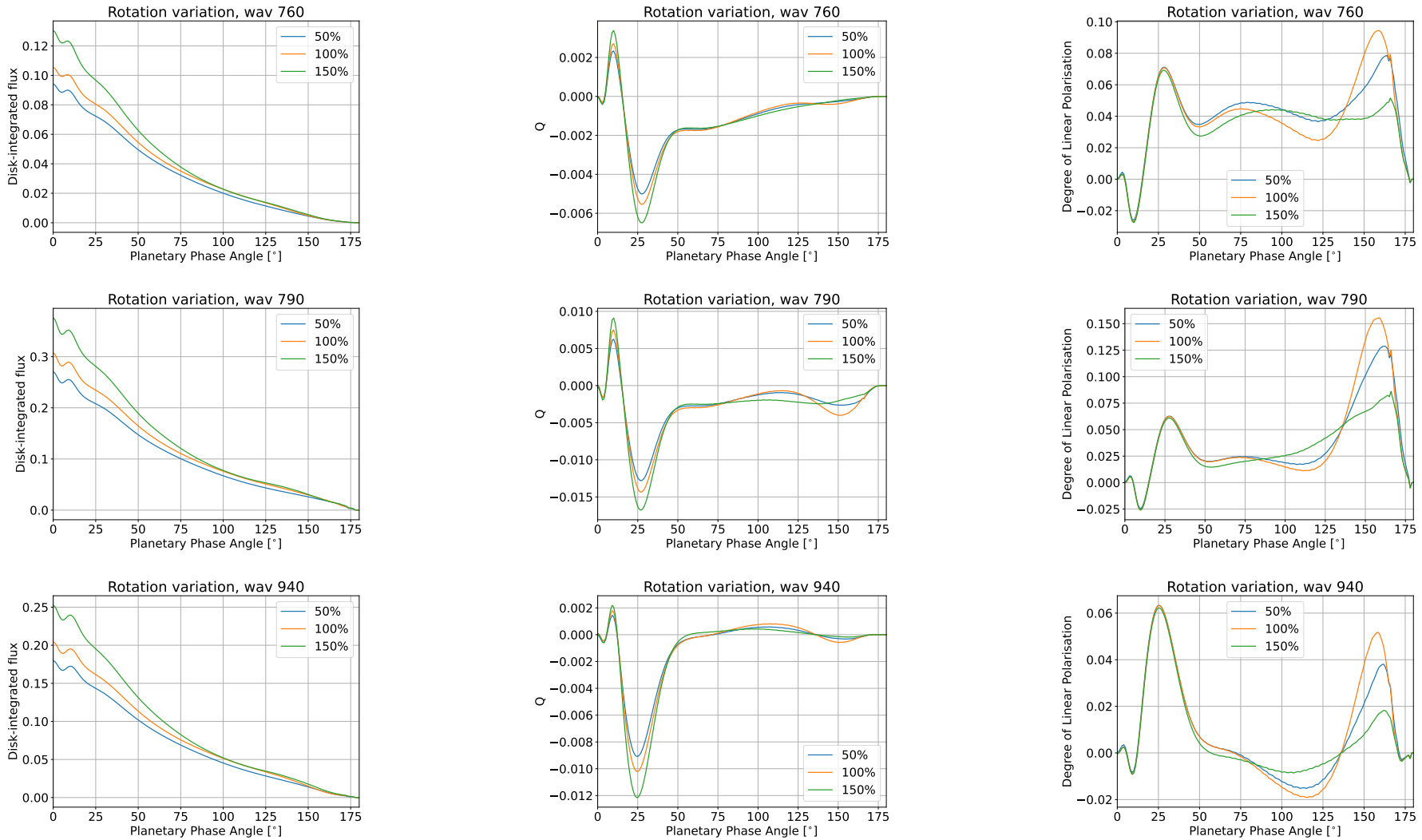

Figure 6.6: Phase curves for various rotational speeds, on wavelengths 760nm (top row), 790nm (middle row) and 940nm (bottom row). The properties shown are flux (left column), Q (middle column) and degree of linear polarisation (right column). The rotational speeds used in all phase curves are 50% (blue), 100% (orange) and 150% (green) of Earth's value.
Note: also here, the little wobble around 165 degrees phase angle in Q and P originates from a little bug in the signal calculation code, but it does not affect the results or conclusions whatsoever.

6.3. Influence of integration time

Integration time, i.e. the time during which photons are collected of a specific target, is a fundamental feature in exoplanetary observations, and in astronomy in general. During the integration, the rotation of the planet and local variations in the cloud cover will change the cloud pattern that is 'visible' to the observer. As the cloud pattern varies, it is expected that over time, every point on the planet will have seen a cloud pass by. Cumulatively, this will have an effect on the received signal from the planet, and lead to deluded conclusions, as a fully clouded planet would be 'observed'. Hence, this section will study the effect of the integration time on the signal. The analysis will be based on different averaging methods of the cloud cover, and how representative each is. The general question to be answered is: what will be left to see in the signal after a certain integration time?

First, we take a look at the visualisation in Figure 6.7 on the left. This plot shows the average cloud cover over three days, of which the last day coincides with Figure 6.7 on the right. The rotational speed in planet used in this section is 100%. The shown pattern is made based on the hand-averaging method, explained hereafter. The principle of when time passes, every pixel will have been clouded is true in this case, as the planet is more clouded than the one day instance in Figure 6.7 on the right. However, this effect mostly washes away small cloud free areas, while leaving alone the entire cloud free band near the equator. This means that despite the extra clouds, still the influence of the rotation could be visible in the signal. What the effect is of the integration time specifically on the observed width of the bands in the cloud pattern should be studied in more detail in further research.

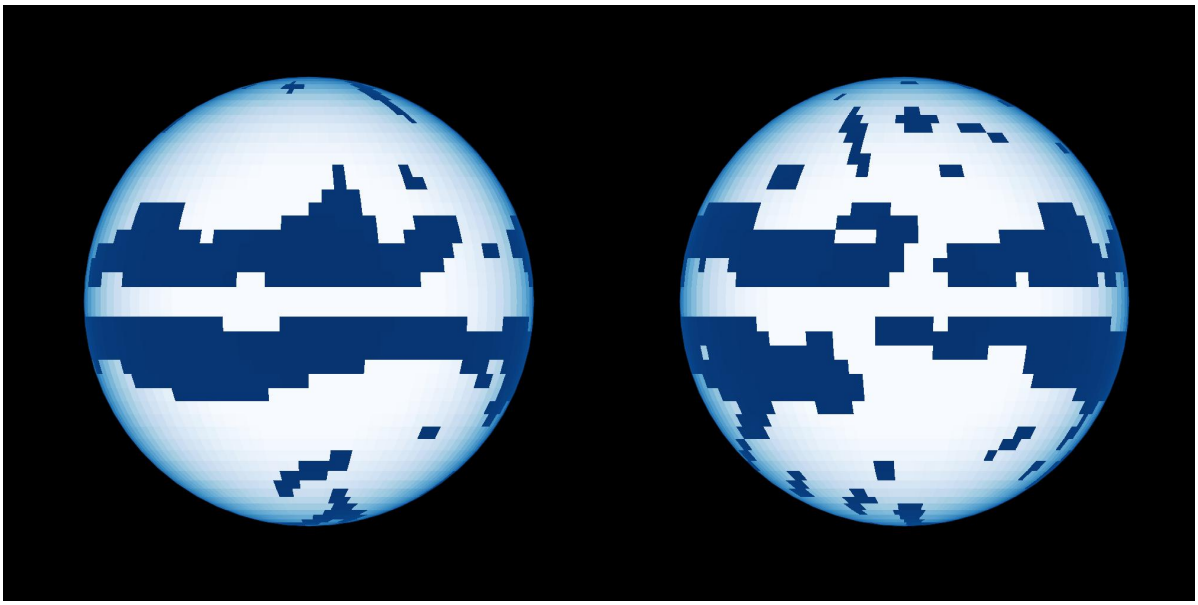

Figure 6.7: Full-planet plots of a water planet over 3 days of simulation on the left and over 1 day on the right, both at 0 degrees phase angle. The 3-day average is taken over the three last days of three years of simulation, while the 1-day average is the last day of three years of simulation, and hence the last day of the 3-day case. Blue denotes oceans and white denotes clouds. The figures represent a binary cloud cover map to compare the difference over three days integration time.

6.3.1. Study of the varying signal over time

To put a measure on the influence of integration time, the differences between an averaged signal and the daily signal are determined. Examples of a comparison between these signals can be seen in Figure 6.8. There are three averaging methods used: SPEEDY's output, averaging by hand, and setting a threshold (after which averaging by hand is applied). These methods all average the cloud cover before a map is made or signals are calculated.

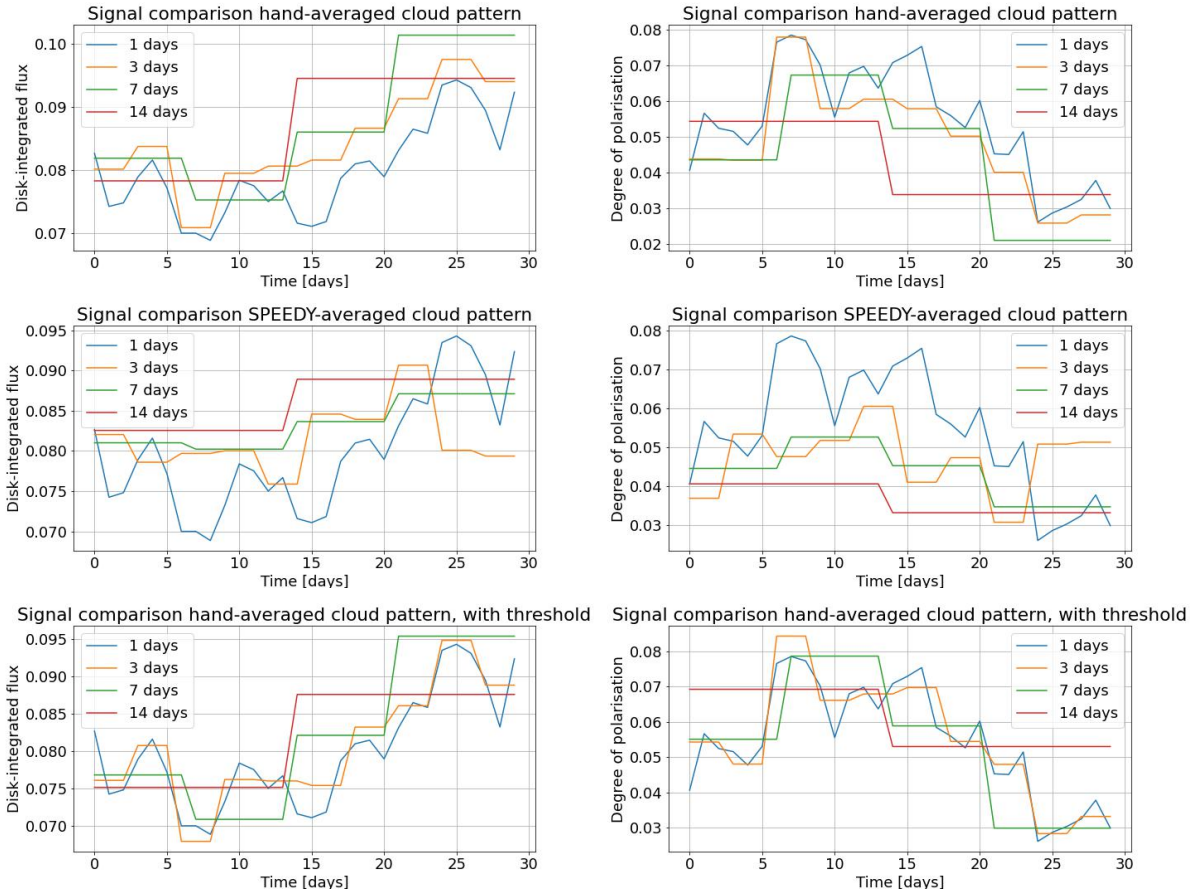

Figure 6.8: Signal over time during one month for averages over multiple days. The month used is December after three years of simulation. The left column shows flux and the right column shows degree of linear polarisation. The rows show the different averaging methods, with the hand-averaged results at the top, the SPEEDY-averaged results in the middle and the hand-averaged results with a threshold on the bottom.

Definition of averaging methods

First, the hand-averaging method will be explained. This is deemed the most representative method for observation purposes. The daily output cloud cover is taken from SPEEDY for a number of days, and then the average of this cloud pattern is taken as pattern for the time span. This is different from letting SPEEDY provide a multiple-day, for example weekly, output cloud pattern directly in the following way: SPEEDY averages the fields, such as vorticity, temperature and humidity, which it uses in its simulations, and afterwards calculates the average cloud cover at once, instead of first calculating all cloud covers and then averaging. For climatological purposes, this is the most representative method. With this method, the patterns over time become more clear, instead of fading into a uniform average. Hence, it is natural that this method is implemented in the climate model, and the average for observational purposes needs to be calculated separately.

To bring the two methods closer together, a threshold is used. It is thought that this threshold will counteract the effect that over time all pixels get clouded. It works as follows: when a pixel has a cloud cover of more than 50% for more than half of the time, it is seen as clouded. If the average cloud cover lies above 50%, but the previous requirement is not fulfilled, the pixel is nevertheless assumed cloud free.

Differences over integration time

To define a measure for the differences in signal over integration time, the focus lies on the hand-averaging method, afterwards the other methods will be discussed.To represent several integration times, the cloud cover was averaged over 3, 7 and 14 days. The difference between the signal from

the averaged cloud cover and the daily cloud cover was determined for every day of the month, for every phase angle and for every previously selected wavelength. The month used is the last month of the simulation, meaning December of the third year. The maximum difference per wavelength for both flux F and polarisation P is given in Table 6.1, in particular the relative and the absolute differences respectively. The values in the table are accompanied by the phase angle α at which this difference occurred.

Table 6.1: Differences over time between the signal of hand-averaged cloud patterns and the signal of daily cloud patterns. α denotes phase angle. For each wavelength the maximum difference over time and phase angle of the signal is given.

		350nm	$\alpha[^\circ]$	750nm	$\alpha[^\circ]$	760nm	$\alpha[^\circ]$	790nm	$\alpha[^\circ]$	940nm	$\alpha[^\circ]$
3	F (rel)	0.0363	37	0.135	165	0.105	111	0.135	177	0.167	176
day	P (abs)	0.0187	98	0.0505	133	0.0340	132	0.0477	133	0.0275	133
7	F (rel)	0.0540	77	0.134	167	0.131	77	0.129	77	0.135	79
day	P (abs)	0.0273	85	0.0276	133	0.0195	131	0.0261	134	0.0154	134
14	F (rel)	0.0469	73	0.132	169	0.120	66	0.122	69	0.127	69
day	P (abs)	0.0240	86	0.0309	133	0.0206	132	0.0290	133	0.0165	133

A lot of information can be derived from this table. Wavelength 350nm shows the smallest differences, especially in flux. This follows from this wavelength being in the continuum part of the spectrum, unaffected by clouds or surface. Taking this as the 'control' wavelength was thus a valid assumption.
In terms of integration time, the 3-day average often shows larger differences than the 7- and 14-day average, which is against what one would expect. It is assumed that this is an instantaneous effect of one outlier, which is less likely to happen when more days are averaged.
In general, no conclusion can be drawn of the influence of the phase angle on the difference, as no clear trend can be identified. Except for 350nm, the wavelength at which the largest polarisation difference occurs is quite constant around 133 degrees. Furthermore, for the 7- and 14-day average, except for 750nm, the phase angle at which the maximum flux difference occurs is also rather constant.

Comparison of averaging methods
Figure 6.8 shows the signal during one month for averages of 1 day, 3 days, 7 days and 14 days, for the different averaging methods. These figures are based on a wavelength of 750nm, because this wavelength has the largest errors in Table 6.1 (it is a rather arbitrary choice, but one wants to quantify the errors regarding the cloud pattern, thus than any wavelength above 550nm would be representative, according to the phase curves in Figures 6.10 and 6.11), and a phase angle of 90 degrees, as this is the angle around which real observations are expected to take place. What can be derived from this figure is twofold: a comparison between the various averaging methods, and a hint on the limitations of integration time on deriving certain features such as rotational speed.

To start, the averaging methods will be discussed. In general, the averaging from the hand-averaged method follows the trends of the original data more than from the SPEEDY-averaged method: for example, the 14-day signal is the average of the two respective 7-day signals, which is not the case for SPEEDY's output. The assumption of the hand-averaging method being more representative than the SPEEDY-averaging method hence proves its purpose. Simply looking at the pattern over time, the SPEEDY-averaging method is much less representative of the 1-day pattern than the hand-averaging method.
The flux of the hand-averaged signal is higher than that of the daily signal. This is a consequence of when the signal is averaged, every pixel will have been clouded at one point. Here the method with threshold comes in. The threshold lowers the flux and as a result, the 1-day pattern is very well represented by the multiple-day average.
In the polarisation, it is again clear that the hand-averaging method is more representative than the SPEEDY-averaging method. As Q is mostly determined by cloud free pixels, some effects from introducing the threshold can be seen in the P-signal. On top of that, a lower flux raises the polarisation. Nevertheless, the method including threshold is also for polarisation a good approximation for the 1-day signal.

Application to integration time
Now it is left to get a feeling of what a good integration time would be. No more can be concluded than to say that it depends greatly on the application. In this case, the second half of the month is more clouded than the first half. As it is December, this can be for example a seasonal effect, as the temperature and incoming solar flux are changing gradually during the month. If one intends to observe merely this, the 14-day average would be enough. If one wants to observe the dynamics of the clouds, the integration time should get as short as possible. Basing conclusions on the most-representative hand-averaging method, it can simply be said that the longer the integration time, the less accurate the signal pattern becomes.

6.3.2. Spectra and phase curves

From the flux and polarisation spectra for the 1-day signal and both averaging methods in Figure 6.9, not much difference can be seen between the 1-day signal and the 3-day averages. This is beneficial for measuring the rotation features, as the integration time can be longer without interfering much with the results. One thing that could be noticed, is the glint feature in the orange and red lines. From Figure 6.4, it could be seen that glint is most present at these phase angles. It is then also here the only difference between the spectra that can be noticed, although small, in both flux and polarisation. This means that the averaging method and the integration time can slightly alter the way the glint is profiled. To be sure, again a look will be taken at the phase curves.

The phase curves are displayed in Figures 6.10 and 6.11. In these figures, both averaged signals (again over three days) and the signal of the three individual days over which the average was taken are displayed. All general phase curve features remarked in Figures 6.5 and 6.6 can also be noticed here.
Once more, it should be noticed that the hand-averaging method is more representative than the SPEEDY-averaging method, as it is a smooth mean of the three daily signals. The effect of SPEEDY averaging fields instead of cloud maps profiles itself mostly in the width of the glint peak, rather than in the height of the peak or polarisation features. Also in the flux, no clear difference can be seen. According to Trees and Stam, 2019, the width of this glint peak depends on albedo of the planet, in this case thus how many clouds are present and what the distribution of these clouds is. Taking a look at the daily signals, the width of the peak can also vary as a temporal effect, however in this case the height of the peak follows accordingly with the width. At this point, no further explanation can be given. Further research would be necessary to discover what influences the temporal widening of the peaks. In conclusion, the same essence as in Section 6.3.1 can be extracted. Assuming the hand-averaging method, the signal nicely repreesnts the average of the individual signals. It should be remarked and taken into account however, that the variation in signal between the individual days is also quite large, especially regarding the glint peak. What the temporal resolution of the signal should be, depends on the application. The suitable integration time then follows respectively. As the signals are averaged, the integration time will not have a large influence on the distinguishment of rotational speeds in section 6.3.1.

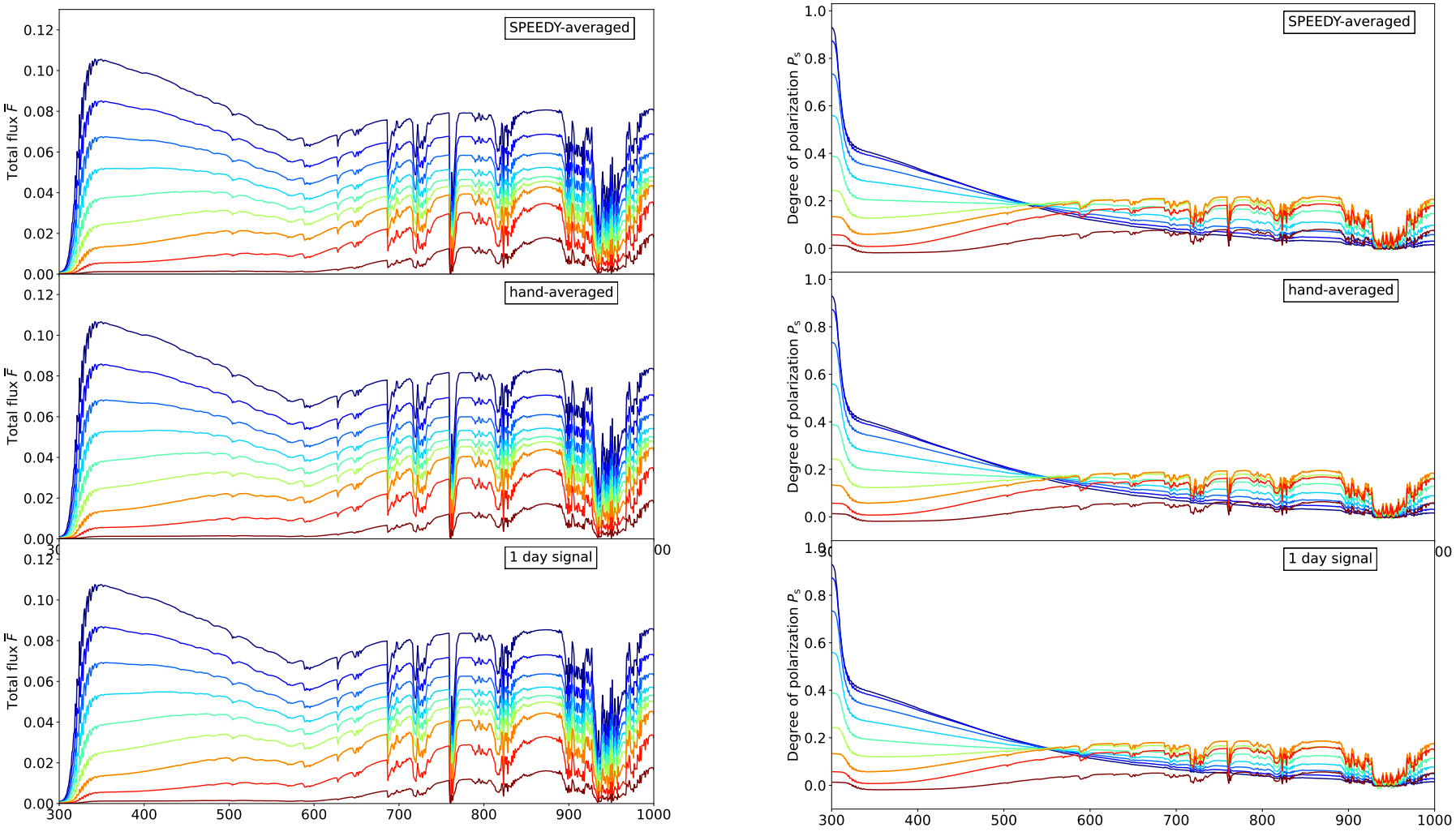

Figure 6.9: Spectra for a 3-day average from SPEEDY on the top, a 3-day average calculated by hand in the middle, and a daily signal on the bottom, for phase angles 90° (dark blue) to 170° (dark red) in steps of 10 degrees. The left figure shows the reflected flux F against wavelength, while the right figure shows the degree of linear polarisation P against wavelength.

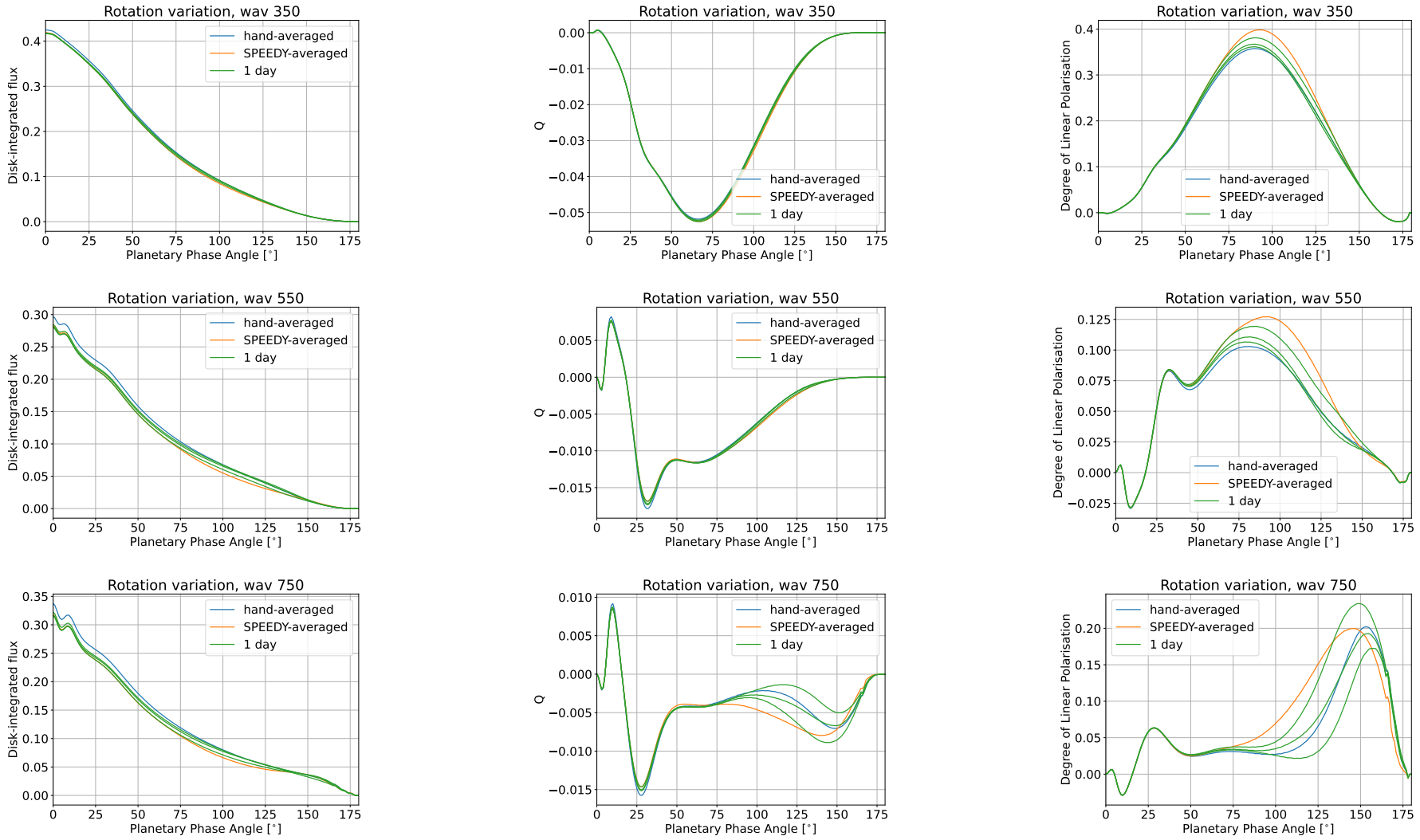

Figure 6.10: Phase curves for the various averaging methods and integration times, on wavelengths 350nm (top row), 550nm (middle row) and 750nm (bottom row). The properties shown are flux (left column), Q (middle column) and degree of linear polarisation (right column). In all plots, blue shows the results of a 3-day average defined by the hand-averaging method, orange by the SPEEDY-averaging methods, and the three green lines show the phase curves of the three individual daily signals over which the averages were calculated.
Note: also here, the little wobble around 165 degrees phase angle in Q and P originates from a little bug in the signal calculation code, but it does not affect the results or conclusions whatsoever.

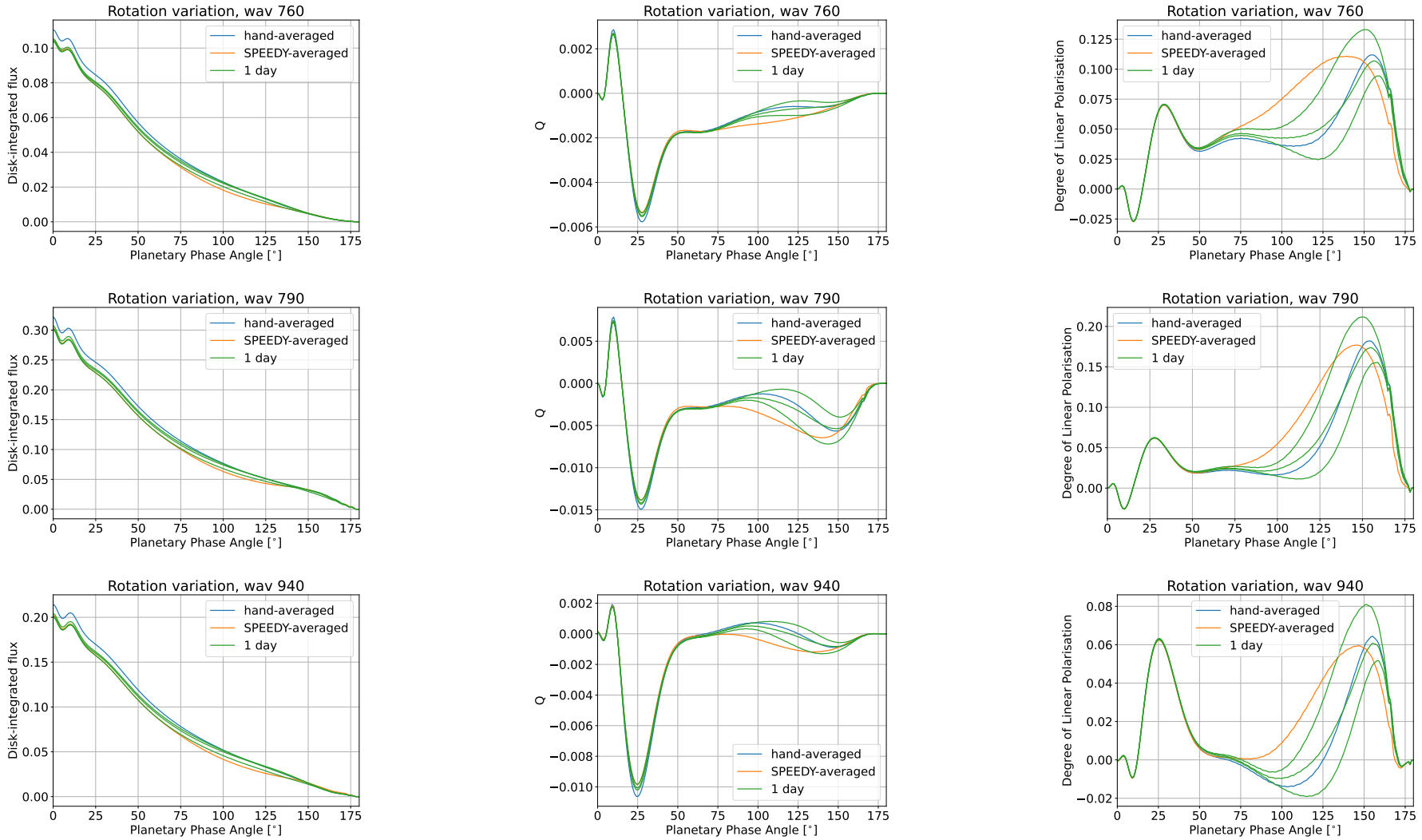

Figure 6.11: Phase curves for the various averaging methods and integration times, on wavelengths 760nm (top row), 790nm (middle row) and 940nm (bottom row). The properties shown are flux (left column), Q (middle column) and degree of linear polarisation (right column). In all plots, blue shows the results of a 3-day average defined by the hand-averaging method, orange by the SPEEDY-averaging methods, and the three green lines show the phase curves of the three individual daily signals over which the averages were calculated.
Note: also here, the little wobble around 165 degrees phase angle in Q and P originates from a little bug in the signal calculation code, but it does not affect the results or conclusions whatsoever.

7

Conclusions

The primary objective for this thesis was stated as follows:

> ”To find if a relation between clouds in the atmosphere and (liquid) water on the surface of exoplanets exists, and if so to define this relation, by the climate model SPEEDY”.

This objective is supported by preset subgoals. The objective and subgoals can be formulated as questions, which aid in structuring the thesis.
This chapter answers the research questions and draws conclusions on the results of the project. The conclusions are formed on three different aspects: the application of SPEEDY in exoplanetary science, the actual relation between clouds and surface water, and the representation in signals.

7.1. The application of SPEEDY to exoplanets

Climate model SPEEDY has been used to simulate the atmosphere of the exoplanets in question. As this model is developed for Earth, it needed to be adapted to be able to be used for exoplanets. Earthly features are taken out and four exoplanet cases were defined to be implemented: an ocean planet, a planet covered by oceans with a large round dry continent in the middle, the same planet with the continent covered by vegetation, and this last planet with the addition of polar ice caps.

The simulated cloud patterns followed expectations, especially compared to control case Earth. This strongly suggesting that the model is flexible enough to be applied to other planets than Earth, at least in the behaviour of the results. Nevertheless, for certain combinations of parameters, the experiments became unstable and the code crashed. This shows that the parametrisation of the model cannot easily be applied to any planet. It was observed that the closer the parameter combination lied to Earth, and also the simpler the case was (for example a water planet as compared to continents), the less runs became unstable.
In conclusion, SPEEDY appears to be applicable to exoplanets, but is limited to specific ranges of parameters. These ranges of parameters preferably lie close to those of Earth.

7.2. The relation between clouds and surface water on exoplanets

To find a relation between clouds and surface water, parameters are varied in the four cases and their influence on the cloud pattern is studied. The parameters that are varied are solar flux, obliquity, eccentricity, rotational speed, relative humidity thresholds, and surface pressure. They are varied between 50% and 150% of Earth’s value. Rotational speed was found to have the most clearly identifiable influence on the cloud pattern, especially on an ocean planet. Therefore the discussion of results focuses on this case.

Generally, the straightforward conclusion would be: the more water on the surface, the more clouds in the atmosphere. This follows from the observation that there are generally more clouds present above an ocean than above land, which was the case for many parameter combinations applied to the

pre-set cases. So, if many clouds are observed, there is likely to be water. This confirms what was expected beforehand from other climate models described in literature.
However, also other factors can cause the cloud cover to increase, such as surface pressure. Therefore, more specific features can be looked at than simply the amount of surface water. For the specific case of a water planet, the rotation of the planet causes the clouds to form a band pattern. This is the clearest effect of an ocean being present that was extracted from the parameter variations. If such a band pattern could be observed, this means that probably a rotating ocean is occurring. An interruption of the band pattern can then be caused by a continent. Also above land clouds can form bands, but they will have a different temperature pattern. As oceans mediate the temperature, the temperature of the atmosphere is more extreme above land than above oceans.
Another way of recognising the distinguishment between an ocean and continents is the wind. As a coastline is an abrupt transition in surface, the moving air will bump against it and turn around. This feature could be derived from observing the dynamics of the clouds over time. An sich the wind is too little to indicate an ocean, but as aforementioned, so is the cloud pattern. An observer therefore wants to identify a combination of these features, to indicate the presence of an ocean.

Generally, recognising surface water on a planet from its cloud pattern through the observation of a band pattern would be the easiest approach. This however means that only planets which are (almost) fully covered by an ocean can be identified, rather than simply an ocean on a planet with land. The conditions of the identified relation are thus narrow.
To assess the certainty of the relation, a look is taken at the evolution of the cloud pattern over time. The bands are very stable, and all variations can be assumed spatially rather than temporally. A sidenote nevertheless: no anomalies, as in for example temperature or orography, were taken along in the simulation.

7.3. Representation in signals

As a secondary objective, the goal is set to: How can the relation between clouds and surface water on exoplanets be observed with a telescope? To this end, the signals of water planets with various rotational speeds have been calculated and compared. As exoplanetary observations usually take a large integration time, the influence of this on the results is also studied.

The rotational speed of the planet has an influence on both total flux as polarisation of the signal. A higher rotational speed induces a larger cloud cover, and hence generates a higher reflected flux. The polarisation is a bit more complicated, as the amount of glint that can be observed is directly dependent on the cloud pattern itself. At increasing rotational speed, the bands form around the equator, and a cloud-free zone is created which allows the glint signal to pass through. On the other hand, cloud cover increases in general, lowering the glint signal again. The effects of rotation are thus not linear, but they can nevertheless be quantified and their trends can be calculated and observed. If one of the two features, the increase in flux due to rotation or a change in glint signal, are recognised, it is not significant enough to identify an ocean, but if both of them are observed, the certainty rises.
A higher integration time indicates a lower temporal resolution, but might be necessary depending on the application. It is difficult to find a balance and to draw conclusions if no specific application is referred to. The effects in the signals of an ocean planet are however very predictable: if the right averaging method, again depending on the application, is used, the trends in daily signals can be derived from the integrated signal. This means that the signals of rotational speed could be extracted nevertheless.

8

Recommendations

While using and adapting SPEEDY for exoplanet applications, a number of questions and ideas for further research came up that could not be addressed in the available time frame. These are described in this chapter as recommendations such that further research can build on the results of this thesis. The recommendations can be split up in the same aspects as the conclusions.

SPEEDY has a large potential to be used in exoplanetary research. At the moment however, the parameter ranges in which it can be applied are rather close to Earth, as otherwise numerical instabilities start to play a role. Another project could try to broaden the application range and make the model more flexible. This thesis has shown that SPEEDY is a valuable option to be an exoplanetary climate model, but the parametrisation itself should be dived into, to find out exactly what is linked to processes on Earth and what not, and how this can be adapted.
Furthermore, the model planets studied in this thesis have uniform properties and a single continent. This was done as a first order study to analyse the effects of certain parameters globally, which has shown what parameters are interesting for further study and which are not. Further research should study more complicated cases, to see if the identified relations still hold and to get more representative and detailed results. As it is not possible to vary all planetary parameters, further research can base itself on a single or few parameters that were found interesting, as for example rotational speed.
Lastly, an attempt was made at implementing a tidally locked planet into SPEEDY. This was simply done by fixing the solar flux to remain the same at all timesteps, because in this manner the mathematics and parametrisation of SPEEDY itself were not invaded. This approach gave too many numerical problems to be able to proceed: gradients in temperature, energy, cloud cover and others became extremely high, causing the results to diverge. This could not be fixed without changing SPEEDY's computational processes. It is left as a recommendation to implement this feature in the model.
In SPEEDY, many parameters are uncoupled. The stellar flux is for example not linked to orbital parameters whatsoever. As a consequence, the influence of certain parameters, such as eccentricity, could not be quantified fully. Further research should adapt the climate model to opt for coupled parameters, such that their influence can be quantified including all their direct and indirect effects. It should be noted that this would probably increase computational complexity and speed of SPEEDY. As a middle ground, also another climate model can be found to repeat the parameter variations in a coupled manner.

The influence of the surface pressure on the cloud pattern could not fully be explained. Hence, more research would be needed in this area. On top of that, the parameter variation study can generally be extended, but this goes together with the extensions in SPEEDY as described above.
Furthermore, the physical explanation of the results should go one level deeper. For example, in the scope of this thesis, the observation of more clouds being present at a higher rotational speed sufficed. Nevertheless, the question why there are more clouds at a higher rotational speed remains. The cause should be found within the cloud formation process, which is parametrised in SPEEDY. Further research should go deeper into the mechanisms behind the observations from SPEEDY's parameter variations.

Regarding the signal calculations, the influence of land on the results appears to be an important factor in this analysis. This would be a direct next step in this research. The signal-calculation code was already adapted to accept more than two Fourier files, and as such can have a more complicated mask than binary. However, as there was no time left to study this in the thesis, the team is forced to leave this as a recommendation.

The added value of this thesis to scientific community is that the signals are calculated based on 'real' simulated cloud patterns. The goal of this signal calculation was to get an idea of how the signals differ in various situations and how large these differences are. As now a first base is formed, a more thorough analysis would be in place. The cloud patterns should be simulated on a subobserver grid instead of a geographical grid, as is common in Earth-observation research. Hence, the spectra will become more representative for exoplanets. Next, more detailed manners of calculating the signal could be used, such as an instrument model. These recommendations are all steps to bring the research closer to answering the question: what signal can we receive from an exoplanet which exhibits surface water?

A

Verification & Validation

Despite the fact that no new code was developed for this thesis research, existing code was adapted for new purposes. This raises the need for verification and validation. Automatically, some verification and validation was done along the way, which was already presented previously in the report. This chapter bundles and expands this verification and validation.

A.1. SPEEDY

During the process of adapting SPEEDY for exoplanets, the results of every parameter change were carefully studied before changing another parameter, to check if everything went well. Only if one parameter worked, another one was adapted. Secondly, known parameters such as albedo were plotted throughout the experiments, to see if remained as expected. In coupled ocean-model, pre-set parameters such as sea surface temperature are influenced slightly by the atmosphere. Nevertheless, their end values should lie close to the starting point, especially in stable situations, as there is still no lateral heat transfer. This is another way to verify the results.

Regarding validation, there are multiple approaches to be applied. The most simple one is to inspect whether the outcome of the simulation is similar to what can be seen in reality. The results for the simulated planets are assumed to lie close to what is known on Earth, as the model is based on our planet and the simulated planets are limited to have Earth-like properties. The cloud cover shows patterns of patchy clouds, which fulfils the described expectations. Furthermore, convective Hadley-cells become smaller as the rotational speed of the planet becomes larger, as described in Section 5.1. This observation adheres to the physical properties of convection.
The results of the parameter variations were validated by checking if the same effects were present in parameter variations on Earth. As Earth is a complex planet, its climate and cloud pattern can appear chaotic, which makes it hard to recognise patterns. The monthly mean cloud cover on Earth after three months is shown in Figure A.1. Nevertheless, large trends caused by varying the parameters are the same. Examples of this are a global increase in clouds when surface pressure is raised, or a tendency to develop high energy gradients when the solar flux is lowered. On top of that, it can be seen that most clouds form above oceans and that the Sahara desert remain clear, an observation to which the studied cases perfectly agree.

A.2. Sensitivity analysis of the results

As a sensitivity analysis, a closer look is taken at the temporal variation of the results. For many of the simulations, there is both monthly and daily output. To check if using the monthly average for drawing conclusions is valid, the daily output is studied. The daily output was found to not fluctuate much over time, implying that the monthly output can be trusted.

The metric defined in Section 5.1 can also be used to evaluate the stability of the results. The results shown in this thesis are converged situations, as can be assumed using the monthly output validated

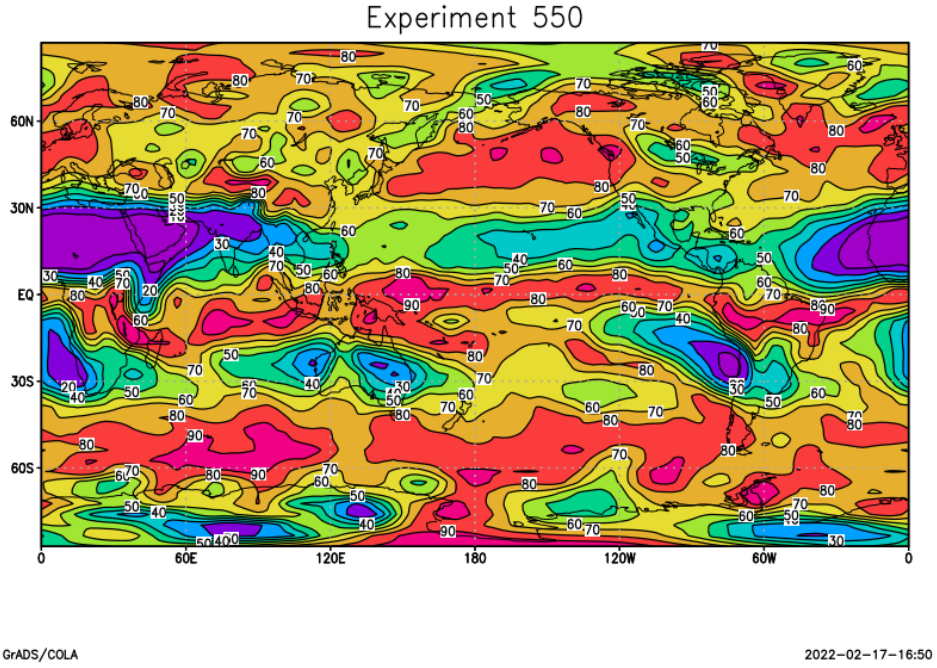

Figure A.1: Deep cloud cover on Earth, after three years of simulation.

above. However, how much can the cloud pattern still vary in a converged situation? To get an idea, the longitude bands over time on Earth are displayed in Figure A.2. As comparison, the same bands are shown for a water planet, in Figure A.3.
At the same latitude, cloud cover on Earth can vary up to 30%, while on an ocean planet the maximum difference lies around 20%. In both figures no trend can be seen from the start of the year towards the end, which shows the variations are due to seasons, anomalies (which are present in the Earth-model, but not in the water planet-model), or even random behaviour of the atmosphere. From this analysis, it can be concluded that the results of a converged ocean planet are as reliable as results of Earth.

A.3. Other Python and Fortran codes

Two Python codes were used: first, a code to process the raw SPEEDY output data in text files, and secondly a code to visualise the reflected signals from the planets' cloud patterns calculated by Fortran code PIXX.
The standard control and grid files processing unit GRADS did not suffice for the purposes of this thesis, and hence the output files were directly needed for further processing by other software. Unfortunately there is no easy way to access and process the control and grid files in Python. SPEEDY also outputs raw text files which can also be used for processing, the right data simply needed to be located in them. To check whether everything went well in the process, the output plots from the Python code were compared with the same plots in GRADS, which are based on the direct control and grid output.

As explained in Chapter 6, the Fortran code to calculate the signals was developed by Victor Trees and Daphne Stam (Trees and Stam, 2022). This code was used as-is, thus did not need to be verified. As validation, the calculated signals were checked against an example case provided by the developers, at every step of the process.
Lastly, some simple code to plot and process the calculated signals was written. Again, this code was compared to and validated with the given example cases.

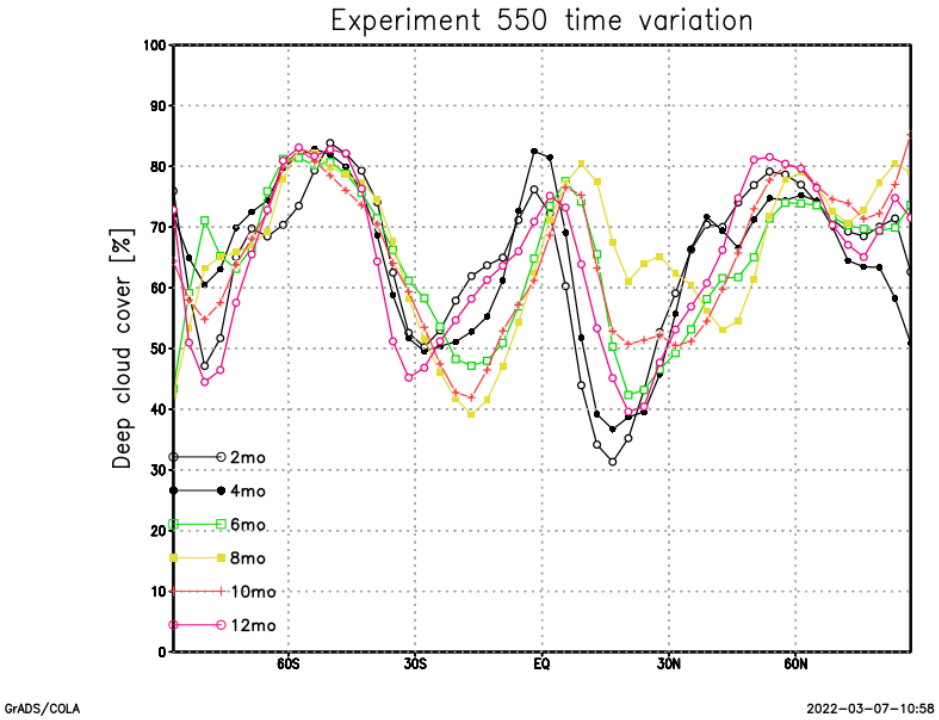

Figure A.2: Average cloud cover per latitude variations over time, for Earth.

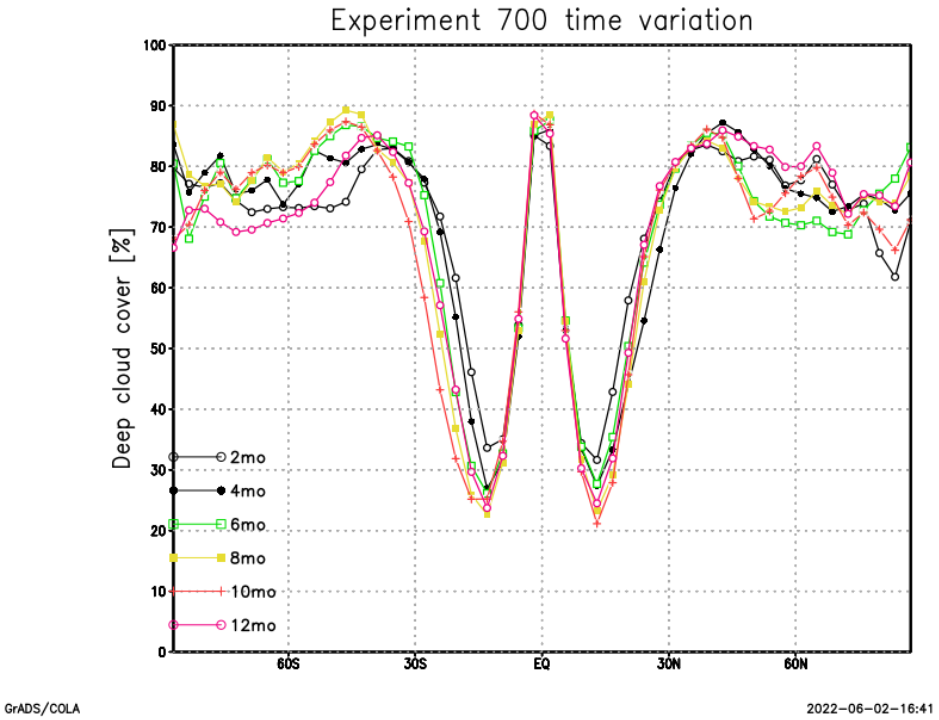

Figure A.3: Average cloud cover per latitude variations over time, for a water planet (case 1, with SST gradient).

B

List of Experiments

For verification purposes, the data of (almost) all experiments has been saved. Table B.1 lists the experiment number and a description. If an experiment is not explicitly used in the report, its individual properties are not specified, only what it was used for.

Table B.1: List of experiments, to link the experiment number to its description.

Number	*Experiment description*
100 - 104	Testing of SPEEDY
106 - 209	Initial parameter analysis
300 - 321	Defining, building and testing cases
322	Attempt to implement tidal lock
323 - 328	Defining, building and testing cases
329	Attempt to implement tidal lock
330	Defining, building and testing cases
331 - 336	Attempt to implement tidal lock
337	Tidal lock of a waterplanet with SST gradient out substellar point
338	Attempt to implement tidal lock
339	Tidal lock of a waterplanet with SST gradient out substellar point with increased surface pressure
340	Tidal lock of a planet with a dry continent (which has the properties of the continent in case 2) and with SST gradient out substellar point
341 - 342	Attempt to implement tidal lock
343	Tidal lock of a planet with a vegetated continent (which has the properties of the continent in case 4) and with SST gradient out substellar point
350 - 367	Parameter variations on gradient case 3 with a smaller time step
400	Default constant-SST case 1
401	Constant-SST case 1 with 50% solar flux
402	Constant-SST case 1 with 50% obliquity
403	Constant-SST case 1 with 50% rotational speed
404	Constant-SST case 1 with 50% eccentricity
405	Constant-SST case 1 with 50% surface pressure
406	Failed experiment
407	Constant-SST case 1 with 50% relative humidity thresholds
408	Constant-SST case 1 with 75% solar flux
409	Constant-SST case 1 with 75% obliquity
410	Constant-SST case 1 with 75% rotational speed
411	Constant-SST case 1 with 75% eccentricity
412	Constant-SST case 1 with 75% surface pressure
413	Failed experiment
414	Constant-SST case 1 with 75% relative humidity thresholds
415	Constant-SST case 1 with 125% solar flux

416	Constant-SST case 1 with 125% obliquity
417	Constant-SST case 1 with 125% rotational speed
418	Constant-SST case 1 with 125% eccentricity
419	Constant-SST case 1 with 125% surface pressure
420	Failed experiment
421	Constant-SST case 1 with 150% relative humidity thresholds
422	Constant-SST case 1 with 150% solar flux
423	Constant-SST case 1 with 150% obliquity
424	Constant-SST case 1 with 150% rotational speed
425	Constant-SST case 1 with 150% eccentricity
426	Constant-SST case 1 with 150% surface pressure
427	Failed experiment
428	Constant-SST case 1 with 150% relative humidity thresholds
429	Constant-SST case 1 with zero obliquity
430	Attempt to implement tidal lock
450	Default constant-SST case 2
451	Constant-SST case 2 with 50% solar flux
452	Constant-SST case 2 with 50% obliquity
453	Constant-SST case 2 with 50% rotational speed
454	Constant-SST case 2 with 50% eccentricity
455	Constant-SST case 2 with 50% surface pressure
456	Failed experiment
457	Constant-SST case 2 with 50% relative humidity thresholds
458	Constant-SST case 2 with 75% solar flux
459	Constant-SST case 2 with 75% obliquity
460	Constant-SST case 2 with 75% rotational speed
461	Constant-SST case 2 with 75% eccentricity
462	Constant-SST case 2 with 75% surface pressure
463	Failed experiment
464	Constant-SST case 2 with 75% relative humidity thresholds
465	Constant-SST case 2 with 125% solar flux
466	Constant-SST case 2 with 125% obliquity
467	Constant-SST case 2 with 125% rotational speed
468	Constant-SST case 2 with 125% eccentricity
469	Constant-SST case 2 with 125% surface pressure
470	Failed experiment
471	Constant-SST case 2 with 150% relative humidity thresholds
472	Constant-SST case 2 with 150% solar flux
473	Constant-SST case 2 with 150% obliquity
474	Constant-SST case 2 with 150% rotational speed
475	Constant-SST case 2 with 150% eccentricity
476	Constant-SST case 2 with 150% surface pressure
477	Failed experiment
478	Constant-SST case 2 with 150% relative humidity thresholds
479	Constant-SST case 2 with zero obliquity
480	Attempt to implement tidal lock
500	Default constant-SST case 3
501	Constant-SST case 3 with 50% solar flux
502	Constant-SST case 3 with 50% obliquity
503	Constant-SST case 3 with 50% rotational speed
504	Constant-SST case 3 with 50% eccentricity
505	Constant-SST case 3 with 50% surface pressure
506	Failed experiment
507	Constant-SST case 3 with 50% relative humidity thresholds
508	Constant-SST case 3 with 75% solar flux
509	Constant-SST case 3 with 75% obliquity

510	Constant-SST case 3 with 75% rotational speed
511	Constant-SST case 3 with 75% eccentricity
512	Constant-SST case 3 with 75% surface pressure
513	Failed experiment
514	Constant-SST case 3 with 75% relative humidity thresholds
515	Constant-SST case 3 with 125% solar flux
516	Constant-SST case 3 with 125% obliquity
517	Constant-SST case 3 with 125% rotational speed
518	Constant-SST case 3 with 125% eccentricity
519	Constant-SST case 3 with 125% surface pressure
520	Failed experiment
521	Constant-SST case 3 with 150% relative humidity thresholds
522	Constant-SST case 3 with 150% solar flux
523	Constant-SST case 3 with 150% obliquity
524	Constant-SST case 3 with 150% rotational speed
525	Constant-SST case 3 with 150% eccentricity
526	Constant-SST case 3 with 150% surface pressure
527	Failed experiment
528	Constant-SST case 3 with 150% relative humidity thresholds
529	Constant-SST case 3 with zero obliquity
530	Attempt to implement tidal lock
550	Default control case Earth
551	Control case Earth with 50% solar flux
552	Control case Earth with 50% obliquity
553	Control case Earth with 50% rotational speed
554	Control case Earth with 50% eccentricity
555	Control case Earth with 50% surface pressure
556	Failed experiment
557	Control case Earth with 50% relative humidity thresholds
558	Control case Earth with 75% solar flux
559	Control case Earth with 75% obliquity
560	Control case Earth with 75% rotational speed
561	Control case Earth with 75% eccentricity
562	Control case Earth with 75% surface pressure
563	Failed experiment
564	Control case Earth with 75% relative humidity thresholds
565	Control case Earth with 125% solar flux
566	Control case Earth with 125% obliquity
567	Control case Earth with 125% rotational speed
568	Control case Earth with 125% eccentricity
569	Control case Earth with 125% surface pressure
570	Failed experiment
571	Control case Earth with 150% relative humidity thresholds
572	Control case Earth with 150% solar flux
573	Control case Earth with 150% obliquity
574	Control case Earth with 150% rotational speed
575	Control case Earth with 150% eccentricity
576	Control case Earth with 150% surface pressure
577	Failed experiment
578	Control case Earth with 150% relative humidity thresholds
579	Control case Earth with zero obliquity
580	Attempt to implement tidal lock
600	Default constant-SST case 4
601	Constant-SST case 4 with 50% solar flux
602	Constant-SST case 4 with 50% obliquity
603	Constant-SST case 4 with 50% rotational speed

604	Constant-SST case 4 with 50% eccentricity
605	Constant-SST case 4 with 50% surface pressure
606	Failed experiment
607	Constant-SST case 4 with 50% relative humidity thresholds
608	Constant-SST case 4 with 75% solar flux
609	Constant-SST case 4 with 75% obliquity
610	Constant-SST case 4 with 75% rotational speed
611	Constant-SST case 4 with 75% eccentricity
612	Constant-SST case 4 with 75% surface pressure
613	Failed experiment
614	Constant-SST case 4 with 75% relative humidity thresholds
615	Constant-SST case 4 with 125% solar flux
616	Constant-SST case 4 with 125% obliquity
617	Constant-SST case 4 with 125% rotational speed
618	Constant-SST case 4 with 125% eccentricity
619	Constant-SST case 4 with 125% surface pressure
620	Failed experiment
621	Constant-SST case 4 with 150% relative humidity thresholds
622	Constant-SST case 4 with 150% solar flux
623	Constant-SST case 4 with 150% obliquity
624	Constant-SST case 4 with 150% rotational speed
625	Constant-SST case 4 with 150% eccentricity
626	Constant-SST case 4 with 150% surface pressure
627	Failed experiment
628	Constant-SST case 4 with 150% relative humidity thresholds
629	Constant-SST case 4 with zero obliquity
630	Attempt to implement tidal lock
697	Default gradient case 1 forced to 14-daily output
698	Default gradient case 1 forced to 7-daily output
699	Default gradient case 1 forced to 3-daily output
700	Default gradient case 1
701	Gradient case 1 with 50% solar flux
702	Gradient case 1 with 50% obliquity
703	Gradient case 1 with 50% rotational speed
704	Gradient case 1 with 50% eccentricity
705	Gradient case 1 with 50% surface pressure
706	Failed experiment
707	Gradient case 1 with 50% relative humidity thresholds
708	Gradient case 1 with 75% solar flux
709	Gradient case 1 with 75% obliquity
710	Gradient case 1 with 75% rotational speed
711	Gradient case 1 with 75% eccentricity
712	Gradient case 1 with 75% surface pressure
713	Failed experiment
714	Gradient case 1 with 75% relative humidity thresholds
715	Gradient case 1 with 125% solar flux
716	Gradient case 1 with 125% obliquity
717	Gradient case 1 with 125% rotational speed
718	Gradient case 1 with 125% eccentricity
719	Gradient case 1 with 125% surface pressure
720	Failed experiment
721	Gradient case 1 with 150% relative humidity thresholds
722	Gradient case 1 with 150% solar flux
723	Gradient case 1 with 150% obliquity
724	Gradient case 1 with 150% rotational speed
725	Gradient case 1 with 150% eccentricity

726	Gradient case 1 with 150% surface pressure
727	Failed experiment
728	Gradient case 1 with 150% relative humidity thresholds
729	Gradient case 1 with zero obliquity
730	Attempt to implement tidal lock
750	Default gradient case 2
751	Gradient case 2 with 50% solar flux
752	Gradient case 2 with 50% obliquity
753	Gradient case 2 with 50% rotational speed
754	Gradient case 2 with 50% eccentricity
755	Gradient case 2 with 50% surface pressure
756	Failed experiment
757	Gradient case 2 with 50% relative humidity thresholds
758	Gradient case 2 with 75% solar flux
759	Gradient case 2 with 75% obliquity
760	Gradient case 2 with 75% rotational speed
761	Gradient case 2 with 75% eccentricity
762	Gradient case 2 with 75% surface pressure
763	Failed experiment
764	Gradient case 2 with 75% relative humidity thresholds
765	Gradient case 2 with 125% solar flux
766	Gradient case 2 with 125% obliquity
767	Gradient case 2 with 125% rotational speed
768	Gradient case 2 with 125% eccentricity
769	Gradient case 2 with 125% surface pressure
770	Failed experiment
771	Gradient case 2 with 150% relative humidity thresholds
772	Gradient case 2 with 150% solar flux
773	Gradient case 2 with 150% obliquity
774	Gradient case 2 with 150% rotational speed
775	Gradient case 2 with 150% eccentricity
776	Gradient case 2 with 150% surface pressure
777	Failed experiment
778	Gradient case 2 with 150% relative humidity thresholds
779	Gradient case 2 with zero obliquity
800	Default gradient case 3
801	Gradient case 3 with 50% solar flux
802	Gradient case 3 with 50% obliquity
803	Gradient case 3 with 50% rotational speed
804	Gradient case 3 with 50% eccentricity
805	Gradient case 3 with 50% surface pressure
806	Failed experiment
807	Gradient case 3 with 50% relative humidity thresholds
808	Gradient case 3 with 75% solar flux
809	Gradient case 3 with 75% obliquity
810	Gradient case 3 with 75% rotational speed
811	Gradient case 3 with 75% eccentricity
812	Gradient case 3 with 75% surface pressure
813	Failed experiment
814	Gradient case 3 with 75% relative humidity thresholds
815	Gradient case 3 with 125% solar flux
816	Gradient case 3 with 125% obliquity
817	Gradient case 3 with 125% rotational speed
818	Gradient case 3 with 125% eccentricity
819	Gradient case 3 with 125% surface pressure
820	Failed experiment

821	Gradient case 3 with 150% relative humidity thresholds
822	Gradient case 3 with 150% solar flux
823	Gradient case 3 with 150% obliquity
824	Gradient case 3 with 150% rotational speed
825	Gradient case 3 with 150% eccentricity
826	Gradient case 3 with 150% surface pressure
827	Failed experiment
828	Gradient case 3 with 150% relative humidity thresholds
829	Gradient case 3 with zero obliquity
850	Default gradient case 4
851	Gradient case 4 with 50% solar flux
852	Gradient case 4 with 50% obliquity
853	Gradient case 4 with 50% rotational speed
854	Gradient case 4 with 50% eccentricity
855	Gradient case 4 with 50% surface pressure
856	Failed experiment
857	Gradient case 4 with 50% relative humidity thresholds
858	Gradient case 4 with 75% solar flux
859	Gradient case 4 with 75% obliquity
860	Gradient case 4 with 75% rotational speed
861	Gradient case 4 with 75% eccentricity
862	Gradient case 4 with 75% surface pressure
863	Failed experiment
864	Gradient case 4 with 75% relative humidity thresholds
865	Gradient case 4 with 125% solar flux
866	Gradient case 4 with 125% obliquity
867	Gradient case 4 with 125% rotational speed
868	Gradient case 4 with 125% eccentricity
869	Gradient case 4 with 125% surface pressure
870	Failed experiment
871	Gradient case 4 with 150% relative humidity thresholds
872	Gradient case 4 with 150% solar flux
873	Gradient case 4 with 150% obliquity
874	Gradient case 4 with 150% rotational speed
875	Gradient case 4 with 150% eccentricity
876	Gradient case 4 with 150% surface pressure
877	Failed experiment
878	Gradient case 4 with 150% relative humidity thresholds
879	Gradient case 4 with zero obliquity
900 - 918	Attempt to implement tidal lock

Bibliography

Checlair, J., Menou, K., & Abbot, D. S. (2017). No snowball on habitable tidally locked planets. *The Astrophysical Journal*, *845*(2), 132. https://doi.org/10.3847/1538-4357/aa80e1

Colose, C. M., Genio, A. D. D., & Way, M. J. (2019). Enhanced habitability on high obliquity bodies near the outer edge of the habitable zone of sun-like stars. *The Astrophysical Journal*, *884*(2), 138. https://doi.org/10.3847/1538-4357/ab4131

Cowan, N. B., Agol, E., Meadows, V. S., Robinson, T., Livengood, T. A., Deming, D., Lisse, C. M., A'Hearn, M. F., Wellnitz, D. D., & Seager, S. (2009). Alien maps of an ocean-bearing world. *The Astrophysical Journal*, *700*(2), 915–923. https://doi.org/10.1088/0004-637X/700/2/915

de Vera, J.-P., & Seckbach, J. (2021). *Habitability of other planets and satellites* (Vol. 28). Springer.

Genio, A. D. D., M. J. Way, N. Y. K., Aleinov, I., Puma, M. J., & Cook, B. (2019). Climates of warm earth-like planets. iii. fractional habitability from a water cycle perspective. *The Astrophysical Journal*, *887*(2), 197. https://doi.org/10.3847/1538-4357/ab57fd

Genio, A. D. D., Way, M. J., Amundsen, D. S., Aleinov, I., Kelley, M., Kiang, N. Y., & Clune, T. L. (2019). Habitable climate scenarios for proxima centauri b with a dynamic ocean. *Astrobiology*, *19*(1), 197. https://doi.org/10.1089/ast.2017.1760

Genio, D., A.D., Brain, D., Noack, L., & Schaefer, L. (2020). *The inner solar system's habitability through time* (Vol. Planetary Astrobiology). University of Arizona Press.

Gillon, M., Triaud, A. H. M. J., Demory, B.-O., Jehin, E., Agol, E., Deck, K. M., Susan M. Lederer, J. d. W., Burdanov, A., Ingalls, J. G., Bolmont, E., Leconte, J., Raymond, S. N., Selsis, F., Turbet, M., Barkaoui, K., Burgasser, A., Burleigh, M. R., Carey, S. J., Chaushev, A., … Queloz, D. (2017). Seven temperate terrestrial planets around the nearby ultracool dwarf star trappist-1. *Nature*, *542*, 456–460. https://doi.org/10.1038/nature21360

Grenfell, J. L., Godolt, M., Cabrera, J., Carone, L., Muñoz, A. G., Kitzmann, D., Smith, A. M. S., & Rauer, H. (2012). Atmospheric characterization via broadband color filters on the planetary transits and oscillations of stars (plato) mission. *Experimental Astronomy*, *50*, 1–49. https://doi.org/10.1007/s10686-020-09660-1

Grenfell, J. L., Leconte, J., Forget, F., Godolt, M., Carrión-González, Ó., Noack, L., Tian, F., Rauer, H., Gaillard, F., Bolmont, É., Charnay, B., & Turbet, M. (2020). Possible atmospheric diversity of low mass exoplanets – some central aspects. *Space Science Reviews*, *216*(2), 98. https://doi.org/10.1007/s11214-020-00716-4

Gu, L., Fan, S., Li, J., Bartlett, S., Natraj, V., Jiang, J. H., Crisp, D., Hu, Y., Tinetti, G., & Yung, Y. L. (2021). Earth as a proxy exoplanet: Deconstructing and reconstructing spectrophotometric light curves. *The Astronomical Journal*, *161*(3), 122. https://doi.org/10.3847/1538-3881/abd54a

Guzewich, S., Way, M., Sohl, L. E., Arney, G. N., Genio, A. D. D., Wolf, E. T., & Kopparapu, R. (2019). Recovering the earth's climate with the rocke3d global climate model.

Herbort, O., Woitke, P., Helling, C., & Zerkle, A. (2020). The atmospheres of rocky exoplanets i. outgassing of common rock and the stability of liquid water. *Astronomy & Astrophysics*, *636*(A71). https://doi.org/10.1051/0004-6361/201936614

Ishiwatari, M., Yoshida, T., Nakajima, K., Takehiro, S. I., Takahashi, Y. O., Hashimoto, G. L., Kuramoto, K., & Hayashi, Y. Y. (2019). Numerical experiments on climate of terrestrial exoplanets: Aqua-planet and land planet.

Jansen, T., Scharf, C., Way, M., & Genio, A. D. (2019). Climates of warm earth-like planets. ii. rotational "goldilocks" zones for fractional habitability and silicate weathering. *The Astrophysical Journal*, *875*(2), 79. https://doi.org/10.3847/1538-4357/ab113d

Kiang, N. Y., Colose, C., Ruedy, R., Barnes, R., Elsaesser, G. S., Harman, S., Kane, S. R., Russell, G. L., Lier-Walqui, M. V., Wolf, E. T., Aleinov, I., Genio, A. D., Guzewich, S. D., Tsigaridis, K., Way, M. J., & Kiang, N. (2021). Land planets in a rocke-3d gcm perturbed parameter ensemble: Fractional habitability.

Klindzic, D., Stam, D., Snik, F., Hoeijmakers, J., Willebrands, M., Karalidi, T., Pallichadath, V., van Dijk, C., & Esposito, M. (2021). Loupe: Observing earth from the moon to prepare for detecting life on earth-like exoplanets. *Royal Society of London. Philosophical Transactions A. Mathematical, Physical and Engineering Sciences*, *379*, 2188. https://doi.org/10.1098/rsta.2019.0577rsta20190577

Komacek, T. D., Fauchez, T. J., Wolf, E. T., & Abbot, D. S. (2020). Clouds will likely prevent the detection of water vapor in jwst transmission spectra of terrestrial exoplanets. *The Astrophysical Journal Letters*, *888*(2), L20. https://doi.org/10.3847/2041-8213/ab6200

Kucharski, F., Molteni, F., & King, M. P. (n.d.). Quick start for speedy version 41.5.

Loftus, K., & Wordsworth, R. D. (2021). The physics of falling raindrops in diverse planetary atmospheres.

Luger, R., Bedell, M., Vanderspek, R., & Burke, C. J. (2019). Tess photometric mapping of a terrestrial planet in the habitable zone: Detection of clouds, oceans, and continents.

Ohno, K., & Okuzumi, S. (2017). A condensation–coalescence cloud model for exoplanetary atmospheres: Formulation and test applications to terrestrial and jovian clouds. *The Astrophysical Journal*, *835*(2), 261. https://doi.org/10.3847/1538-4357/835/2/261

Petralia, A., Alei, E., Aresu, G., Locci, D., Cecchi-Pestellini, C., Micela, G., Claudi, R., & Ciaravella, A. (2020). A systematic study of co2 planetary atmospheres and their link to the stellar environment. *Monthly Notices of the Royal Astronomical Society*, *496*(4), 5350–5359. https://doi.org/10.1093/mnras/staa1929

Robinson, T. D., Meadows, V. S., Crisp, D., Deming, D., A'Hearn, M. F., Charbonneau, D., Livengood, T. A., Seager, S., Barry, R. K., Hearty, T., Hewagama, T., Lisse, C. M., McFadden, L. A., & Wellnitz, D. D. (2011). Earth as an extrasolar planet: Earth model validation using epoxi earth observations. *Astrobiology*, *11*(5). https://doi.org/10.1089/ast.2011.0642

Rossi, L., Berzosa-Molina, J., & Stam, D. M. (2018). Pymiedap : A python–fortran tool to compute fluxes and polarization signals of (exo)planets. *Astronomy & Astrophysics*, *616*(A147). https://doi.org/10.1051/0004-6361/201832859

Rossow, W. B. (1978). Cloud microphysics: Analysis of the clouds of earth, venus, mars, and jupiter. *Icarus*, *36*, 1–50.

Rossow, W. B. (1983). A general circulation model of a venus-like atmosphere. *Journal of the Atmospheric Sciences*, *40*(2), 273–302.

Trees, V., & Stam, D. (2019). Blue, white, and red ocean planets: Simulations of orbital variations in flux and polarization colors. *Astronomy & Astrophysics*, *626*(A129). https://doi.org/10.1051/0004-6361/201935399

Trees, V., & Stam, D. (2022). Ocean signatures in the total flux and polarization spectra of earth-like exoplanets. *accepted for publication in Astronomy & Astrophysics*. https://doi.org/10.1051/0004-6361/202243591

Way, M. J., Anthony D. Del Genio, I. A., Clune, T. L., Kelley, M., & Kiang, N. Y. (2018). Climates of warm earth-like planets. i. 3d model simulations. *The Astrophysical Journal Supplement Series*, *239*(2), 24. https://doi.org/10.3847/1538-4365/aae9e1

Way, M. J., Anthony D. Del Genio, N. Y. K., Sohl, L. E., Grinspoon, D. H., Aleinov, I., Kelley, M., & Clune, T. (2016). Was venus the first habitable world of our solar system? *Geophysical Research Letters*. https://doi.org/10.1002/2016GL069790

Woitke, P., Herbort, O., Helling, C., Stüeken, E., Dominik, M., Barth, P., & Samra, D. (2021). Coexistence of ch4, co2 and h2o in exoplanet atmospheres. *Astronomy & Astrophysics*, *646*(A43). https://doi.org/10.1051/0004-6361/202038870

Wordsworth, R. D., & Pierrehumbert, R. T. (2013). Water loss from terrestrial planets with co2-rich atmospheres. *The Astrophysical Journal*, *778*(2), 154. https://doi.org/10.1088/0004-637X/778/2/154

Wunderlich, F., Scheucher, M., Godolt, M., Grenfell, J. L., Schreier, F., Schneider, P. C., Wilson, D. J., Sánchez-López, A., López-Puertas, M., & Rauer, H. (2020). Distinguishing between wet and dry atmospheres of trappist-1 e and f. *The Astrophysical Journal*, *901*(2), 126. https://doi.org/10.3847/1538-4357/aba59c

Yang, J., Abbot, D. S., Koll, D. D. B., Hu, Y., & Showman, A. P. (2019). Ocean dynamics and the inner edge of the habitable zone for tidally locked terrestrial planets. *The Astrophysical Journal*, *871*(1), 29. https://doi.org/10.3847/1538-4357/aaf1a8

Yang, J., Cowan, N. B., & Abbot, D. S. (2013). Stabilizing cloud feedback dramatically expands the habitable zone of tidally locked planets. *The Astrophysical Journal Letters*, *771*(2), L45. https://doi.org/10.1088/2041-8205/771/2/L45

Zsom, A., Kaltenegger, L., & Goldblatt, C. (2012). A 1d microphysical cloud model for earth, and earth-like exoplanets: Liquid water and water ice clouds in the convective troposphere. *Icarus*, *221*(2), 603–616. https://doi.org/10.1016/j.icarus.2012.08.028

Zugger, M. E., Kasting, J. F., Williams, D. M., Kane, T. J., & Philbrick, C. R. (2011). Searching for water earths in the near-infrared. *The Astrophysical Journal*, *739*(1), 12. https://doi.org/10.1088/0004-637X/739/1/12